UiT The Arctic University of Norway

Faculty of Science and Technology
Departement of Physics and Technology

The Role of Clouds in Arctic Climate

FYS-3900: Master's thesis in Physics - 60 ECTS

Hannah Sundermann

15.05.2024

Abstract

Anthropogenic climate change is causing the Arctic to warm faster than any other region on Earth, a phenomenon also known as Arctic amplification. The warming and its consequences induce, amongst other things, a change in clouds, impacting their role in the Arctic climate by introducing a feedback.
Clouds play an important role in the global radiation budget. They cool the surface by reflecting incoming shortwave radiation and warm it by absorbing and re-emitting longwave radiation. While the cooling effect outweighs the warming on a global mean, clouds warm the Arctic surface. The precise impact of clouds on the Arctic climate, particularly in global climate models, remains uncertain and is subject of ongoing research.
This thesis studies the sensitivity of the Arctic climate to local changes in microphysical cloud properties using the Community Earth System Model 2.1.3 (CESM).
First-order impacts of cloud alterations resulting from climate change were studied. Therefore, a simulation with clouds from a $2\times CO_2$ environment within a climate model set to pre-industrial CO_2 levels was conducted. These changes were only implemented concerning the radiation transfer scheme of CESM. The results show a net warming effect in winter and a cooling effect in summer, with the warming effects predominating.
Additionally, dedicated numerical experiments were conducted to investigate how variations in droplet size distribution, ice crystal sizes, liquid and ice water paths, and cloud fraction influence Arctic temperature, sea ice extent, and radiation fluxes. These experiments aimed to evaluate the model's accuracy in representing cloud microphysical parameters and their alignment with established theoretical frameworks.

Acknowledgements

First of all, I want to thank my supervisor, Rune Grand Graversen, for always finding time to give me valuable advice and to discuss my progress. Thank you for introducing me to the world of global climate modeling, Arctic clouds, and sea ice.

I also want to thank my fellow students, Patsi and Ronnie, for keeping me sane during stressful times and helping me through all kinds of struggles.
Thank you also to Håvard for always being there for me and for listening to all my thoughts; I could not have done this without you.
To my friends back in Germany, thank you for your support from afar.

Lastly, a huge thank you goes to my parents who made this possible. Thank you for always supporting me in pursuing my passions. Thank you also for proofreading parts of this thesis.

Contents

List of Figures

List of Tables

List of Abbreviations

CAM6 Community Atmosphere Model version 6

CESM Community Earth System Model version 2.1.3

FLDS downwelling LW flux at surface

FLNS net LW flux at surface

FSNS net SW flux at surface

IWC ice water content

IWP ice water path

LW longwave

LWC liquid water content

LWP liquid water path

MC Monte-Carlo

SHEBA Surface Heat Budget of the Arctic Ocean

SOM slab-ocean model

SW shortwave

1 Introduction

The Arctic is a unique geographical and climatic region that plays an important role in the global climate. It is usually constrained by the 10 °C isotherm for July. Hence, the Arctic is defined as the regions in the Northern hemisphere where average temperatures in July do not exceed 10 °C [1, 2]. Early definitions for the Arctic take astronomical elements into account; using the Arctic circle at a latitude of 66 °33 ′N as a southern boundary [1, 3, 4].
The Arctic consists of a variety of ecological areas. As the mentioned isotherm aligns with the northern treeline, continental parts of the Arctic are characterised by treeless tundras [1, 2], permafrost (permanently frozen ground) and the Greenland ice sheet [5]. A large part of the Arctic is the Arctic ocean that is typically covered by sea ice [5].
Temperatures show a large spatial variability. In the central Arctic, above the sea ice covered ocean, mean winter temperatures can be as low as −30 °C in January and even colder in the terrestrial Siberia. In Iceland, on the other hand, mean temperatures in January are around 0 °C [5]. Moreover, the Arctic is a generally cloudy place; during the summer months, an average of over 80 % of the Arctic sky is covered with clouds, predominantly low-level clouds. During the winter season, the monthly mean of cloud coverage is between 40 and 60 % [6].
The Arctic plays an important role in the global climate system and changes in Arctic climate have an influence on the climate in other parts of the world, e.g. the mid latitudes [2, 7, 8, 9].
Additionally, while the anthropogenic climate change affects every region on Earth, it is particularly strong in the Arctic; a phenomenon also known as

Arctic amplification [10]. There, climate change is evident in a decline in sea ice extent [9, 11] as a result of a warming of atmosphere [10, 12] and ocean [13, 14]. Moreover, the Greenland ice sheet is shrinking [15] and the permafrost in Siberia is thawing [16, 17].
The melting of the Greenland ice sheet contributes to the rise of global sea levels [18] and, more importantly, the increase of fresh water outflowing from the ice sheet into the ocean has potential to significantly affect the Atlantic meridional overturning circulation leading to severe consequences regarding the global climate [19].
The thawing of the permafrost releases greenhouse gases such as methane and carbon dioxide, further fuelling climate change [16, 17].
Furthermore, as the Arctic sea ice extent declines, the ice thickness decreases, and more ocean area becomes ice-free, the albedo of this region decreases, leading to even more warming and an even further decline in sea ice (ice-albedo feedback) [2, 9, 10, 13, 20].
Clouds play a significant role in both the Arctic and global energy balance by absorbing and re-emitting LW radiation and by reflecting SW radiation as well as by being responsible for precipitation [21].
As the Earth warms due to climate change, a global change in clouds can also be observed [22]. For example, clouds are expected to be found at higher altitudes [23].
Arctic clouds are changing as well. As the sea ice extent declines, Arctic clouds change and an increase in Arctic cloud cover (cloud-ice feedback) can be observed and is associated with a surface warming [2, 24, 25, 26]. Additionally, an increase in Arctic temperature is suggested to lead to more clouds at higher altitudes resulting from instabilities in the lower atmosphere [8, 27]. Moreover, an increase in precipitation has been observed in Arctic regions [28, 29] and further increases are to be expected. Additionally, precipitation is expected to change from snow- to rain-dominated [29].
Overall, cloud changes due to climate change introduce a positive feedback in global climate models [30]. Hence, a local change in Arctic clouds might influence the Arctic climate change further.

Climate modeling emerges as a crucial tool to investigate potential future scenarios [31, 32] and is helping to understand and find connections between different variables [10]. Climate models allow researchers to change particular conditions and parameters in a local or global climate, thereby enabling the study of direct and indirect climate responses and providing insights into the dynamic interactions within the climate system [5, 31].
The first coupled climate model was developed in 1969, coupling an atmosphere with an ocean model [31, 33]. Since then, climate models have undergone further evolution. Not only a deeper understanding of atmospheric physics and chemistry, but also advances in computational power helped to develop more detailed and accurate climate models containing more climatic variables and

interactions. Given their potential, climate models still play an essential role in climate research [34].

As the Earth continues to warm, understanding the complex climate interactions in the Arctic becomes increasingly important. An important element are Arctic clouds, whose role in Arctic climate feedbacks is still a big uncertainty in global climate models and subject of current research [35].

This thesis studies the sensitivity of Arctic climate to local changes of microphysical cloud properties in one global climate model by conducting dedicated numerical climate model experiments with the Community Earth System Model version 2.1.3 (CESM) [36]. After looking at changes of single parameters, local changes of microphysical cloud properties due to climate change are investigated as well as their effects on the Arctic climate.

2

Foundation and Theory

2.1 Types of clouds

Clouds come in various shapes and sizes and can appear at different altitudes in the atmosphere. They can be visually classified as ten different genera that can be further divided into species and then varieties [6, 37]. Additionally, clouds extending to the ground can be classified as fog [6]. A brief overview of the cloud genera and the height where their base is located above the ground (étage) is shown in Tab 2.1.

		Height of cloud base		
Genus	**Level**	**Polar Regions**	**Temperate Regions**	**Tropical Regions**
Cumulonimbus Cumulus Stratocumulus Stratus	Low	up to 2 km	up to 2 km	up to 2 km
Altocumulus Altostratus Nimbostratus	Middle	2-4 km	2-7 km	2-8 km
Cirrocumulus Cirrostratus Cirrus	High	3-8 km	5-13 km	6-18 km

Table 2.1: Overview over cloud types sorted by height of cloud base [6, 37].

Low clouds often contain liquid water, but ice can also be present when the temperatures are sufficiently low [38]. One can find two groups of clouds in the lowest étage, cumuliform and stratiform clouds. *Cumulus* is the latin word for pile [6], Cumulus and Cumulonimbus clouds can be described as towering clouds with great thicknesses but flat bases [6, 37, 38]. *Nimbus* always refers to a cloud that precipitates [6]. Cumulus and cumulonimbus clouds are formed by fast rising air in a statically unstable atmosphere [6, 38]. *Stratus*, on the other hand, is latin for flattened out [6]. Low stratiform clouds experience little to no internal vertical air currents. Stratus clouds are usually a grey layer with a large horizontal extent [6, 37]. Similarly to stratus clouds, stratocumulus clouds appear as one large sheet of cloud, but with distinctive elements like long lines or clumps [6, 37].
As the étages can overlap, nimbostratus clouds are some times defined as low- and other times defined as middle-level clouds. They differ from stratus clouds in that they have a greater vertical extent and that they produce significant amounts of precipitation [6, 37, 38].
Middle clouds also mainly consist of liquid water, but ice crystals can also be present to form mixed-phase or ice clouds [38].
Altum is height in latin [6]. Altocumulus clouds are mid-level clouds made up of small elements of various forms (e.g. clumps, rolls or plaques). These clouds are thin and can be similar to stratocumulus, just found at a higher altitude [6, 37, 38]. Altostratus clouds differ from stratus clouds in the height at which they are found. They consist of a greyish layer covering the sky wholly or just partly. They can be thin enough so that the Sun can be seen through them and their precipitation usually does not touch the ground [6, 37, 38].
In high clouds, ice is the predominant water phase. They are generally thin and do not produce precipitation [6, 38].
The latin word *cirrus* refers to a lock of hair [6]. Cirrus clouds are white with a fibrous structure and/or a silky sheen [37]. Cirrocumulus clouds are high clouds consisting of small elements such as grains or ripples [37, 38]. Cirrostratus clouds appear as a transparent veil-like sheet with either a smooth or fibrous apperance [37, 38].
The fibrous appearance of cirriform clouds is due to strong winds in the upper troposphere and the ice particles becoming large. The ice particles then evaporate slowly, making it possible for the wind to move them over large distances [6].

2.2 Formation of clouds

2.2.1 Nucleation of cloud particles

Clouds form from supersaturated air [21], i.e. when the relative humidity of the air exceeds 100 % [6]. The relative humidity φ_r of the air is defined as:

$$\varphi_r = \frac{\varphi_a}{\varphi_s} = \frac{e}{e_s}, \tag{2.1}$$

with the absolute and saturation humidities being φ_a and φ_s, respectively, the vapor pressure e and the saturation vapor pressure e_s [39]. Saturation describes the state when, over a surface of pure water, there are as many molecules evaporating from this surface into gas as there are gas molecules condensing back to the liquid phase. If this equilibrium is not reached yet, and more molecules are evaporating than condensing, the air above the water surface is unsaturated. If the rate of condensing is greater than that of evaporation, the air is supersaturated [21, 40]. The saturation vapor pressure is highly dependent on the temperature, and so is the relative humidity. The dependence on temperature T of the saturation vapor pressure e_s over a liquid phase surface can be be derived using the Clausius-Clapeyron-equation [21]:

$$\frac{\mathrm{d}e_s}{\mathrm{d}T} = \frac{L}{T\,(\alpha_2 - \alpha_1)}, \tag{2.2}$$

where L is the specific latent heat of vaporising and α_1 and α_2 are the specific volumes of liquid and gaseous water, respectively [21]. Since $\alpha_1 \ll \alpha_2$, Eq. (2.2) can be approximated to:

$$\frac{\mathrm{d}e_s}{\mathrm{d}T} = \frac{L}{T\alpha_2}. \tag{2.3}$$

Using the ideal gas law:

$$e_s\alpha_2 = R_v T, \tag{2.4}$$

with the specific gas constant $R_v = {}^{R}/_{M}$ with M being the molar mass of water and R being the molar gas constant, the Clausius-Clapeyron-equation can be further modified to:

$$\frac{\mathrm{d}e_s}{\mathrm{d}T} = \frac{Le_s}{R_v T^2}. \tag{2.5}$$

By integration, this becomes:

$$\int_{e_0}^{e_s} \frac{\mathrm{d}e'_s}{e'_s} = \int_{T_0}^{T} \frac{L}{R_v T'^2}\mathrm{d}T' \tag{2.6}$$

$$\Leftrightarrow \log\left(\frac{e_s}{e_0}\right) = \frac{L}{R_v}\left(\frac{1}{T_0} - \frac{1}{T}\right). \tag{2.7}$$

Here, the temperature dependence of the latent heat is neglected as the temperature ranges in the atmosphere are sufficiently small [21]. This approximation works fine on small temperature ranges. T_0 and e_0 are chosen such that e_0 is the saturation vapor pressure at T_0 [21].
Now, the saturation vapor pressure e_s can be approximated to:

$$e_s = e_0 \exp\left(\frac{L}{R_v}\left(\frac{1}{T_0} - \frac{1}{T}\right)\right) \tag{2.8}$$

and the dependence of the saturation vapor pressure on the temperature becomes evident.
In the Earth's atmosphere, supersaturation most often occurs when air cools adiabatically[41]. This happens e.g. when it rises and expands [21].
Theoretically, cloud droplets can either form homogeneously when there is no condensation nucleus, i.e. an aerosol particle, and heterogeneously when there is some particle as condensation nucleus [6].
First, the case of homogeneous nucleation of a water droplet with radius r is discussed. The net energy related to the formation of this droplet can be written as:

$$\Delta E = 4\pi r^2 \sigma - \frac{4}{3}\pi r^3 n \left(\mu_v - \mu_l\right), \tag{2.9}$$

where σ is the surface tension or surface energy, n is the number of liquid water molecules per unit volume in the droplet and μ_v and μ_l are the Gibbs free energies per gaseous and liquid water molecule, respectively. Hence, the first term on the right hand side refers to the energy required to form the surface area, a vapor-liquid interface, of the droplet. The second term refers to the change in energy in the system due to the phase change of the gaseous water molecules [6, 21].
For a droplet to stably form, the energy in the system has to decrease and $\Delta E < 0$ [6, 21].
To make the equation clearer, the next step is to substitute the Gibbs energies in the second term on the right hand side.
Using the definition of Gibbs free energy for a reversible process:

$$\mathrm{d}G = V\mathrm{d}p - S\mathrm{d}T, \tag{2.10}$$

with volume V, pressure p, entropy S and temperature T and the ideal gas law:

$$pV = Nk_\mathrm{B}T, \tag{2.11}$$

where N is the number of molecules and k_B the Boltzmann constant, and assuming a constant temperature, Eq. (2.10) becomes:

$$\mathrm{d}G = \frac{Nk_\mathrm{B}T}{p}\mathrm{d}p. \tag{2.12}$$

Integrating between an arbitrary reference pressure value p_0 and the vapor pressure e or the saturation vapor pressure e_s over a plane surface of water at temperature T gives:

$$\int_{G_0}^{G_{v,l}} \mathrm{d}G = \int_{p_0}^{e_{v,l}} \frac{Nk_\mathrm{B}T}{p} \mathrm{d}p \tag{2.13}$$

$$\Leftrightarrow G_{v,l} - G_0 = Nk_\mathrm{B}T \log\left(\frac{e_{v,l}}{p_0}\right), \tag{2.14}$$

where G_v and G_l refer to the free Gibbs energy of gaseous and liquid water, respectively and e_v and e_l are referring to the the vapor pressure e and the saturation vapor pressure e_s, respectively. Using:

$$\frac{G}{N} = \mu, \tag{2.15}$$

Eq. 2.9 becomes [6, 21, 42]:

$$\Delta E = 4\pi r^2\sigma - \frac{4}{3}\pi r^3 nk_\mathrm{B}T \log\left(\frac{e}{e_s}\right). \tag{2.16}$$

When the air is not supersaturated and $e \leq e_s$, $\log \frac{e}{e_s}$ becomes 0 or negative and ΔE is always positive. Since the system favours states with less energy, droplet formation will not occur. If the air is supersaturated and $e > e_s$, ΔE is either positive or negative depending on r. At first, ΔE increases with increasing r until it reaches a maximum at $r = r^*$ from where it decreases with increasing r. This shows that droplets with radii smaller than r^* will still tend to evaporate but droplets that have reached radii greater or equal to r^* due to e.g. collision before they could evaporate will continue to grow from condensation [6, 21].

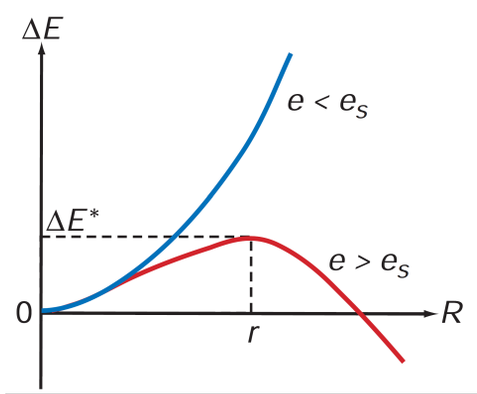

Figure 2.1: Net energy ΔE of droplet formation as a function of the droplet radius R for supersaturated ($e > e_s$) and non-saturated ($e < e_s$) air [21, p. 210, Fig. 6.1].

An expression for this critical radius r^* can be found by satisfying the condition:

$$\frac{\partial(\Delta E)}{\partial r} = 0, \tag{2.17}$$

which results in *Kelvin's equation* [6, 21]:

$$r^* = \frac{2\sigma}{nk_\mathrm{B}\log\left(e/e_s\right)}. \tag{2.18}$$

It can be seen that r^* is dependent on the degree of supersaturation ($(e/e_s - 1)\cdot 100\%$) as well as the temperature T, as σ and e_s are dependent on temperature. However, under atmospheric conditions the dependence on T has a rather weak influence on r^* [6]. Eq. 2.18 shows that the critical radius decreases with increasing supersaturation. For (super)saturations close to 100 %, the critical radius diverges.
For droplets to form homogeneously, supersaturations of at least 300 % are required [6]. Homogeneous nucleation is hence rather hypothetically as air that is that strongly supersaturated hardly ever occurs. Additionally, the air in Earth's atmosphere is very seldom perfectly clear and free of aerosols, hence favouring heterogeneous nucleation [6, 43].
Heterogeneous nucleation requires much lower supersaturations than homogeneous nucleation and thus is the predominant way of the formation of cloud droplets in the atmosphere. Here, water collects on a wettable aerosol particle (*cloud condensation nucleus* or *CCN*). Wettable means that the surface tension between the water and the surface of the particle is sufficiently low for the water to be able to cover it as a horizontal film. Eq. (2.18) still applies if the CCN is insoluble in water. Here, the critical radius r^*, however, also includes the radius of the CCN as it is the radius of the curvature of the water film. Hence, it is greater for a droplet forming on a CCN than a homogeneous formed droplet with the same amount of molecules. Thus, reaching the critical radius is more likely. The larger the aerosol particle, the more likely it is for a surviving drop to form on it [6, 21].
If the particle is water-soluble, it dissolves (partly) in the water condensing on it and resulting in a droplet consisting of a solution. The saturation vapor pressure of water over the solution droplet is generally lower than over a same-sized pure water droplet. Thus, e/e_s is smaller and r^* is greater for a solution compared to a pure water droplet, making it easier for nucleation to take place [6, 21].

If the temperature in a cloud is sufficiently low, water in the cloud will appear in solid phase (ice) rather than as a liquid. Similar to the formation of liquid water droplets, ice crystals can homogeneously be nucleated from water vapor, but this process requires temperatures below −65 °C and supersaturations around 1000 %. Since the latter never occurs in Earth's atmosphere, ice particles in

clouds are never homogeneously nucleated directly from water vapor. Instead, they are nucleated from liquid droplets [6, 21].
Liquid water can appear in clouds even at temperatures below 0 °C. It is then referred to as supercooled, an unstable state [21]. Supercooled water can be found in clouds at temperatures as low as −38 °C [6]. The homogeneous nucleation of ice from water droplets can be described similarly to the formation of water droplets from vapor. Analogically, an expression for a critically radius r_i^* can be found that is a function of temperature [6]:

$$r_i^* = \frac{2\beta_i \sigma_i}{\alpha_i n_i k_B T \log\left(e_s / e_{si}\right)}, \tag{2.19}$$

where α_i, β_i are coefficients referring to the size and shape of the ice particle (that is a polyhedron rather than a sphere like a droplet), σ_i is the surface tension of an ice-liquid interface, n_i is the number of molecules per unit volume of ice and e_{si} is the saturation vapor pressure with respect to ice. Here, r_i^* refers to the sphere that is just contained within the ice particle [6].
Experiments show that under laboratory conditions, homogeneous nucleation of ice particles takes place at temperatures lower than −35 °C and thus can usually only occur in clouds in high altitudes [21].
The ice crystals observed in clouds at higher temperatures than $\sim$ −35 °C hence formed through heterogeneous nucleation, again referring to nucleation onto a foreign particle's, the ice nucleus', surface [6, 21]. Analogically to the heterogeneous nucleation of liquid water droplets, the nucleus increases the initial size of the ice particle, making it more likely to reach the critical size (see Eq. (2.19)) [21]. Suitable nuclei are insoluble in water, have a diameter lager than 0.1 μm and should have a lattice structure comparable to that of ice. While these characteristics are favourable, they are in no means sufficient or necessary for a good ice nucleus [6, 21, 44].
The nucleation process can be differentiated into different modes. If the ice particle forms directly from water vapor onto an ice nucleus, this process is called *deposition nucleation*. If a water droplet comes into contact with an ice nucleus in the air and freezes, the nucleation process is referred to as *contact freezing* [6, 21, 45]. If the cloud condensation nucleus acts as the ice nucleus, the process is called *condensation freezing*. If any other ice nucleus that causes the freezing is contained within the droplet, the process is referred to as *immersion freezing* [6, 45].
Unlike spherical water droplets, ice crystals can take on different shapes [6, 21, 46, 47]. *Magono and Lee, 1966* [46] identified about 80 distinct ice and snow crystal shapes. The broadest classification of cloud ice crystals categorises them as either plate- or column (prism)-like, with hexagonal plates and columns with a hexagonal base area representing the simplest shapes in these categories [6, 21, 47]. Single crystals can aggregate to form more complex shapes [21, 46]. As a frequently observed example, bullet rosettes are a form of aggregated ice crystals made up of bullets, hexagonal columns with a pyramid-shaped top

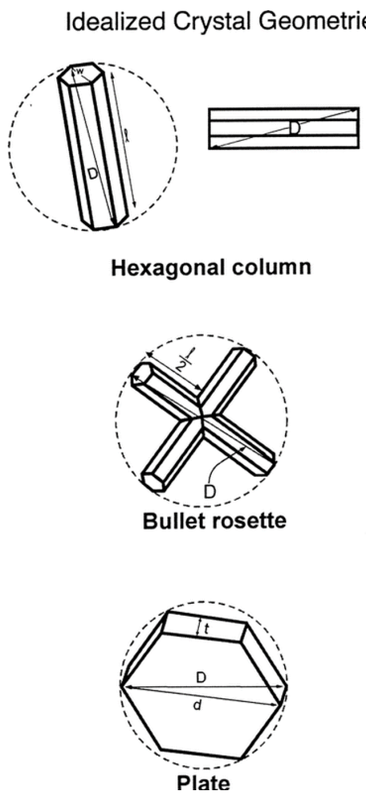

Figure 2.2: Illustration of the shape and dimensions of hexagonal columns, plates and bullet rosettes [48, Fig. 1].

[46, 48]. A schematic illustration of the mentioned ice crystal shapes can be seen in Fig. 2.2.

2.2.2 Growth of cloud particles and precipitation

Existing cloud particles can now further grow or shrink [6, 21].
Liquid water droplets grow by *condensation* or *collision and coalescence* with other droplets. They can shrink due to *evaporation* [6, 21].
Condensation occurs in a saturated environment when water vapor diffuses towards the droplet, evaporation occurs when the air around the droplet is unsaturated [6]. The growth rate is inversely proportional to the radius of the droplet. Hence, smaller droplets grow faster than larger droplets [21]. Liquid cloud droplets (radius $\sim 10\,\mu$m [21, 49]) can not grow to sizes of raindrops (radius $\sim 1000\,\mu$m [21]) just by condensation. Hence, another mechanism, collision and coalescence, becomes important [21]. On one hand, gravitation accelerates the droplets towards the Earth. On the hand, frictional forces slow them down. The terminal fall describes the speed of the droplet when buoyant

and drag forces are equal to gravity, hence the droplet does not experience acceleration anymore [50]. Small droplets have lower terminal fall speeds than large drops until the terminal fall speed saturates at a radius of about 3 mm [6, 21]. On their way downwards, larger drops may pass smaller droplets or collide with them [6, 21]. The collision efficiency describes the ratio of the effective collision cross section and the geometrical collision cross section. Given two droplets with radii r_1 and r_2 and the critical distance y between the center points of these droplets at which they would collide grazingly, the collision efficiency can be written as [21]:

$$E = \frac{y^2}{(r_1 + r_2)^2}. \tag{2.20}$$

y is not equal to $r_1 + r_2$ as the smaller droplet will follow the streamlines around the larger drop [21]. Hence, the collision efficiency is highly dependent on the airflow around the collector drop [6]. The larger the collector drop is, the larger is the collision efficiency if the ratio between the radii is held constant [6, 21].
A collision, though, will not automatically lead to coalescence of two cloud particles. Particles can also continue to exist as two separate particles after a collision and not coalesce. The coalescence efficiency is defined as the ratio of collisions resulting in coalescence. It is highest for large drops colliding with small droplets, decreases as the size of the droplet increases and then increases again as the droplets' radii approach in size. Coalescence is dependent on the ratio between the impact energy and the surface energy. If an electric field is present, coalescence becomes more likely [21].
The final collection efficiency is the product of the collision and coalescence efficiency [6, 21].

Ice crystals grow by *deposition*, *riming* or *aggregation*. They shrink by *sublimation* [6, 21].
Deposition and sublimation are equivalent to condensation and evaporation for liquid droplets [6].
Aggregation occurs when two ice crystals collide and attach to each other. The former happens, similarly to liquid droplets, when the ice crystals have different terminal fall speeds. The latter is highly dependent on temperature as well as the structure of the ice crystals. It generally does not occur at temperatures below $-20\,^{\circ}\mathrm{C}$ and becomes especially likely at temperatures above $-5\,^{\circ}\mathrm{C}$ [6, 21].
Riming occurs when ice crystals collide with liquid drops which then freeze on contact. Here, the collection efficiency depends on the size of the water droplet as well as the size and shape of the ice particle and its terminal fall speed. Generally, it is close to 0 for very small droplets, increases with increasing droplet size and then again drops to almost 0 for the largest droplets [6].
Ice particles can also change phase and melt into liquid cloud droplets. For that

to happen, they have to come in contact with water or air with temperatures above 0 °C [6].

Cloud droplets and ice crystals that fall onto Earth's surface are referred to as precipitation. Liquid droplets fall as rain or drizzle, depending on their radius. Ice particles can fall as snow, hail or graupel [6, 21].

2.3 Radiative effects of clouds

Clouds are an important factor regarding the global energy balance because they interact strongly with incoming and outgoing radiation. Cloud particles (water droplets or ice crystals) absorb and re-emit LW radiation and reflect SW radiation. While the former induces a greenhouse effect that is warming the climate system, the latter is an albedo effect leading to cooling [21, 51].
The interaction of spherical particles such as droplets with electromagnetic radiation can be described using various theories, depending on the size of the particle and the wavelength of the radiation [21, 52, 53].
First, a dimensionless size parameter x is defined as:

$$x = \frac{2\pi r}{\lambda}, \tag{2.21}$$

with the particle radius r and the wavelength λ of the incident radiation [21, 54].
When $x \ll 1$, the scattering is described using Rayleigh scattering and when $x \gtrsim 1$, Mie scattering theory (Mie theory) is used [54]. For $x \gg 1$, geometric optics are applied [21].
In the visible spectrum, x is $\ll 1$ for air molecules, ~ 1 for cloud droplets and $\gg 1$ for rain droplets [21]. x as a function of particle radius r and wavelength λ of incoming radiation is shown in Fig. 2.3 to illustrate the connection between the different scattering regimes and different wavelengths and particle sizes.
Since Mie theory is the most relevant theory for the scattering of SW radiation on cloud particles, its main aspects will be briefly discussed here. One of the important aspects from Mie theory is that with increasing radius r of the particle, the amount of radiation scattered in a forward direction increases [21, 55].
The optical depth of a cloud τ_c can be written as:

$$\tau_c = \beta_e z_c, \tag{2.22}$$

where β_e is the extinction coefficient and z_c is the thickness of the cloud [52].
The extinction parameter β_e is a measure for the attentuation of radiation when passing through a unit length of a medium, e.g. a cloud. It can be defined

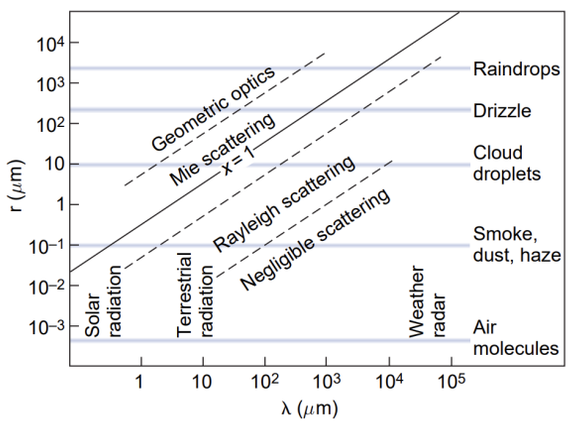

Figure 2.3: Regimes for different scattering theories dependent on wavelength λ of incoming radiation and radius r of the scattering particle [21, p. 123, Fig. 4.11].

as:

$$\beta_e = \int \hat{\sigma_e} \mathrm{d}n(r), \tag{2.23}$$

with the extinction cross section $\hat{\sigma_e}$ and $\mathrm{d}n(r) = \frac{\mathrm{d}n}{\mathrm{d}r}\mathrm{d}r$ representing the droplet size distribution, i.e. the number n of particles with a respective radius r [52]. The LWP Σ_l of a cloud is the amount of liquid cloud water within a unit-area column of atmosphere [21, 52]. The LWP of a cloud is defined as the total amount of liquid water in a cloud in a vertical column of atmosphere per unit area [56] and can be described as:

$$\Sigma_l = z_c \frac{4\pi\rho_w}{3} \int r^3 \mathrm{d}n(r), \tag{2.24}$$

where ρ_w is the density of water and a spherical geometry of water droplets is assumed [52].
For the extinction cross section $\hat{\sigma_e}$ applies:

$$\hat{\sigma_e} = Q_e \pi r^2, \tag{2.25}$$

where Q_e is the extinction efficiency or the fraction of the incoming radiation removed through the interaction with the spherical particle [52, 57]. For large x, when the radius of the sphere is much greater than the wavelength of the incoming radiation, Mie-theory suggest that $Q_e \longrightarrow 2$. Thus, the extinction cross section approaches $\hat{\sigma_e} \longrightarrow 2\pi r^2$ in the limit of large particles and SW radiation [58] and the optical depth of a cloud τ_c can be written as, combining this limit with Eqs. (2.22), (2.23) and (2.24) [52]:

$$\tau_c = \frac{3\Sigma_l \int 2\pi r^2 \mathrm{d}n(r)}{4\pi\rho_w \int r^3 \mathrm{d}n(r)}. \tag{2.26}$$

The scattering-equivalent mean droplet radius is defined as [52, 58]:

$$r_e = \frac{\int r\pi r^2 \mathrm{d}n(r)}{\int \pi r^2 \mathrm{d}n(r)}. \tag{2.27}$$

Unlike a simple mean radius, this scattering-equivalent mean droplet radius is weighted with the droplet cross section of the droplet. This is useful as the amount of light scattered by spherical particles is proportional to their cross sections [58].
Using Eq. (2.27), the optical depth of a cloud can be written as [52, 57]:

$$\tau_c = \frac{3\Sigma_l}{2\rho_w r_e}. \tag{2.28}$$

The albedo is a measure for the fraction of incoming radiation that is reflected on a certain surface [59]. A cloud's albedo can reach values of up to 0.9, depending on its characteristics, i.e. the type of cloud, its thickness, and microphysical properties [21, 59, 60], as well as the solar zenith angle [52].

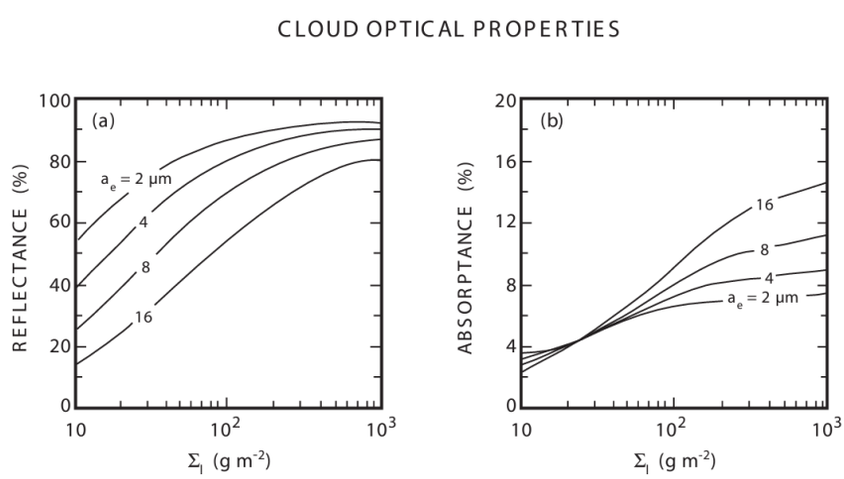

Figure 2.4: Fractions of reflected (left) and absorbed (right) SW wavelengths in clouds with different droplet sizes a_e dependent on the LWP Σ_l [52, p. 310, fig 9.34][61].

The single-scattering albedo $\tilde{\omega}$ is the ratio of scattering and extinction efficiencies Q_s and Q_e, respectively [62] and is defined as [58]:

$$\tilde{\omega} = \frac{Q_s}{Q_e} = \frac{Q_e - Q_a}{Q_e} = 1 - \frac{Q_a}{Q_e}, \tag{2.29}$$

where Q_a is the absorption efficiency and $\hat{\sigma_a}$ and $\hat{\sigma_e}$ are the absorption and extinction cross sections, respectively. Using Eq. (2.25), Eq. (2.29) can be written

as:

$$\tilde{\omega} = 1 - \frac{\hat{\sigma_a}}{\hat{\sigma_e}}. \tag{2.30}$$

Further, the following is valid [58]:

$$\hat{\sigma_a} = k_i \frac{4 r_e G}{3}, \tag{2.31}$$

$$\hat{\sigma_e} \cong 2G. \tag{2.32}$$

Here, $k_i = {}^{4\pi m_i}/_{\lambda}$ is the absorption coefficient that is dependent on the wavelength λ of the incident radiation and the imaginary part of the refractive index m of the absorbing medium. $G = \int \pi r^2 \mathrm{d}n(r)$ is the total cross section area [58]. Thus, the following relation for $1 - \tilde{\omega}$ can be found [58]:

$$1 - \tilde{\omega} \cong \frac{2}{3} k_i r_e. \tag{2.33}$$

$1 - \tilde{\omega}$ is a measure of the fraction of the radiation removed from the incident beam by absorption [63]. As $k_i \sim {}^1/_{\lambda}$, Eq. (2.33) illustrates that the shorter the wavelength of incoming radiation is, the larger is the fraction of removed light that is absorbed rather than scattered. Fig. 2.4 (right) shows that in the SW spectrum, with an increasing droplet radius, the absorbance of those wavelengths increases. This is also supported by Eq. (2.33).
Furthermore, the albedo increases with the optical depth of a cloud [64, 65]. As shown in eq. 2.28, the optical depth of a cloud is proportional to its LWP. Hence, an increase in the LWP leads to an increase in optical depth and thus results in a higher albedo. This is also shown in fig. 2.4 (left).
Additionally, it can be seen that the smaller the water droplets are, the higher is the albedo [66, 57]. This is also illustrated in Fig. 2.4 (left) and Eq. (2.28) supports this too; as the mean effective radius r_e decreases, the optical depth τ_c increases [57] and the albedo increases with the optical depth of a cloud [64, 65]. As shown in Eq. (2.28), the optical depth of a cloud is proportional to its LWP. Hence, an increase in the LWP leads to an increase in optical depth and thus results in a higher albedo. This is also shown in Fig. 2.4 (left).
Also, a higher cloud droplet number concentration leads to an increase in albedo [65].
Liquid water droplets also have a stronger effect on SW radiation compared to ice crystals [64], i.e. liquid phase clouds are up to 4 times more reflective than ice clouds [67].
The radiative properties of non-spherical ice crystals are more difficult to obtain than those of spherical water droplets as Mie theory does not apply here [58]. Still, one can define the optical depth τ_i of an ice cloud similar to that of a liquid phase cloud:

$$\tau_i = \beta_e z_i = z_i \int \hat{\sigma_e} \mathrm{d}n(L), \tag{2.34}$$

where β_e is the extinction coefficient, z_i is the thickness of the ice cloud, σ_e is the extinction cross section and $n(L)$ is the distribution of the major dimension L of the ice crystals [58].
Assuming randomly oriented hexagonal ice crystals, in the limit of geometric optics, σ_e can be written as:

$$\sigma_e = \frac{3D}{2}\left(\frac{\sqrt{3}D}{4} + L\right), \tag{2.35}$$

with the minimum dimension D of the crystal [58].
The single-scattering absorption of for such ice crystals can be derived similarly to that of liquid droplets [58]:

$$1 - \tilde{\omega} = \frac{\sigma_a}{\sigma_e} \sim \frac{k_i\sqrt{3}LD^2}{D\left(\sqrt{3} + 4L\right)}, \tag{2.36}$$

using again that σ_a is proportional to the absorption coefficient k_i and the volume V. The volume of a hexagonal ice crystal can be expressed as [58]:

$$V = \frac{3\sqrt{3}}{8}LD^2. \tag{2.37}$$

Interaction of LW radiation and cloud particles can be either described using Mie theory, as previously presented, or using Rayleigh Scattering. As mentioned earlier, this depends on the size of the cloud particle as well as the incident wavelength (see Eq. (2.21)). Often, Mie theory is still used to describe the interaction of cloud particles and LW radiation [58, 63]. When considering Rayleigh scattering and spherical particles (i.e. water droplets), though, the absorption efficiency can be approximated to:

$$Q_a = \frac{8\pi r}{\lambda}\mathfrak{Im}\left(\frac{m^2-1}{m^2+2}\right) = 4x\,\mathfrak{Im}\left(\frac{m^2-1}{m^2+2}\right), \tag{2.38}$$

where m is the refractive index of the sphere, r the radius of the particle and λ the wavelength of the incoming radiation. x is the size parameter (see Eq. (2.21)) [68].
The scattering efficiency can in this case is written as [68]:

$$Q_s = \frac{8}{3}\frac{16\pi^4 r^4}{\lambda^4}\left|\frac{m^2-1}{m^2+2}\right|^2 = \frac{8}{3}x^4\left|\frac{m^2-1}{m^2+2}\right|^2. \tag{2.39}$$

If the refractive index m is only weakly depending on λ over an interval, the following holds for Q_a and Q_s and sufficiently small particles [68]:

$$Q_a \sim \frac{r}{\lambda}, \quad Q_s \sim \frac{r^4}{\lambda^4}. \tag{2.40}$$

This follows from Eqs. (2.38) and (2.39). It shows that both the scattering as well as the absorption efficiency decrease with increasing wavelength but the absorption efficiency decreases faster. Additionally, both efficiencies increase with increasing droplet radius r.
Liquid water has an absorption minimum in the visual range. Several absorption bands can be found in the infrared (LW) range that are associated with vibrations of the molecules. Absorption in the UV range is attributed to electrons absorbing energy, thus becoming excited and transitioning to higher energy orbitals [68].

The greenhouse effect is associated with molecules in the atmosphere, especially so-called greenhouse gases such as CO_2 and H_2O, absorbing and re-emitting LW radiation emitted by Earth's surface and at other levels of the atmosphere. The emitted radiation is not solely directed away from the surface into space, some part of it is also redirected towards the surface. Hence, more radiation than just the incoming solar radiation is reaching Earth's surface, causing a larger warming compared to if no atmosphere was present. Clouds also cause a greenhouse effect [21, 60].
Liquid phase clouds are optically thick regarding LW radiation when their LWP Σ_l exceeds about $20\,\mathrm{g/m^2}$. Its impact on the radiation can then be described similarly to that of a blackbody [52]. Other observational studies of Arctic clouds indicate LWPs of $50\,\mathrm{g/m^2}$ [69] and $30\,\mathrm{g/m^2}$ [64] as the minimal water content for blackbody behaviour.
Ice clouds, on the other hand, absorb much less LW radiation, but also behave as a blackbody if the IWP is sufficiently large [52].
The name blackbody describes a physical body whose surface absorbs all incoming radiation. Hence, no incoming radiation gets transmitted or reflected [21].
A blackbody also emits radiation according to *Planck's law* [21, 40, 70]:

$$\varrho(\nu, T)\mathrm{d}\nu = \frac{8\pi h\nu^3}{c^3}\frac{1}{\exp\left(h\nu/k_\mathrm{B}T\right) - 1}\mathrm{d}\nu, \tag{2.41}$$

where T is the temperature of the blackbody, h is the Planck constant, ν is the frequency of the radiation, c the speed of light and k_B the Boltzmann constant [40]. The a derivation of Planck's law can be found in the appendix A.
A cloud's greenhouse effect is hence also dependent on its temperature. Clouds at higher altitudes are usually colder than the Earth's surface and hence absorb the upwelling LW radiation from the surface and emit LW radiation as a colder blackbody and thus with a different spectrum that has a maximum at a greater wavelength [21, 53]. The greenhouse effect is thus also dependent on the cloud's height.
A cloud's albedo is neither dependent on its height nor its temperature [52, 53]. The absorbance of a cloud increases with increasing droplet size and increasing LWP (see Fig. 2.4 (right), considering Mie theory) [52].

In a global mean, a cloud's albedo effect outweighs its greenhouse effect, so that clouds are usually associated with an overall cooling effect on Earth's surface [21, 51].
In conclusion, the radiative properties of a cloud depend on the phase of the water (liquid or solid phase), the droplet/ice crystal size and their concentration, the thickness of the cloud as well as its shape and temperature [51, 64, 71].

2.4 Clouds in the Arctic

Looking at a whole year, an average of about 70 % of the Arctic is covered by clouds [72, 73]. During the warmer seasons, the cloud cover is generally greater than during the colder seasons [6, 72].
In the Arctic, liquid phase and ice clouds as well as mixed-phase clouds can be found [74]. Additionally, liquid water is found in Arctic clouds all year round [35, 71, 75]. Solely liquid phase clouds most often appear close to the ground. Liquid water found in clouds at altitudes of a few kilometers is associated with mixed-phase clouds and the highest clouds in the Arctic contain only ice crystals [74]. Compared to mid and low latitudes, mixed-phase clouds are found at much lower altitudes in the Arctic [76]. This has of course to do with the lower temperatures in the Arctic compared to mid and low latitudes. In the Arctic, ice clouds reach temperatures as low as -60°C and liquid water can still be found in mixed-phase clouds at -40°C. Clouds containing only liquid water have been observed at -24°C [74].
From October 1997 until October 1998, the Surface Heat Budget of the Arctic Ocean (SHEBA) project took place in a region north of Alaska [77].
Purely liquid phase clouds observed during SHEBA were mostly occurring in summer, mixed-phase clouds in spring and autumn and solely ice clouds appeared in all seasons [49].
The most frequently observed type of mixed-phase clouds during that time were low-level stratiform clouds [78].
Arctic clouds are often low [72, 79] and optically thin with a low water content, hence observing them, especially from space and during winter, can be challenging [75, 79, 80].
Microphysical properties of Arctic clouds can vary significantly from cloud to cloud as well as within a single cloud [49, 80, 81]. Within a single cloud, the largest variations can be found vertically where e.g. the mean droplet radius and liquid water content generally increase with height above the cloud base [49, 81, 82]. During SHEBA, average values for the droplet radius and LWP in liquid clouds were observed to be 6.5 μm and 45 $\mathrm{g/m^2}$, respectively. In ice clouds, ice particles are generally larger in summer than in winter with an average diameter of 73 μm. The annual average IWP in Arctic ice clouds was observed to be 30 $\mathrm{g/m^2}$ [49]. In mixed-phase clouds observed during SHEBA, ice particles

were also larger in summer than in winter. Here, the average annual diameter is 93 μm. The average IWP in mixed-phase clouds during those observations was 42 g/m^2, the average LWP was 61 g/m^2 [78].
Observations during SHEBA found Arctic clouds in the observed region at 85 % of the times. Clouds were more frequent in summer than in winter [75]. A similar seasonal variability in cloud coverage has been observed in other areas of the Arctic as well. In the Eurasian Arctic, for example, the cloud coverage is largest in autumn and smallest in spring [72]. Generally, there is a spatial variability of cloud coverage in the Arctic with a similar seasonal variability [83].
Low-level liquid clouds with bases below 4.3 km above ground have the highest influence on the radiation budget in the Arctic, including both LW and SW radiation [64].
Diamond dust or cloudless ice crystal precipitation is a crystalline condensation in the Arctic air while no clouds are present. It only occurs when the air temperature is low enough, hence it is usually found from October to April [84]. Earlier studies suggested a rather large impact of diamond dust on the Arctic radiation budget [85], but it was found that it has little to no effect [84]. *Intrieri and Shupe, 2004* [84] suspect that rather thin liquid clouds that had not been observed, were the reason for the previous assumption.
Observations during SHEBA suggest cloud phase and cloud fraction to have more influence on the surface radiation budget compared cloud base temperature and other microphysical properties [86].
In contrast to the global mean where clouds are associated with a general cooling effect [21, 51], Arctic clouds generally have a warming effect on the surface temperature except for a short time during summer when they have a cooling effect due to the low surface albedo [80, 87, 88, 89].
Clouds do not only have an influence on the Arctic climate by interacting with radiation [35], they are also responsible for precipitation [6]. Snow, e.g., has an insulating effect on sea ice. Thicker snow covers in cold months lead to slower sea ice growth unless there is so much snow on the ice that it gets flooded. Flooding is way more frequent in the Antarctic than in the Arctic. [90].
Sea ice and clouds have an effect on each other [83, 91]. In warmer months, for example, clouds over open ocean contain more liquid water due to inter alia enhanced evaporation and a higher surface temperature compared to sea ice covered areas [91].
Several studies suggest a positive cloud-ice feedback, meaning less sea ice could lead to more clouds which then, due to an enhanced greenhouse effect, warm the surface and promote sea ice melt [24, 25, 26].
Sea ice plays an important role in the Arctic and global climate system. Its albedo (up to 0.85) is significantly higher than that of open ocean (ca. 0.07) and it acts as an insulator between the cold atmosphere and warmer ocean prohibiting turbulent heat exchanges between those two [90, 92]. The ice-albedo feedback is an important positive climate feedback that originates in

the large albedo difference of sea ice and open ocean. As the sea ice melts, more radiation is absorbed by the open ocean compared to the one covered in ice. This leads to a warming of the surface and atmosphere which then enhances sea ice melt [52, 90, 93].

3 Methods

3.1 Community Earth System Model

In this work, all experiments are performed using a slab-ocean model (SOM) version of the CESM [36]. The CESM is a global climate model that is fully coupled and developed of seven different components that interact via a coupler. It was created by the National Center for Atmospheric Research [94]. The component models are atmosphere, ocean, land, sea ice, land ice, river and waves [95]. This project will mainly focus on the atmosphere component, the Community Atmosphere Model version 6 (CAM6).

In the SOM version of CESM, the ocean is simplified to a single, well-mixed layer with a temperature T_0 and an internal heat flux Q. Q is determined by a control run of the model with a fully coupled ocean and is based on a linear interpolation of the monthly mean flux of energy into the ocean. It is important that the annual and global means of the Q-flux is 0 to ensure no sources or sinks of heat are being introduced relative to the control run [96].

3.1.1 Cloud Microphysics and Radiation scheme

The model distinguishes between three different types of clouds: ice clouds, liquid clouds and snow clouds. In mixed-phase clouds, the liquid and ice phase clouds are treated individually. Each cloud type i has a respective cloud fraction c_i, optical depth τ_i, single-scattering albedo ω_i and asymmetry parameter g_i

[97].
The optical depth τ_i of a cloud is a measure for the amount by which radiation diminishes as it travels vertically through a cloud layer [21]. The single-scattering albedo ω_i quantifies the balance between scattering and absorption, indicating the fraction of radiation removed from an incident beam of radiation through extinction that removed by scattering [21, 52]. Lastly, the asymmetry parameter g_i is a measure for the difference in backward and forward scattering. For Rayleigh scattering, e.g., $g_i = 0$ while $g_i > 0$ for Mie scattering [52].
The variables used to calculate the interaction of a liquid cloud with LW and SW radiation are the LWP Σ_l and two parameters related to the droplet size distribution, μ and λ (see [98, Eq. (19)], [99]).
The number n of droplets with diameter D is gamma distributed:

$$n(D) = \frac{\lambda^{\mu+1}}{\Gamma(\mu+1)} D^{\mu} \exp(-\lambda D) . \tag{3.1}$$

The optical properties of a liquid cloud are found in a lookup table regarding μ and $1/\lambda$ and are then used to calculate the size-integrated mass-specific extinction coefficient k_{ext}, the single-scattering albedo ω and asymmetry parameter g as well as the mass-specific absorption in the LW spectrum [97].

To determine the optical properties of ice clouds, the model takes into account the in-cloud IWP Σ_i, the cloud fraction of ice clouds and the effective diameter d_i of the ice particles within the cloud. The effective diameter of ice particles is calculated as follows [97]:

$$d_i = \frac{3\rho}{\lambda_i \rho_i}, \tag{3.2}$$

where λ_i is the slope parameter corresponding to the gamma distribution of ice particle sizes, $\rho = 500\,\mathrm{kg/m^3}$ is the bulk density for cloud ice and $\rho_i = 917\,\mathrm{kg/m^3}$ is the bulk density of pure ice. As for the crystal shapes, the model assumes 50 % quasi-spherical, 30 % irregular ice particles and 20 % bullet rosettes [97]. Physically, d_i represents the theoretical distance a photon can travel through a particle without experiencing internal reflections or refraction. d_i is a measure for all particles of the size distribution [100]. Ice cloud optical properties are calculated using the modified anomalous diffraction approximation, a simplification of Mie theory [100].

Optical properties of snow clouds are calculated similarly to those of ice clouds using optical properties from a lookup table [97].

The combined cloud parameters used for the cloud-radiation interaction are

then calculated as follows [97]:

$$C = \max\{C_i\}, \tag{3.3}$$

$$\tau = \sum_{i \in \text{type}} \tau_i \frac{C_i}{C}, \tag{3.4}$$

$$\omega = \sum_{i \in \text{type}} \tau_i \omega_i \frac{C_i}{\tau C}, \tag{3.5}$$

$$g = \sum_{i \in \text{type}} \tau_i \omega_i g_i \frac{C_i}{\tau \omega C}. \tag{3.6}$$

These are then passed on to the radiative transfer model RRTMG [101].

3.2 Experiments

The cloud parameters applied in this work are the droplet size distribution in liquid phase clouds, the size of the ice crystals in ice phase clouds, the liquid and ice water contents of the clouds as well as the cloud fraction, namely λ and μ of the droplet size distribution in liquid phase clouds, the effective radiative diameter of ice crystals d_i in ice phase clouds,the in-cloud LWP and IWPs Σ_l and Σ_i in liquid and ice phase clouds respectively as well as the overall cloud fraction c_f. These are the parameters determining the radiation scheme in the CESM.
The Arctic is defined as the region above a latitude of 70°.
First, individual runs for each cloud parameter with pre-industrial CO_2 levels are performed with an applied forcing by modifying one microphysical parameter in Arctic clouds. This way, the influence each cloud parameter on the Arctic climate can be studied. The modifications in cloud parameters are introduced in year 41 of each run to ensure the model is already in equilibrium before introducing the changes. The experiments will be run for 70 years in total and the last 20 years (51-70) of each run will be analysed, if not indicated otherwise. For the runs with pre-industrial CO_2 levels, the restart files are obtained from a previous SOM run conducted by the institute to save time and memory.
All modifications made are only relevant to the radiation model and do not interact with other components of the CESM.
Then, the changes of those cloud parameters due to climate change will be investigated by performing two experiments with the climate model, one with pre-industrial (1850) atmospheric CO_2 content (284.7 ppm) and one with a forcing by doubling the atmospheric CO_2 content (569.4 ppm). The latter value is chosen as an estimate for the increase in CO_2 levels due to anthropogenic climate change. It is still higher than the actual value today, but a reasonable value for the future as CO_2 levels have been constantly increasing during the

past decades [102].
Monthly averages of the parameters in each run are considered to quantify how they change in the Arctic due to the forcing.
In the following, the conducted experiments are briefly described, with an overview provided in Table 3.1, detailing experiment names and modifications. Seasonal variations are considered in certain experiments, with winter defined as January, February, and March, and summer as July, August, and September. These experiments are denoted with `_winter` or `_summer` after their run name.

Run name	Σ_l	μ	Λ	Σ_i	d_i	c_f
`ctrl`						
`2CO2`						
`+liq`	$+0.2\Sigma_i$			0.8		
`no_liq`	0			$+\Sigma_l$		
`+ice`	0.8			$+0.2\Sigma_l$		
`no_ice`	$+\Sigma_i$			0		
`2liq`	2					
`+pgam`		1.5				
`+lamc`			1.5			
`+dei`					1.5	
`-cld`						0.5
`no_cld`						0
`cld_force`	$=\Sigma_l^{2CO2}$	$=\mu^{2CO2}$	$=\lambda^{2CO2}$	$=\Sigma_i^{2CO2}$	$=d_i^{2CO2}$	$=c_f^{2CO2}$

Table 3.1: Overview over all the conducted experiments. Numbers indicate factors by which a certain parameter is multiplied. "+" preceding a number indicates an amount added to the parameter, while "=" preceding a number indicates specific values to which parameters are set. Except for `2CO2`, all experiments are run with pre-industrial CO_2 levels (284.7 ppm), while `2CO2` is run with doubled CO_2 levels (569.4 ppm).

3.2.1 Control runs

The control run without any forcings will be referred to as `ctrl`. The experiment with a forcing due to the doubling of pre-industrial CO_2 levels is called `2CO2`.

3.2.2 Cloud fraction

To investigate the general influence of clouds on Arctic climate, the cloud fraction c_f is modified.

During the experiment `-cld`, the cloud cover fraction is reduced by the factor 0.5, hence half of the clouds in the Arctic are removed. This is implemented during all of the months as well as only during summer or winter in the experiments `-cld_summer` and `-cld_winter`, respectively.
The experiment `no_cloud` does not consider clouds in the Arctic at all. Here, c_f in the Arctic is set to 0.

3.2.3 Liquid and ice water path

To examine the influence of cloud phase on Arctic climate, the LWP and IWP are modified.
In the experiment `+liq`, an increase in liquid cloud water is implemented by adding 20% of the in-cloud IWP Σ_i to the in-cloud LWP Σ_l. At the same time, Σ_i is reduced by 20% which results in a change in ratio of liquid and ice cloud water, but leaves the total amount of water in the clouds unchanged. This is equivalent to melting 20% of the ice crystals found in Arctic clouds.
Similarly, in the `+ice` experiment, 20% of Σ_l is added to Σ_i and the same amount is subtracted from Σ_l. Illustratively, 20% of the liquid cloud droplets get frozen in Arctic clouds. Again, the overall water content in the Arctic clouds stays the same.
During the experiment `2liq`, a forcing is introduced by doubling Σ_l. Variations of this experiment include `2liq_summer` and `2liq_winter` where the doubling of Σ_l is implemented in only summer and winter, respectively.
Additionally, experiments with just liquid water and just ice clouds are conducted. They are called `no_ice` and `no_liq`, respectively. During the former, all ice in Arctic clouds is transformed into water. During the latter, all liquid water is turned into ice crystals.

3.2.4 Size distribution parameters

To investigate the effect of droplet and ice crystal size distributions, the parameters regarding those are modified.
In the experiments `+pgam` and `+lamc`, μ and λ of the liquid droplet size distribution are increased by the factor 1.5, respectively. The increase of μ leads to the distribution being wider and the maximum is shifted towards the right if λ is kept constant. An increase in λ without changing μ, on the other hand, leads to a narrower size distribution and the maximum is shifted towards the left. This is illustrated in Fig. 3.1.
In the experiment `+dei`, the effective radiative diameter of ice (d_i) is increased by the factor 1.5, hence enlarging the ice crystals.

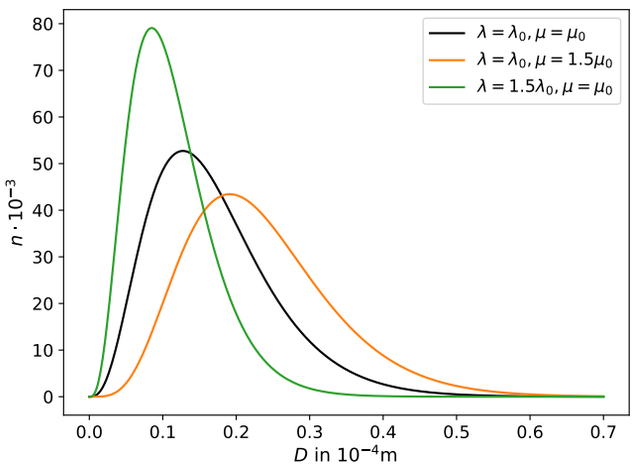

Figure 3.1: Droplet size distributions for different λ and μ, where $\lambda_0 = 0.235 \cdot 10^{-6}\ {}^{1}/_{\mathrm{m}}$ and $\mu_0 = 3$ were chosen arbitrarily.

3.2.5 Doubling of CO_2

Lastly, I use the `2C02` and `ctrl` experiments to determine the changes of clouds in an environment with double the amount of CO_2 in the atmosphere. Using 30 years (years 51-80) of both experiments, I calculate the difference of the parameters in each month averaged over those 30 years. The difference is calculated at each grid point and each pressure level, giving a 3D mask which is then added to all microphysical cloud parameters and the cloud fraction in an experiment with preindustrial CO_2 levels. I hereby make sure to keep all the parameters within their limits, e.g. ensuring that $0 < c_f < 1$ or $\Sigma_{i,l} > 0$. This way, I can conduct an experiment studying the first order changes introduced by clouds changing due to climate change, corresponding to a doubling of the atmospheric CO_2. The changes implemented here do not only concern a single microphysical property but rather a combination of all of them.
This experiment is called `cld_force`.

3.3 Analysis

Climate variables of interest include the reference height temperature averaged over the Arctic, sea ice extent, and LW and SW fluxes used to estimate the clouds' greenhouse and albedo effects. Monthly output is obtained for each variable.
The sea ice extent is defined similarly to how the NSIDC (National Snow & Ice Data Center) does as the area that is covered by at least 15% of sea ice [103].

Hence, every grid cell with a sea ice fraction > 0.15 contributes to the sea ice extent.
The control run `ctrl` will act as a reference for comparison.

3.3.1 Greenhouse effect

Using the LW fluxes, the clouds' greenhouse effect G_C can be calculated. The combined greenhouse effect of clouds, atmosphere and aerosols G can be defined as the difference in upwelling LW flux at the surface ($F_{\mathrm{LW}}^{\mathrm{U,S}}$) and at the top of the atmosphere ($F_{\mathrm{LW}}^{\mathrm{U,T}}$) [104]:

$$G = F_{\mathrm{LW}}^{\mathrm{U,S}} - F_{\mathrm{LW}}^{\mathrm{U,T}}. \tag{3.7}$$

The CESM only outputs values for the net and downwelling LW flux at the surface ($F_{\mathrm{LW}}^{\mathrm{N,S}}$ and $F_{\mathrm{LW}}^{\mathrm{D,S}}$, respectively), which can be combined to give $F_{\mathrm{LW}}^{\mathrm{U,S}}$:

$$F_{\mathrm{LW}}^{\mathrm{U,S}} = F_{\mathrm{LW}}^{\mathrm{N,S}} - F_{\mathrm{LW}}^{\mathrm{D,S}}, \tag{3.8}$$

using that the net LW flux is directed upwards. Thus, G can be calculated as follows:

$$G = F_{\mathrm{LW}}^{\mathrm{N,S}} - F_{\mathrm{LW}}^{\mathrm{D,S}} - F_{\mathrm{LW}}^{\mathrm{U,T}}. \tag{3.9}$$

To find G_C, the difference between the clear-sky, hence cloud-free, greenhouse effect G_{CS} and the combined greenhouse effect G is calculated. As the $F_{\mathrm{LW}}^{\mathrm{U,S}}$ is dependent on the surface temperature, it is identical in the clear-sky and cloudy scenario. Then, G_C can be written as:

$$G_C = F_{\mathrm{LW}}^{\mathrm{U,T}} - F_{\mathrm{LW}}^{\mathrm{U,T,CS}}. \tag{3.10}$$

G_C can only be seen as a measure for the cloud greenhouse effect under certain circumstances. The emissivity of a cloud changes with, e.g., temperature [21, 53]. Hence, the same cloud would yield different G_C values in a, e.g., colder environment.

3.3.2 Albedo

To find a measure for the cloud albedo effect A, the downwelling SW flux at the surface is considered in the cloudy-sky as well as the clear-sky version of the model output ($F_{\mathrm{SW}}^{\mathrm{D,S}}$ and $F_{\mathrm{SW}}^{\mathrm{D,S,CS}}$, respectively). A can then be defined as the amount of radiation removed of the downwelling beam by the clouds:

$$A = F_{\mathrm{SW}}^{\mathrm{D,S}} - F_{\mathrm{SW}}^{\mathrm{D,S,CS}}. \tag{3.11}$$

3.3.3 Calculation of mean control values

The mean Arctic near-surface temperature, the mean sea ice extent as well as the mean LW and SW fluxes for the control run are computed using a MC simulation. To rule out natural variability and long-term patterns in the climate, during each iteration of the MC simulation, 20 random years between the years 41 to 80 will be picked.

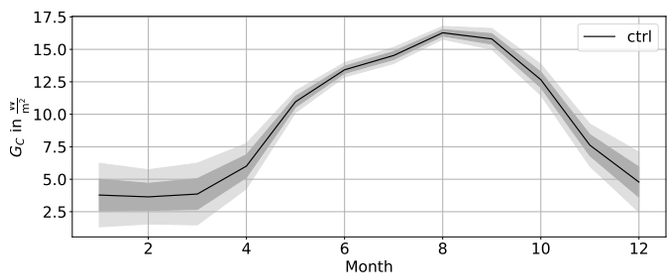

Figure 3.2: Monthly mean cloud greenhouse effect in the Arcitc with 1- and 2-σ ranges (dark grey and light grey, respectively), derived by using a MC simulation.

Each year can only be picked one time during each iteration. Then, the 20-year-mean of each climate parameter is calculated. This step is repeated 5000 times. Lastly, the mean and standard deviation of these values is calculated.
As an example, the monthly means of the Arctic cloud greenhouse effect derived by the MC simulation are shown in Fig. 3.2. Here, the black line shows the mean value of the MC simulation, the dark grey area corresponds to the 1-σ-range and the the light grey area corresponds to the 2-σ-range, with σ being the standard deviation. This means, assuming a normal distribution, that about 95.4 % of the simulated 20-year means are within that range.

4

Sensitivity Studies

4.1 Cloud fraction

First, the general influence of clouds in the Arctic is studied by changing the cloud fraction in the Arctic. Removing all clouds in the Arctic by decreasing the cloud fraction c_f to 0, does not significantly change the mean Arctic temperature compared to the control run when considering the reference height temperature averaged over the Arctic and the last 20 years, years 51-70, of the simulation (`no_cld`, see Tab. 4.1). On first sight, this is not consistent with literature suggesting an overall warming effects of clouds on Arctic temperature [80, 87, 88, 89].

Run name	`ctrl`	`no_cld`	`-cld`	`-cld_summer`	`-cld_winter`
$\bar{T}$ in °C	-15.5 ± 0.2	-15.4	-18.7	-15.7	-16.2

Table 4.1: Mean temperature $\bar{T}$ in °C in the Arctic, averaged over the years 51-70 of each `-cld` experiment. The value for `ctrl` was derived by a MC simulation.

However, considering the monthly means of the reference height temperature in the Arctic over the mentioned 20-year period, a significant warming can be observed in summer and autumn, while a significant cooling can be observed in winter and spring (see Fig. 4.1). In June and December, almost no difference in mean Arctic reference height temperature can be found. In June, this corresponds to the start of the sea ice melt (see Fig. 4.2).

The largest warming can typically be observed in September and October. Here, it is more than 3 °C warmer in `no_cld` compared to `ctrl`. Additionally, during July, August and November, a warming greater than 1 °C is observed. During winter and spring, the absence of clouds has a large cooling effect, yielding a difference between the mean monthly temperatures of `ctrl` and `no_cld` greater than 2 °C in March, April and May (see Fig. 4.1). These findings are also consistent with literature, as clouds in the Arctic have a warming effect on the surface temperature except for in summer [80, 87].

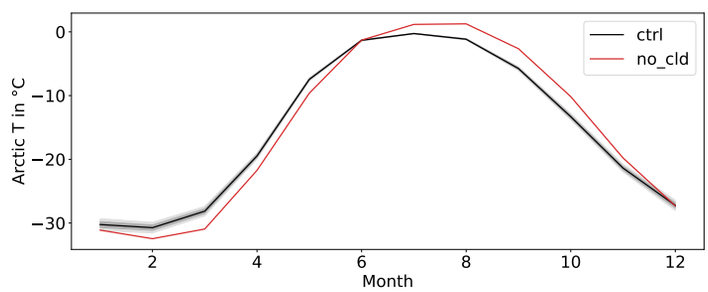

(a) Monthly means

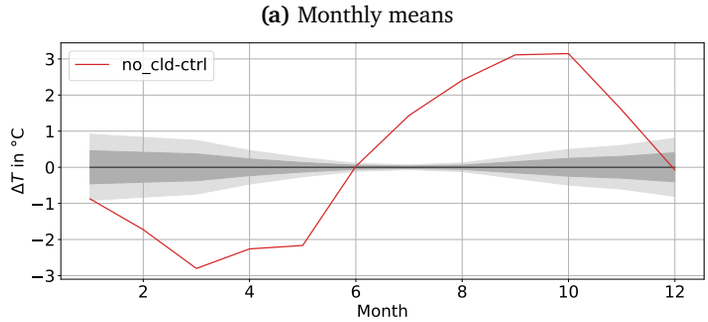

(b) Differences

Figure 4.1: 20-year Monthly means of the reference height temperature and difference between these monthly means averaged over the Arctic of the `no_cld` (red, over the years 51-70) experiment and `ctrl` (black, derived by a MC simulation) experiment. The shaded areas show the 1- and 2-σ ranges of `ctrl` (dark grey and light grey, respectively)

It can also be seen that the mean Arctic temperature stays below 0 °C at any time in `ctrl`, but is above 0 °C in July (1.2 °C) and August (1.3 °C) in `no_cld`. Higher temperatures in summer promote sea ice melt. Hence, the sea ice minimum in September is considerably lower in `no_cld` compared to `ctrl`. During the winter months though, there is little to no deviation in sea ice extent (see Fig. 4.2). Generally colder temperatures during the freezing season can potentially compensate the loss of sea ice, at least in terms of area. The thickness of the ice is not considered here, but one could speculate thinner and less multi-year ice `no_cld`.

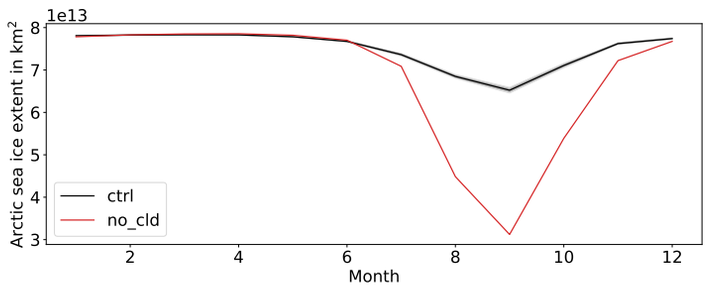

Figure 4.2: Monthly means averaged over the years 51-70 of Arctic sea ice extent of the `no_cld` (red) and `ctrl` (black) experiments.

An absence of clouds leads to incoming solar radiation not being reflected or absorbed by them. Hence, especially in summer, more solar radiation is reaching the surface (see Fig. 4.3). The large peak in summer can be explained with the fact that more sunlight is generally reaching the Arctic during the summer months. Additionally, a reduced surface albedo due to a smaller sea ice extent leads to less SW radiation being reflected. Since the net SW flux is directed downwards, it increases here.

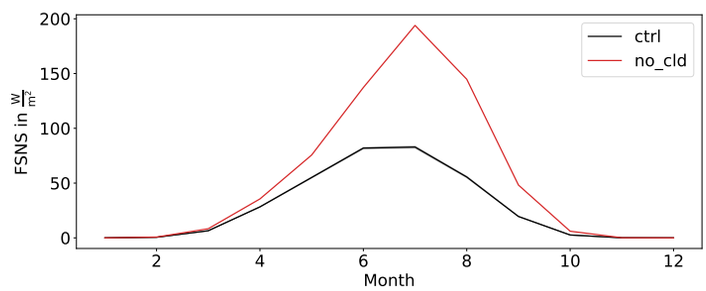

Figure 4.3: 20-year averages (years 51-70) of the monthly means of the FSNS of the `no_cld` (red) and `ctrl` (black , derived by a MC simulation) experiments. The net SW flux is directed downwards.

When there are no clouds present, there is also no greenhouse effect induced by them (see Fig. 4.5a). Hence, the downwelling LW flux at the surface (see Fig. 4.4a) is smaller during `no_cld` than during `ctrl`. The upwards directed net LW flux, though, is greater during `no_cld` than during `ctrl` during all months (see Fig. 4.4b). This can also be explained by the absence of the clouds' greenhouse effect not trapping the LW radiation but rather letting more of the upwelling LW radiation escape. Additionally, during summer, when the temperature is higher during `no_cld`, both the atmosphere and the surface emit more LW radiation due to the warmer temperatures.
Even though the clouds' greenhouse effect G_C in `ctrl` is largest in summer,

and hence the difference in G_C is largest in summer (see Fig. 4.5b), summer temperatures are generally warmer during `no_cloud`. This indicates that in summer, when sea ice is at its lowest, the clouds' albedo effect outweighs their greenhouse effect.

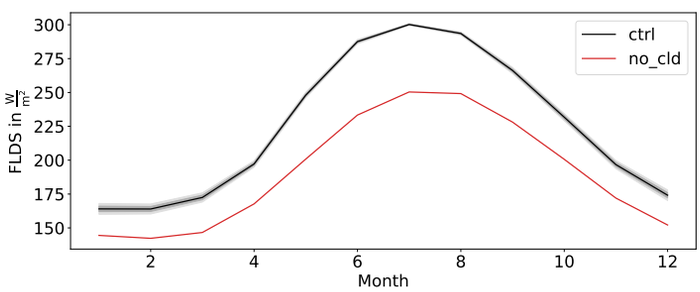

(a) downwelling LW flux at surface (FLDS) in the Arctic.

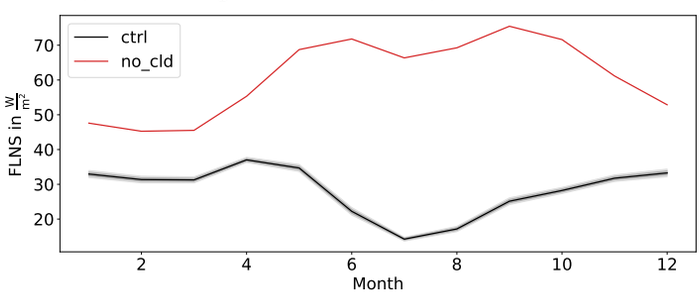

(b) FLNS in the Arctic.

Figure 4.4: 20-year averages of the monthly means of the Arctic LW fluxes at the surface of the `no_cld` (red, over the years 51-70) and `ctrl` (black, derived by a MC simulation) experiments. The net LW flux is directed upwards, the downwelling LW flux is directed downwards.

For further insights into the radiation fluxes and spatial resolution of reference height temperature in the Arctic concerning the `no_cld` scenario, please refer to the appendix (see Ch. B.1).

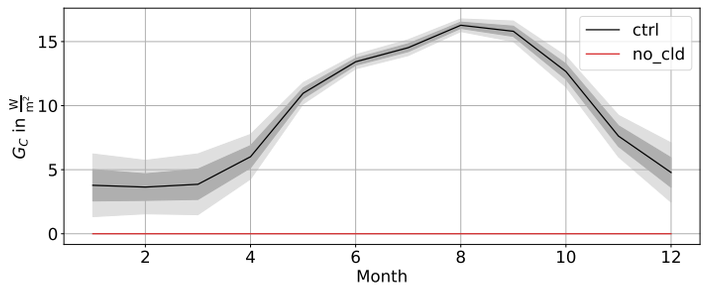

(a) Monthly means

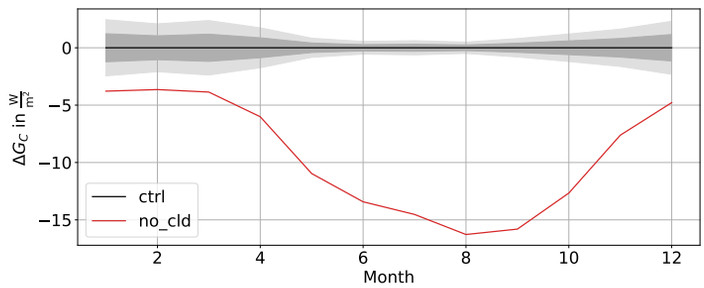

(b) Differences

Figure 4.5: 20-year averages of the monthly means of the Arctic cloud greenhouse effect of the `no_cld` (red, over the years 51-70) and `ctrl` (black, derived by a MC simulation) experiments.

Now, the `-cld` experiments are considered. Decreasing the Arctic cloud fraction c_f by 50 % in all months leads to a decrease in mean Arctic reference height temperature averaged over the years 51-70 of each simulation (see Tab. 4.1). The `-cld` experiment yields the lowest temperature, about 3 °C colder than during `ctrl`. The cooling observed during `-cld_summer` is insignificant compared to `ctrl` and within its 1-σ range.

When considering the monthly 20-year mean temperature (see Fig. 4.6), it can be seen that `-cld` yields lower average monthly values than `ctrl` in all months. The largest differences between these two experiments can be found in autumn and early winter, with temperature deviations up to 6 °C. The colder temperatures, especially in the freezing season, cause a larger sea ice extent and the sea ice to potentially grow thicker, and colder temperatures in the melting season lead to less melt and a larger sea ice extent during the minimum in September (see Fig. 4.7). A larger sea ice extent and thicker sea ice would inhibit energy fluxes between the ocean and the atmosphere, hence cool the Arctic climate, especially during winter. Less clouds in winter would also contribute to a colder climate, mainly due to a reduction in greenhouse effect (see Fig. 4.9).

In summer, on the other hand, less clouds should have a warming effect on the

Arctic which can not be observed here. The temperature differences between `-cld` and `ctrl` are smallest in summer, but this is mostly due to sea ice melt locking reference height temperatures at around 0 °C. This, the significantly colder temperatures during winter as well as the greater sea ice extent (and possible greater sea ice thickness) perhaps damp the warming effect the lack of clouds should have in summer.

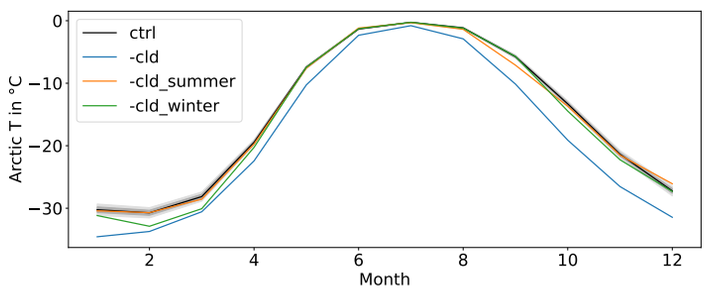

(a) Monthly means of the reference height temperature averaged over the Arctic of the `-cld` experiments.

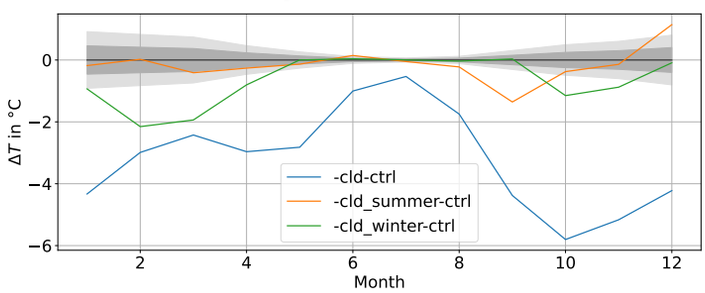

(b) Difference between `-cld` and `ctrl` monthly means of the reference height temperature Arctic average.

Figure 4.6: Monthly means of the reference height temperature and difference between these monthly means averaged over the Arctic and years 51-70 of the `-cld` experiments. The 20-year monthly means of `ctrl` were derived using a MC simulation.

Looking at the net SW flux at the surface (see Fig. 4.8a), larger net SW flux at the surface can be found for `-cld` compared to `ctrl`. The increase can be explained by the fact that less clouds lead to a lower albedo of the atmosphere and thus, less reflected SW radiation. Hence, more SW radiation is reaching the surface (see Fig. 4.8).
At the same time, a decrease in cloud greenhouse effect can be observed (see Fig. 4.9), enhancing the cooling. When additionally considering `-cld_summer`, it can be seen that the greenhouse effect attains a similar level compared to `-cld` during the summer months, when the forcing is applied. The slightly higher greenhouse effect during `-cld_summer` can be explained with the higher

temperatures in the corresponding months (see Fig. 4.6) compared to `-cld` as the greenhouse effect of clouds is temperature dependent [53]. Additionally, the lower amount of sea ice during the summer time (see Fig. 4.7) could lead to more clouds in the atmosphere due to the cloud-ice feedback [24, 25, 26]. The higher net SW flux during `-cld_summer` in summer can be explained with a lower surface albedo due to significantly less sea ice compared to `-cld`.

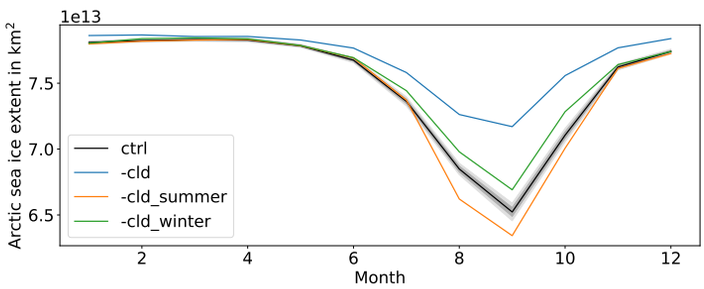

Figure 4.7: 20-year averages (years 51-70) of the monthly means of Arctic sea ice extent of the `-cld` experiments. The values for `ctrl` were derived using a MC simulation.

During the analysed 20-year period, the average near-surface Arctic temperature decreases slightly by about 0.2 °C when the c_f is reduced by 50 % during the summer months. This change is within the 1-σ range of `ctrl`. When c_f is reduced during the winter months, on the other hand, the the average near-surface Arctic temperature decreases by about 0.7 °C. The latter aligns well with theoretical expectations, as reducing the cloud cover removes part of the warming effect clouds have during winter (`-cld_winter`, see Ch. 2.4). Since the temperature change during `-cld_summer` is insignificantly small, it can be assumed that removing clouds during summer does not have an impact on Arctic reference height temperatures.
When looking at the average monthly mean Arctic temperatures (see Fig. 4.7), though, it can be seen that the greatest warming in `-cld_summer` does not occur in summer, as one could expect [87]), but in December. On the other hand, in September, a significant cooling can be observed. Here, temperatures are more than 1 °C higher compared to `ctrl`. During the other months, no significant deviation from `ctrl` can be observed. The colder September could be explained with the fact that there is not as much incoming solar radiation in September as there is e.g. in July and August (see Fig. 4.8a). Hence, one could speculate the warming effect of Arctic clouds to be dominating during this month. When reducing the cloud fraction, this warming effect gets smaller and it gets colder.
When considering the greenhouse effect (see Fig. 4.9), it can be seen that the greenhouse effect is smaller in `-cld_summer` during the months when the

forcing is applied compared to `ctrl`. This is a consequence of the reduced cloud cover.
During `-cld_summer`, there is less sea ice, mainly during summer (see Fig. 4.7). This can be explained with the reduced cloud cover in summer, letting more SW radiation reach the surface and melt the ice. This does not become apparent in the temperature difference as the phase transition from solid ice to liquid water locks temperatures at around 0 °C.

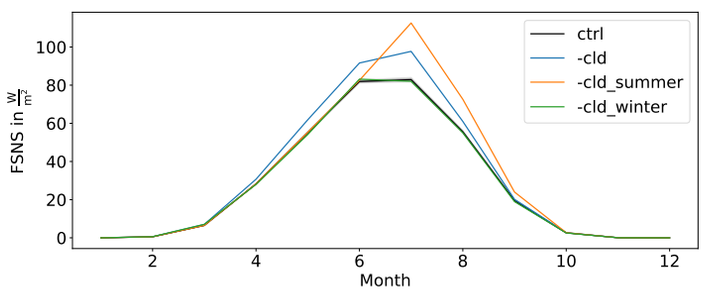

(a) Monthly means of the FSNS

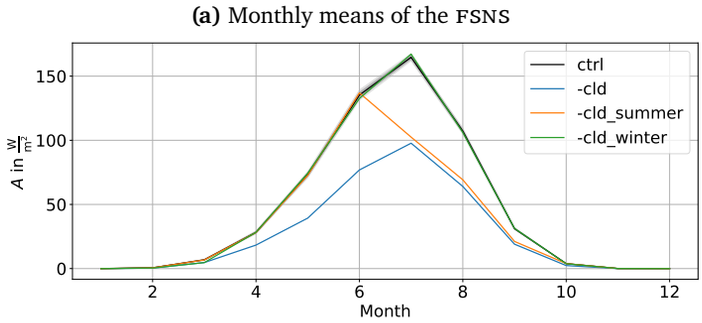

(b) Monthly means of the Arctic cloud albedo effect

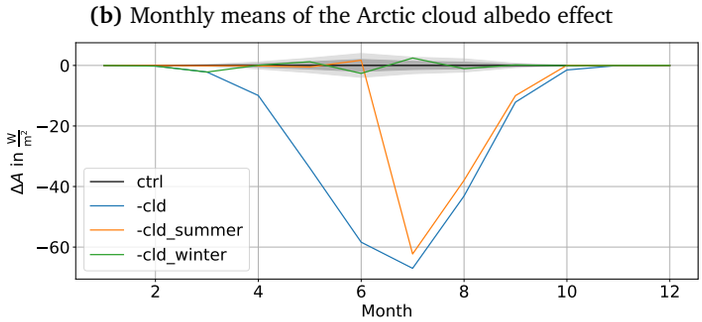

(c) Differences between the monthly means of the Arctic cloud albedo effect

Figure 4.8: 20-year averages of the monthly means of the FSNS, the Arctic cloud albedo effect A of the `-cld` (over the years 51-70) and `ctrl` (derived by a MC simulation) experiments and the difference between the Arctic cloud albedo effect monthly means. The net SW flux is directed downwards.

The higher temperatures in December could be explained by thinner sea ice allowing more heat to be exchanged between the warm ocean and cold atmosphere. However, this explanation does not account for the minor cooling trends observed in November and January. Therefore, the warming trend observed specifically in December may stem from alternative factors not directly linked to cloud cover, requiring additional research for a comprehensive understanding.

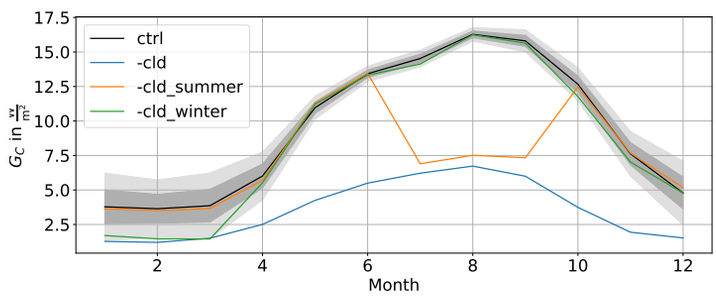

(a) Monthly means

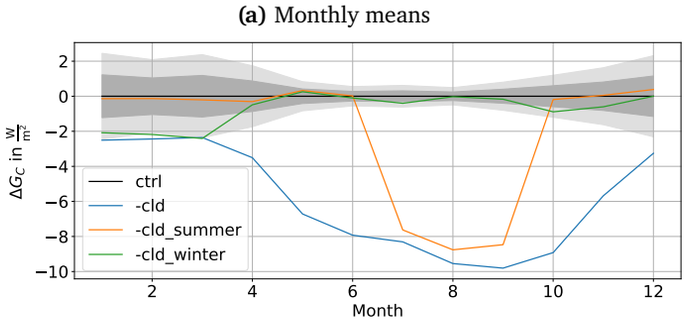

(b) Differences

Figure 4.9: 20-year averages of the monthly means of the Arctic cloud greenhouse effect of the `-cld` experiments (over the years 51-70) and `ctrl` (derived by a MC simulation) experiments.

During `-cld_winter`, the maximal temperature differences occur in February and March when it is about 2 °C colder than during `ctrl` (see Fig. 4.6b). These colder temperatures can be explained by the reduced greenhouse effect due to the reduced cloud cover in winter (see Fig. 4.9). During the January, February and March, the months in which the forcing is applied, a lower greenhouse effect can be observed (see Fig. 4.9) due to the reduction in cloud cover. Since it is generally colder or equally warm during the other months compared to `ctrl`, sea ice can grow thicker and melt slower during the melting season with respect to extent, resulting in a greater sea ice extent during the minimum in September (see Fig. 4.7). The larger amount of sea ice then acts as an insulator between the ocean and the atmosphere, leading to cooler temperatures during

late autumn and winter.
Changing c_f during the first three months of year does not have a significant influence on the net SW flux at the surface and the cloud albedo effect (see Fig. 4.8). This is due to the small amount of sunlight reaching the Arctic during that time of year.
Overall, reducing c_f in winter has a larger impact on temperatures by cooling and a resulting positive impact on sea ice, while reducing c_f in summer has little influence on temperatures, but a negative impact on sea ice.

4.2 Liquid and ice water path

As a next step, the amount of liquid water in Arctic clouds is doubled. Hereby, the total amount of Arctic cloud condensate increases as well (see Figs. B.12-B.14). If this forcing is applied in all months, a cooling of about 2 °C can be observed (see Tab. 4.2, `2liq`). At a first glance, this seems to contradict literature and the previous experiments where clouds were found to have an overall warming effect on the Arctic, as the warming effect during spring, autumn and winter is outweighing the cooling effect during summer [80, 87, 88, 89] and an increase in optical depth due to increase in liquid water path (see Eq. 2.28). Thus, one would expect an increase in cloud condensate to warm the Arctic.

Run name	`ctrl`	`2liq`	`2liq_summer`	`2liq_winter`
$\bar{T}$ in °C	-15.5 ± 0.2	-17.4	-17.1	-15.7

Table 4.2: Mean temperature $\bar{T}$ in °C in the Arctic, averaged over the years 51-55 of the `2liq` experiments.

It can be seen, though, that during `2liq`, the mean Arctic reference height temperature averaged over the years 51-70 of the simulation is lower in all months compared to `ctrl` (see Fig. 4.10). The largest difference to `ctrl` can be found in October when it is about 4 °C colder.
Colder temperatures lead to a greater sea ice extent, a slower sea ice melt (see Fig. 4.11) and is probably probably resulting in thicker sea ice. The larger sea ice extent inhibits energy exchanges between the ocean and the atmosphere. This has a large effect in autumn when temperatures are decreasing again and the ice is beginning to freeze. This can explain the peak in temperature difference between `2liq` and `ctrl` in October.
During `2liq`, the sea ice extent is on average greater in October than in all other months during `ctrl`. In November and December, the sea ice extent during `ctrl` has increased, less energy is going from the ocean to the atmosphere and the difference in reference height temperature is decreasing.

An explanation for an initial increase in sea ice during `2liq`, which is then part of a feedback loop by cooling the atmosphere, can be found when considering the SW fluxes (see Fig. 4.12). During the months when sunlight is reaching the Arctic, a decrease in net SW flux at the surface can be observed. This is due to a significantly increased cloud albedo effect by increasing the LWP [64, 65] (see Figs. 4.12b and 4.12c). Therefore, during the melting season, less sunlight is reaching, warming and melting the ice.

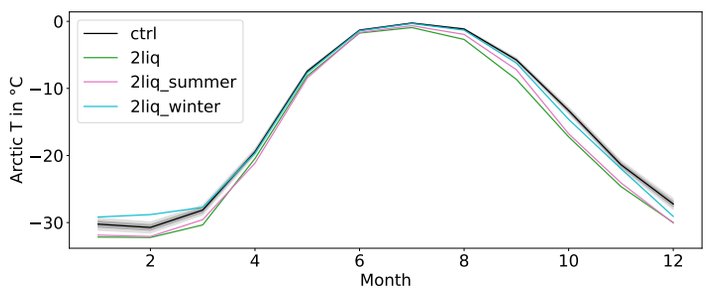

(a) Monthly means

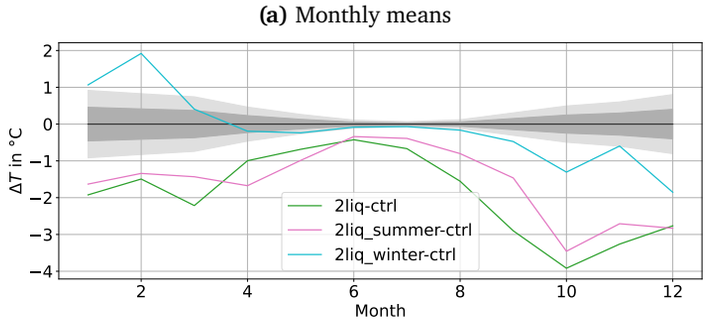

(b) Differences

Figure 4.10: Monthly means of the reference height temperature and difference between these monthly means averaged over the Arctic and years 51-70 of the `2liq` experiments. The 20-year monthly means of `ctrl` were derived using a MC simulation.

An increase in cloud condensate is also associated with an increased greenhouse effect [52, 64, 69]. During `2liq`, an increase in greenhouse effect is only observed in spring and summer (see Fig. 4.13). This can be explained by, for one, the amount of liquid water that is added. Generally, there is more liquid water in clouds during summer compared to the winter season (see Fig. B.12). Thus, doubling the liquid water in a given month adds a larger amount of liquid cloud condensate in summer compared to in winter. Therefore, the increase of greenhouse effect is larger in summer than in winter in `2liq`. Additionally, the greenhouse effect illustrated in Fig. 4.13 is only a measure of greenhouse effect in that exact environment. Since absorption and emissivity of the cloud

are dependent on temperature [21, 53], the greenhouse effect of `2liq` winter clouds would look different when placed, for instance, in the `ctrl` environment. Colder clouds, e.g., are radiating less than warmer clouds which explains the decrease in greenhouse effect during autumn and winter (see Fig. 4.13b). Additionally, the increase in greenhouse effect during winter and the increase in albedo effect during summer cannot simply be compared because the amount of added liquid cloud condensate is not similar. One could suspect adding an equal amount of liquid cloud condensate during winter and summer to give a more balanced result. To support these assumptions, the same forcing is applied only during the summer months (`2liq_summer`) and only during the winter months (`2liq_winter`). During `2liq_summer`, a decrease of the Arctic mean reference height temperature can be found during the years 51-70. Here, the average temperature decreases by about 1.5 °C (see Tab. 4.2). The reasoning here is similar to `2liq`: a higher cloud albedo in summer (see Fig. 4.12) inhibits sea ice melt, and a greater sea ice extent (see Fig. 4.11) leads to a higher surface albedo as well as a better insulation between the warmer ocean and the colder atmosphere. All this leads to a general decrease in temperature. The increased greenhouse effect in summer (see Fig. 4.13) is outweighed by the albedo effect. The peak in temperature difference in October during `2liq_summer` (see Fig. 4.10b) can also be attributed to the same underlying factors present during `2liq`.

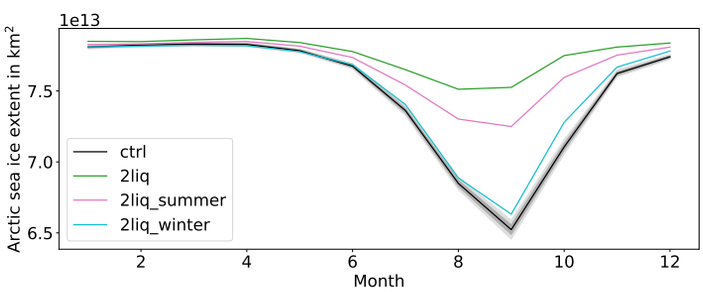

Figure 4.11: 20-year averages (years 51-70) of the monthly means of Arctic sea ice extent of the `2liq` experiments. The values for `ctrl` were derived using a MC simulation.

During `2liq_winter`, a insignificant decrease of 0.2 °C can be observed. This change is within the 1-σ range of `ctrl`. It can be seen, though, that during the months the forcing is applied, the mean Arctic reference height temperature increases (see Fig. 4.10). This coincides with an increased greenhouse effect during that time (see Fig. 4.13). The magnitude of the difference in temperature is not as large as during `2liq` and `2liq_summer`. A reason for that is, as already mentioned, the amount of cloud liquid added to the clouds. The absolute difference between the modified and unmodified `2liq_winter` winter cloud

is not as large as that of a summer cloud during `2liq` or `2liq_summer`. The increase of liquid cloud condensate in winter does not affect the albedo effect of the Arctic cloud as there is little or no incoming sunlight to reflect (see Fig. 4.12).

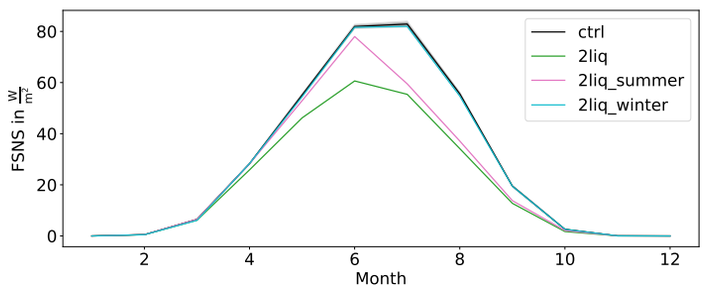

(a) Monthly means of the FSNS

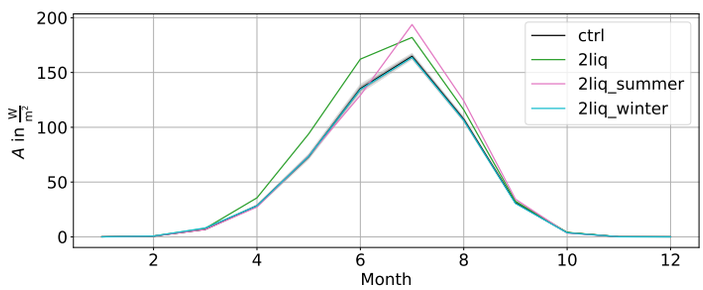

(b) Monthly means of the Arctic cloud albedo effect

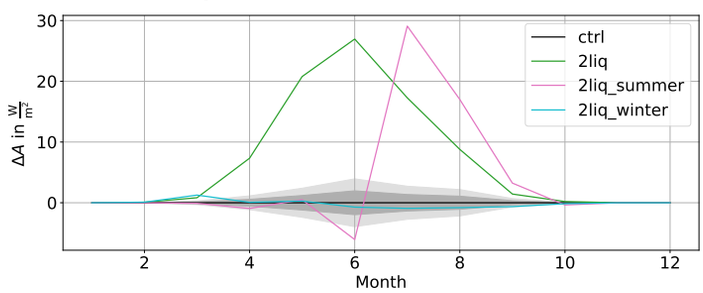

(c) Differences between the monthly means of the Arctic cloud albedo effect

Figure 4.12: 20-year averages of the monthly means of the FSNS, the Arctic cloud albedo effect A of the `2liq` (over the years 51-70) and `ctrl` (derived by a MC simulation) experiments and the difference between the Arctic cloud albedo effect monthly means. The net SW flux is directed downwards.

Still, the forcing applied in `2liq_winter` seems to cause some kind of feedback, leading to a cooling during the rest of the year (see Fig. 4.10) which then leads to a larger sea ice extent in summer and autumn. This is most likely not cloud-

related, as a decrease in cloud albedo can be observed during summer and `2liq_winter` (see Fig. 4.12c). The decrease in greenhouse effect (see Fig. 4.13) can find its origin in an overall lower temperature.

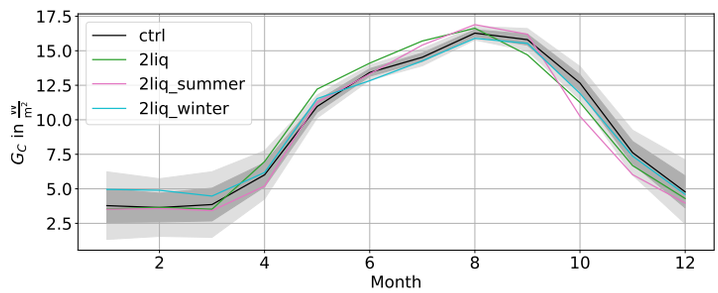

(a) Monthly means

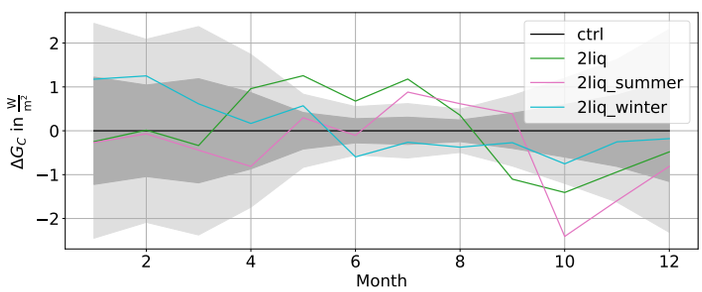

(b) Differences

Figure 4.13: 20-year averages of the monthly means of the Arctic cloud greenhouse effect of the `2iq` experiments (over the years 51-70) and `ctrl` (derived by a MC simulation) and their differences.

Next, the ratio of liquid water to ice in Arctic clouds is varied. Hereby, the total amount of water in the clouds is not changed (see Figs. B.8 - B.11).

Run name	`ctrl`	`+liq`	`no_ice`	`+ice`	`no_liq`
$\bar{T}$ in °C	-15.5 ± 0.2	-15.9	-15.3	-15.8	-18.4

Table 4.3: Mean temperature $\bar{T}$ in °C in the Arctic, averaged over the years 51-70 of each experiment changing the ratio of liquid and ice water but not the total cloud water amount. The value for `ctrl` was derived by a MC simulation.

When converting parts or all of Arctic cloud ice into liquid, the total amount of liquid water in the cloud does not change significantly (see Figs. B.9 and B.10) as liquid cloud condensate is up to two magnitudes more abundant than ice cloud condensate.
Thus, the `+liq` and `no_ice` experiments will not be discussed here. However,

for the sake of completeness, a short discussion of these experiments is included in the appendix (see Ch. B.2.1).

Lastly, the amount of frozen cloud condensate is increased while the LWP is decreased by an equal amount.
During `+ice` and `no_liq`, the 20-year mean Arctic reference height temperature is decreasing (see Tab. 4.3). When only 20 % of the liquid water droplets are frozen (`+ice`), the 20-year mean temperature decreases by about 0.3 °C which is within the 2-σ range of `ctrl`. When all liquid water is converted into ice (`no_liq`), the temperature decreases significantly by about 2.9 °C.
Considering the monthly mean temperatures averaged over the analysed time period (see Fig. 4.14), it can be seen that it is significantly colder in all months during `no_liq`. The month with the largest deviation from `ctrl` is October, when it is about 5.8 °C colder. In June and July, when the deviation from `ctrl` is smallest, it is about 1 °C colder during `no_liq`. Because of the colder temperatures throughout the year, sea ice can grow to a larger extent and potentially thicker, and it melts slower (see Fig. 4.14).

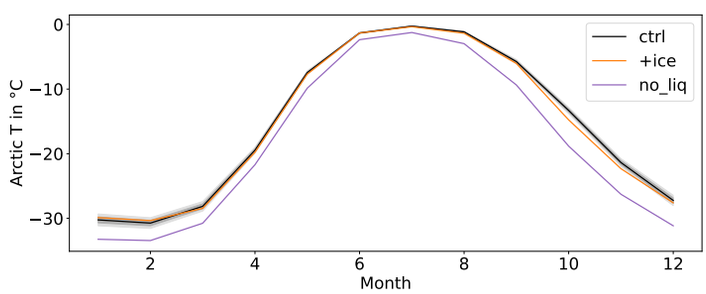

(a) Monthly means

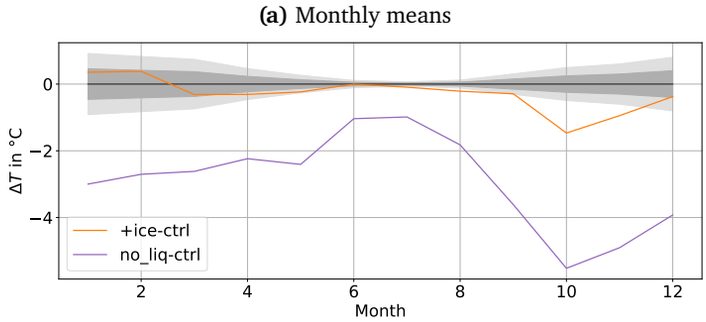

(b) Differences

Figure 4.14: Monthly means of the reference height temperature and difference between these monthly means averaged over the Arctic and years 51-70 of the experiments with decreased LWP and increased IWP. The 20-year monthly means of `ctrl` were derived using a MC simulation.

A greater sea ice extent leads to a higher surface albedo in the Arctic, leading to the net surface SW flux in the Arctic being increased in late spring while the cloud albedo effect is significantly decreased during `no_liq` (see Fig. 4.17). The decrease in albedo can be attributed to liquid cloud particles being more reflective compared to ice crystals [67].

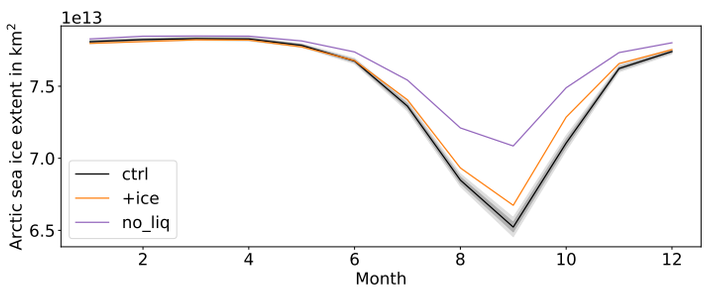

Figure 4.15: Monthly means averaged over the years 51-70 of Arctic sea ice extent of the experiments with decreased LWP and increased IWP. The 20-year monthly means of `ctrl` were derived using a MC simulation.

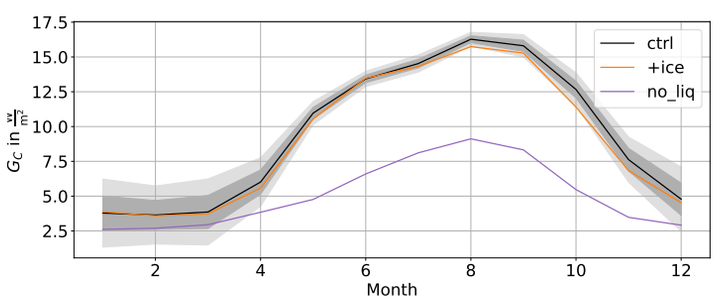

(a) Monthly means

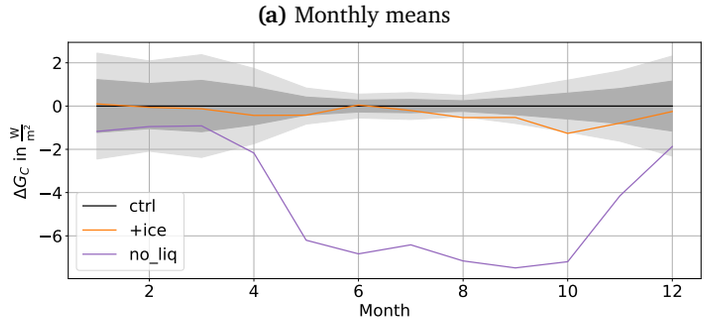

(b) Differences

Figure 4.16: 20-year averages of the monthly means of the Arctic cloud greenhouse effect of the experiments with decreased LWP and increased IWP (over the years 51-70) and `ctrl` (derived by a MC simulation) and their differences.

The main factor contributing to the cooling effect of ice clouds compared to liquid and mixed phase clouds is the greenhouse effect that is significantly decreased in the Arctic during `no_liq`, especially during spring, summer and autumn (see Fig. 4.16). The decrease in greenhouse effect originates in less cloud condensate due to colder temperatures and a larger sea ice extent (see Fig. B.11). Additionally, ice clouds have a smaller impact on LW radiation compared to liquid phase clouds [52, 64, 88].

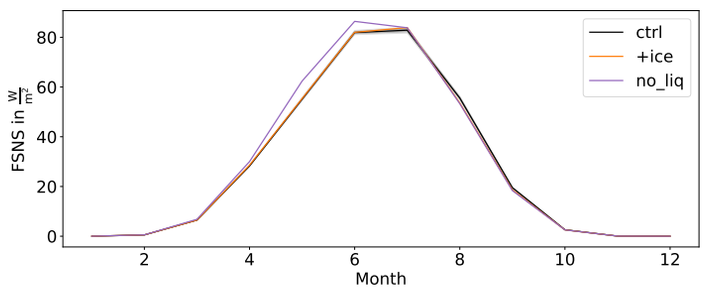

(a) Monthly means of the FSNS

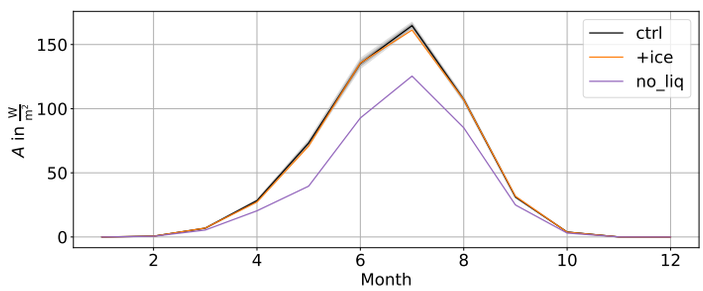

(b) Monthly means of the Arctic cloud albedo effect

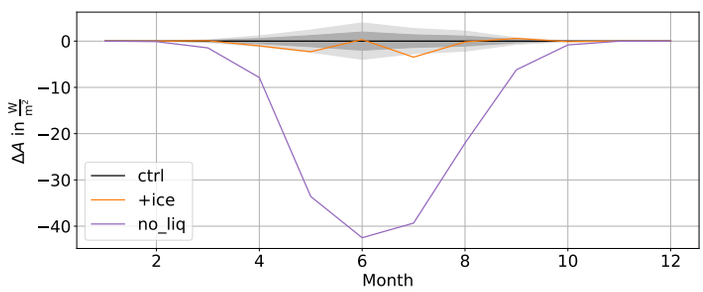

(c) Differences between the monthly means of the Arctic cloud albedo effect

Figure 4.17: 20-year averages of the monthly means of the FSNS, the Arctic cloud albedo effect A of the `ctrl` (derived by a MC simulation) and experiments with decreased LWP and increased IWP (over the years 51-70) and the difference between the Arctic cloud albedo effect monthly means. The net SW flux is directed downwards.

During `+ice`, it is only significantly colder during October (about 1.7 °C) and November (about 1 °C) compared to `ctrl` when considering the 20-year mean reference height temperatures in the Arctic. Here, no denoting change in greenhouse effect or albedo can be observed (see Figs. 4.16 and 4.17).
Additionally, in October, a slight decrease in cloud condensate can be found, but no significant change in combined cloud condensate is observed during the other months (see Fig. B.8). This could be explained with the cloud-ice feedback. Due to the slightly colder temperatures between 0 to 0.5 °C throughout the year, there is a greater sea ice extent during summer and autumn (see Fig. 4.15) which could lead less cloud condensate in the atmosphere. Compared to `no_liq`, this effect is not as significant mainly because the difference in sea ice extent between this experiment and `ctrl` is not as substantial.

All figures regarding the liquid and ice water content of the experiments discussed in this section can be found in the appendix (see Ch. B.2.2). To conclude this set of experiments, it can be seen that the ratio of liquid and ice cloud condensate does play a big role in the interaction with radiation, both LW and SW. Especially the liquid cloud condensate is important here. An increase in liquid cloud condensate in summer cools the Arctic and has a positive effect on sea ice extent. When eliminating the liquid water, temperatures drop especially in winter. When eliminating the ice, no significant changes can be observed.

4.3 Size distribution parameters

Next, the sensitivity of the climate regarding the size distribution parameters is investigated.

Run name	`ctrl`	`+dei`	`+pgam`	`+lamc`
$\bar{T}$ in °C	-15.5 ± 0.2	-15.9	-14.1	-17.9

Table 4.4: Mean temperature $\bar{T}$ in °C in the Arctic, averaged over the years 51-70 of each size distribution parameter experiment. The value for `ctrl` was derived by a MC simulation.

When increasing the effective radiative diameter d_i of the ice crystals (`+dei`), no strong change in mean Arctic reference height temperature averaged over the years 51-70 of the simulation can be observed compared to `ctrl`. On average, the temperature increases by 0.4 °C (see Tab. 4.4) which is within the 2-σ range of `ctrl`. The lower ice water path in clouds (see Fig. 4.18), combined with the smaller influence of ice crystals on radiation compared to liquid cloud

condensate [88, 52, 64, 67], may explain why the liquid component of clouds plays a more dominant role in the radiation regime and changes in d_i do not significantly impact the Arctic climate.
Looking at the mean Arctic temperatures for each month, though, some significant deviations from `ctrl` can be observed (see Fig. 4.19). The monthly mean Arctic temperature, averaged over the years 51-70 of the simulations, in November, for example, is about 1 °C lower compared to `ctrl`.
Furthermore, it can be seen that it is generally colder in all months with an exception of February. During the summer months, there is little to no difference between the control run and the `+dei` experiment, supported by a moderating effect of sea ice melt maintaining temperatures at around 0 °C. The cooling tendency of enlarged ice crystals is supported by the slightly reduced greenhouse effect during `+dei` compared to `ctrl` (see Fig. 4.21). Even though all monthly values regarding the greenhouse effect durin `+dei` lie within the 1-σ range of `ctrl`, the mean values are generally lower with an exception of June.
Taking the sea ice extent into account (see Fig. 4.20), a significant deviation from `ctrl`, especially during summer and autumn, can be observed. There, more sea ice during the extent minimum in September and the surrounding months can be observed during `+dei`. This corresponds a reduced greenhouse effect.

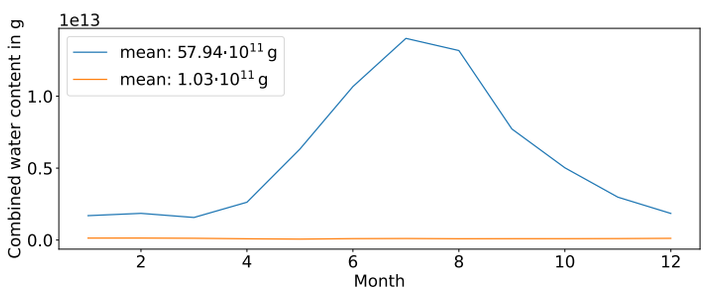

Figure 4.18: Monthly average values of Arctic LWP and IWPs and their mean values over the years 51-70 of `+dei`.

When looking at the monthly mean of the net SW flux at the surface averaged over the years 51-70 (see Fig. 4.22a), it can be seen that it is very similar during `ctrl` and `+dei` in all months. This suggests that the size of ice particles does not have a large influence on shortwave radiation and thus the albedo of the ice and mixed-phase clouds, or at least the albedo effect induced by the liquid cloud droplets is clearly dominating here.

Now, the sensitivity of the Arctic climate regarding the droplet size distribution parameters is investigated. As shown in Fig. 3.1, an increase in λ (`+lamc`) leads to an increase in the number of smaller droplets and a decrease in the number

of larger droplets. An increase in μ (+pgam), on the other hand, leads to a decrease in the number of smaller droplets and an increase in the number of larger droplets.
During the years 51-70 of +lamc, a decrease in mean Arctic temperature of about about 2.4 °C compared to ctrl can be observed. During the same time interval, the mean Arctic temperature of +pgam increased by about 1.4 °C (see Tab. 4.4).

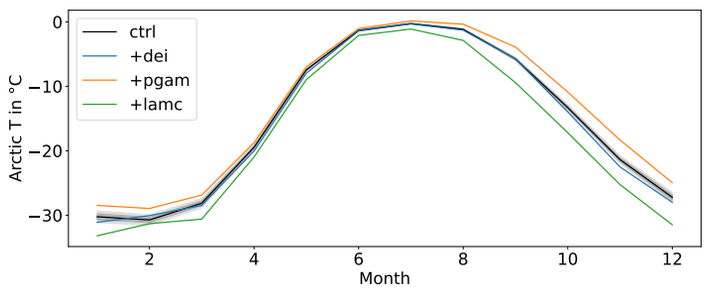

(a) Monthly means

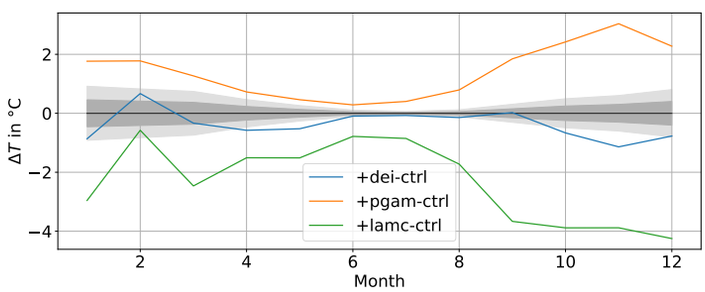

(b) Differences

Figure 4.19: Monthly means of the reference height temperature and difference between these monthly means averaged over the Arctic and years 51-70 of the size distribution parameter experiments. The 20-year monthly means of ctrl were derived using a MC simulation.

This change can also be seen when considering the averaged monthly means of the reference height temperature during that time interval (see Fig. 4.19). During +lamc, it is significantly colder compared to ctrl in every month except for February. Here, it is still colder, but the deviation from ctrl is within the 2-σ range.
The largest differences can be observed in the last third of the year, when it is up to 4 °C colder than during ctrl. This cooling can be explained by the increase of the clouds' optical depth leading to an increase in albedo (see Eq. (2.28), [52, 57], see Figs. 4.22b and c). Hence, less solar radiation is reaching the surface (see also Fig. 4.22a). During the second half of the year, there are also smaller average greenhouse effect induced by clouds (see Fig. 4.21).

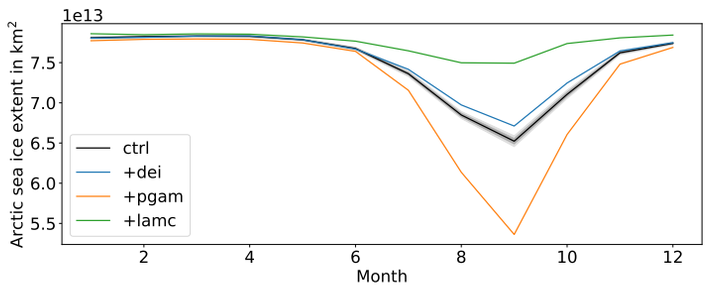

Figure 4.20: Monthly means averaged over the years 51-70 of Arctic sea ice extent of the size distribution parameter and `ctrl` experiments.

A decrease in the greenhouse can also be explained by the smaller cloud droplets. Additionally, a larger sea ice extent can lead to less cloud water in the atmosphere during summer and autumn (cloud-ice feedback [24, 25, 26]). Figs. 4.23a and 4.23b illustrate this as well. Here, it can be seen that there is less cloud water (in any phases) in the Arctic atmosphere during `+lamc`, especially from August to November. Less cloud condensate within the clouds would also lead to a reduced greenhouse effect.

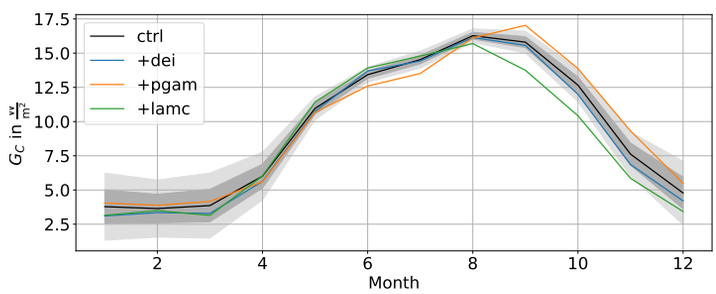

(a) Monthly means

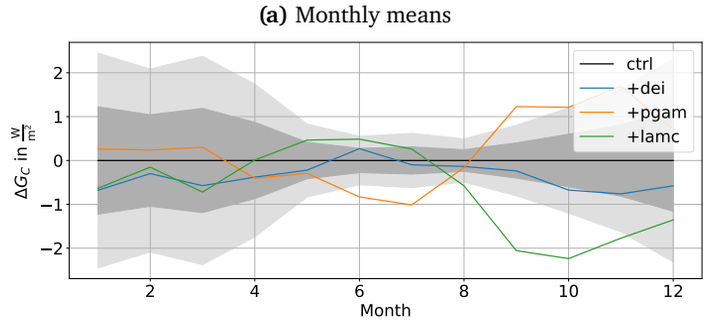

(b) Differences

Figure 4.21: 20-year averages of the monthly means of the Arctic cloud greenhouse effect of the size distribution parameter experiments (over the years 51-70) and `ctrl` (derived by a MC simulation) experiments and their differences.

Sea ice changes significantly in `+lamc` compared to `ctrl`. Especially during the sea ice minimum, a lot more sea ice can be found during `+lamc`, certainly a consequence of the overall lower temperatures. Even though the thickness of the ice is not considered here, one could suspect the ice to grow thicker, too.

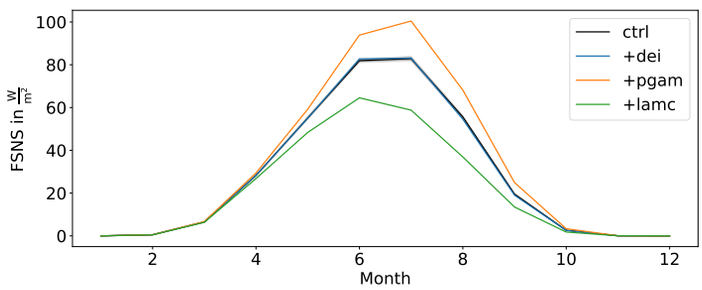

(a) Monthly means of the FSNS

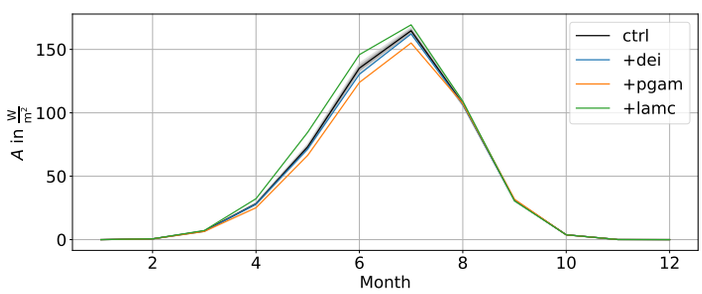

(b) Monthly means of the Arctic cloud albedo effect

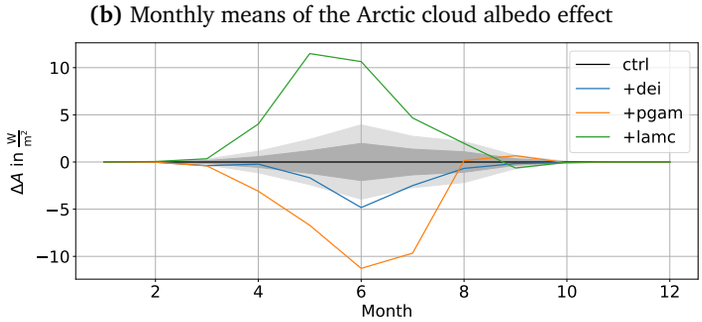

(c) Differences between the monthly means of the Arctic cloud albedo effect

Figure 4.22: 20-year averages of the monthly means of the FSNS, the Arctic cloud albedo effect A of the size distribution parameter (over the years 51-70) and `ctrl` (derived by a MC simulation) experiments and the difference between the Arctic cloud albedo effect monthly means. The net SW flux is directed downwards.

During the `+pgam` experiment, the mean Arctic temperature averaged over the

years 51-70 is significantly warmer than during `ctrl` in all months (see Fig. 4.19). Here, the largest differences between `+pgam` and `ctrl` can be found in autumn and winter, with a maximum difference of 3 °C in November. During summer, this difference is the smallest, most likely due to the sea ice melt.
The general warming of the Arctic can be explained by a smaller albedo due to larger cloud droplets (see Fig. 4.22) as well as an increased greenhouse effect during winter. More SW radiation is reaching the surface during all months with sun above the horizon (see Fig. 4.22a).
Furthermore, compared to `ctrl`, there is on average less sea ice during all months of the years 51-70 of `+pgam`. An increase in temperature leads to more sea ice melt, an earlier melt onset resulting in less ice during the winter season.

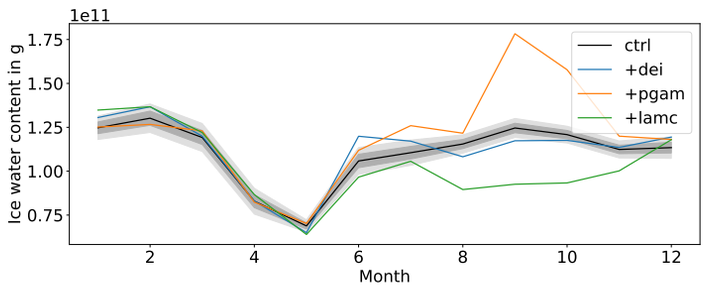

(a) Ice water path

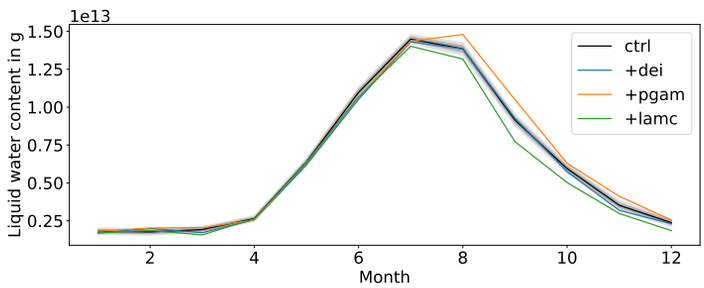

(b) LWP

Figure 4.23: 20-year monthly means of LWP and IWP in the Arctic for the size distribution parameter experiments (over the years 51-70) and `ctrl` (derived by a MC simulation).

The ice is probably also thinner, there is less multi-year ice and more energy can get exchanged between the atmosphere and the ocean which is additionally supporting the warming. Less sea ice also results in more cloud condensate (see Figs. 4.23a and b).

Overall, generally increasing the size of the liquid cloud droplets leads to an increase in Arctic temperature with negative effects regarding the sea ice extent.

Generally decreasing the size of the liquid cloud droplets leads to a cooling of the Arctic with a positive effect regarding the sea ice extent. Increasing the size of ice crystals does not have a noteworthy effect on Arctic temperatures.

4.4 Doubling of CO_2

After examining the effects of individually varying cloud microphysical parameters in the preceding experiments, the following experiment will investigate the effects of a combination of cloud microphysical properties.
Therefore, the amount of CO_2 in the atmosphere is doubled which leads to a general increase of mean Arctic reference height temperatures by about 12 °C (see Tab. 4.5). Here, the value for 2C02 was derived by using a MC simulation as explained in Ch. 3.2.1.
Alongside this warming trend, changes in cloud microphysical properties occur concurrently. Fig. 4.24 illustrates those changes by showing the mean value of each cloud parameter and month, averaged over the all Arctic grid points and all levels for `ctrl` and 2C02. These mean values do not match the exact alterations implemented in `cld_force` but should give a brief idea of general trends. In `cld_force`, each grid point and level is treated individually.

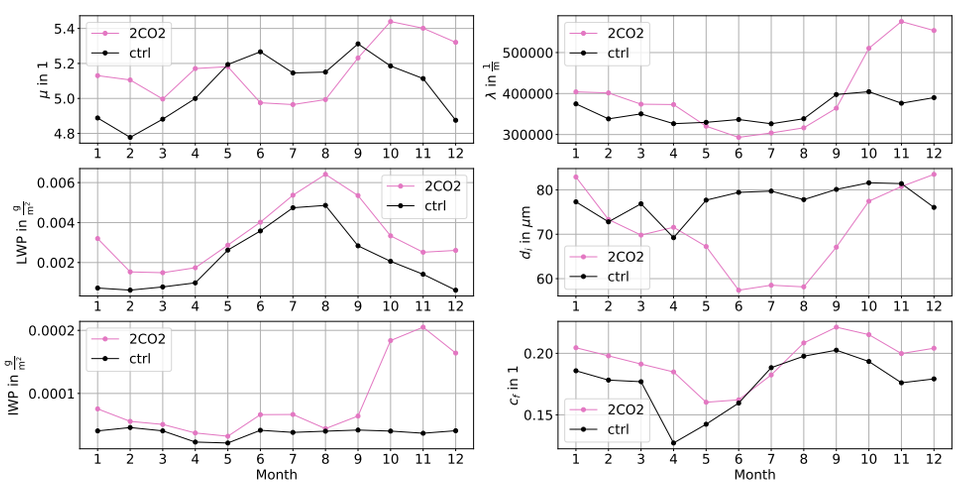

Figure 4.24: Mean values of microphysical cloud properties relevant for interaction with radiation averaged over the Arctic, all pressure levels and the years 51-80 of `ctrl` and 2C02.

It can be seen, e.g., that LWP and IWP in the Arctic seem to increase throughout the whole year. At the same time, ice crystals seem to decrease in size during summer as well as the two liquid cloud droplets size parameters μ and λ. A

general increase in cloud fraction can also be observed except in July.

When adding the differences between the `ctrl` and `2CO2` clouds to an experiment with preindustrial CO_2 levels, the first order impacts the climate change induced cloud changes have on the pre-industrial climate. However, it has to be considered that underlying feedbacks triggered by the initial implementation of those changes might cause additional changes, leading to slightly different clouds than during `2CO2` (see Fig. B.15).

Run name	`ctrl`	`2CO2`	`cld_force`
$\bar{T}$ in °C	-15.5 ± 0.2	-3.3 ± 0.2	-15.0

Table 4.5: Mean temperature $\bar{T}$ in °C in the Arctic, averaged over the years 51-70 of `cld_force`. The values for `ctrl` and `2CO2` were derived by a MC simulation.

Here, the mean Arctic reference height temperature increases by about 0.5 °C when considering the average temperature over the years 51-70 of the simulation (see Tab. 4.5). The changes were again implemented in year 41.

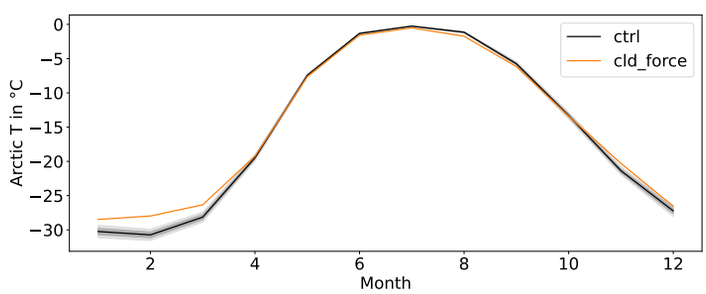

(a) Monthly means

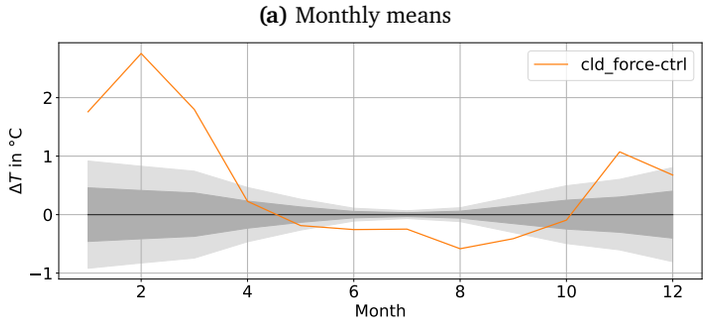

(b) Differences

Figure 4.25: Monthly means of the reference height temperature and difference between these monthly means averaged over the Arctic and years 51-70 of the `cld_force` experiment. The 20-year monthly means of `ctrl` were derived using a MC simulation.

The biggest differences between the monthly means of the 20-year average reference height temperature of `ctrl` and `cld_force` can be found during winter and early spring (see Fig. 4.25). Here, temperatures can be up to 3,°C warmer during `cld_force`. Conversely, in summer, a cooling of up to 0.5,°C is evident, with the most significant cooling observed in August.
Overall, a cooling trend is noticeable from May to October, while a warming trend can be observed from November to April. The extent of warming during these months exceeds that of the cooling period. This might also be related to sea ice melt locking temperatures at around 0 °C.

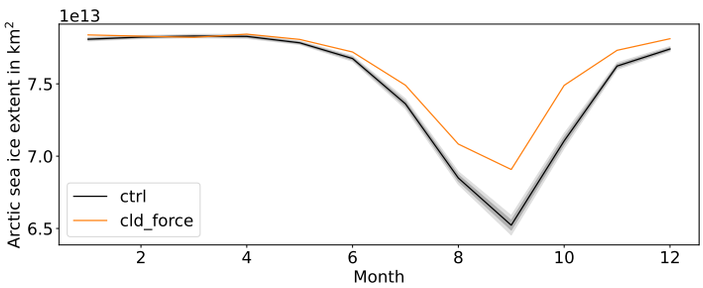

Figure 4.26: 20-year averages (years 51-70) of the monthly means of Arctic sea ice extent of the `cld_force` experiment. The values for `ctrl` were derived using a MC simulation.

Colder temperatures in summer are most likely related to the increased albedo effect (see Fig. 4.27) compared to `ctrl`. Especially the increased water path (see also Fig. B.16) contributes to this. A simultaneous decrease in λ and μ, as found as a general trend (see Fig. 4.24), would result in an increase in the number of larger cloud droplets and a decrease in the number of smaller cloud droplets which would lead to a lower albedo.The same holds true when d_i is reduced. Hence, the effect of the increased cloud condensate is dominating regarding the clouds' albedo effect.
A significantly increased greenhouse effect can also be observed in summer as well as throughout the whole year (see Fig. 4.28). This is most likely also related to the increased cloud condensate and cloud fraction. In summer though, the albedo effect is outweighing the greenhouse effect, hence it gets colder.
The colder temperatures in summer lead to a slower sea ice melt, resulting in a smaller sea ice minimum (see Fig. 4.26).
During winter, the absolute change in liquid cloud condensate is greatest (see Fig. B.16). Consequently, the largest increase in greenhouse effect compared to `ctrl` can be observed during the winter months (see Fig. 4.28).

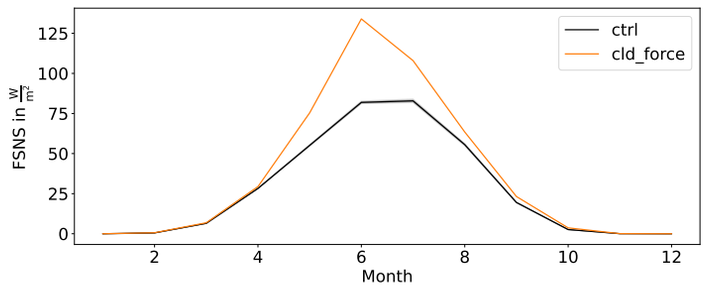

(a) Monthly means of the FSNS

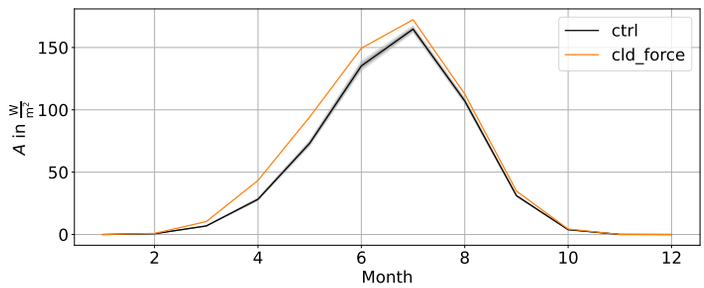

(b) Monthly means of the Arctic cloud albedo effect

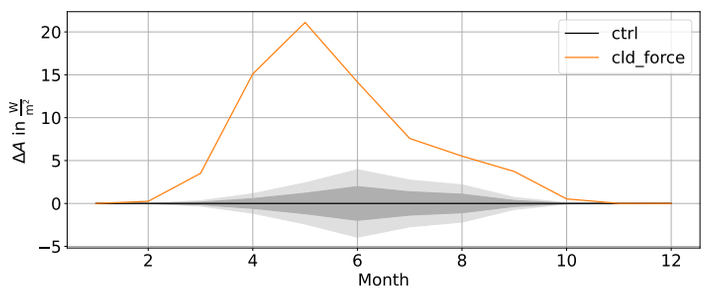

(c) Differences between the monthly means of the Arctic cloud albedo effect

Figure 4.27: 20-year averages of the monthly means of the FSNS, the Arctic cloud albedo effect A of `cld_force` (over the years 51-70) and `ctrl` (derived by a MC simulation) and the difference between the Arctic cloud albedo effect monthly means. The net SW flux is directed downwards.

Because of little to no incoming solar radiation, the albedo effect of clouds becomes insignificant in winter (see Fig. 4.27). Now, the greenhouse effect is dominating which explains the observed warming. An increase in μ and λ during the winter season (see Fig. 4.24) leads to an increase in the number of small cloud droplets and a decrease in the number of larger cloud droplets. One would expect a decrease in absorbance due to these changes [58, 68] and a resulting decrease in greenhouse effect, but again, the general increase of cloud condensate is probably dominating here. A potentially larger cloud

fraction could also be contributing to an increased greenhouse effect.

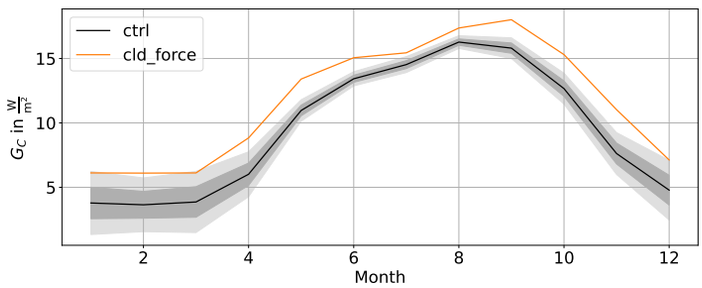

(a) Monthly means

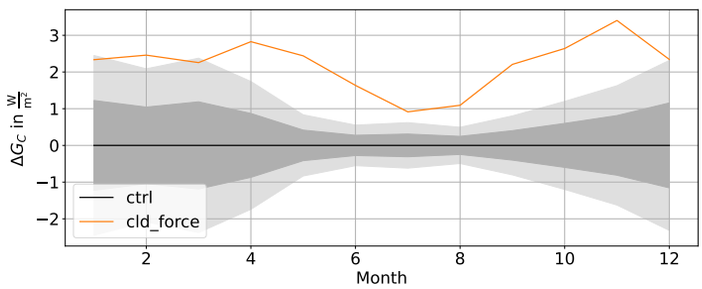

(b) Differences

Figure 4.28: 20-year averages of the monthly means of the Arctic cloud greenhouse effect of `cld_force` (over the years 51-70) and `ctrl` (derived by a MC simulation) experiments.

Overall, it can be seen that the Arctic cloud changes induced by global climate change positively influence the warming, especially in winter. In summer, they have a negative impact on Arctic warming by cooling the climate and inhibiting sea ice melt.

5

Discussion of Methodology

With the results of the experiments presented and discussed, it is essential to also critically evaluate the methodologies employed, identify any limitations, and discuss potential options for improvement.
First of all, the determination of mean values and their uncertainties in `ctrl` and `2CO2` assumes a normal distribution, which may not hold true for all variables, e.g. sea ice extent which is constrained by available area. For this particular example, this is more important in winter when most of the Arctic ocean is covered by sea ice. However, it is merely a minor detail.
A larger improvement of quality of the results could be achieved by prolonging the simulation time, allowing the evaluation of 30 or more years to eliminate long-term fluctuations. Alternatively, a similar MC approach as in `ctrl` and `2CO2` could be applied to all experiments.
Furthermore, this work considered the Arctic as a uniform region, applying the same changes to clouds across the whole area. More realistic outcomes could be attained by incorporating greater spatial variability into the implemented changes. An attempt for achieving that has already been made in `cld_force`.
Additionally, during the analysis of the results, a distinction of the different regions in the Arctic would have been insightful to differentiate between various Arctic regions to assess the impacts of cloud changes over, for instance, open ocean, sea ice, or land.
On a temporal scale, climate changes due to cloud alterations have been examined monthly and the effect of seasonal as well as all-year-round cloud changes have been studied. Here, the choice of summer months during the `_summer` experiments could be reconsidered. July, August and September were chosen

to include months with a large amount of incoming solar radiation as well as the sea ice minimum. *Intrieri et al., 2002* [87] observed clouds to warm the Arctic surface during all months with an exception of a short period in summer, namely late June and July. Therefore, reconsidering the choice of summer months to include only June and July, or, to maintain a three-month period, June, July, and August, may offer potential merit.

Implementing experiments with non-uniform cloud changes on a temporal scale would also account for more realistic results. Efforts in this direction have already been made in `cld_force`.

More realistic results can also be attained when considering more realistic changes. The changes implemented in this work do not necessarily represent future changes due to climate change. `2CO2` showed how cloud parameters change regarding a global warming resulting from a doubling of atmospheric CO_2 content (see Fig. 4.24). Here, it can be seen that, for instance, both, LWP and IWP, increase in this scenario. The experiments conducted and discussed in Ch. 4.2, with an exception of `2liq`, only change the ratio of liquid and ice water content in Arctic clouds.

Hence, in addition to `cld_force`, experiments with changes of a single microphysical property according to `2CO2` can give further insights on the impact that parameter has on the Arctic climate.

All experiments could also be improved by accounting for the underlying cloud changes. When the environment changes due to a feedback induced by the implemented cloud changes, cloud microphysical properties respond. Thus, before modification, they do not align exactly with those in `ctrl`. Moreover, microphysical properties that are not modified can change significantly and can have a large impact on radiation. An example of that are the `+lamc` and `+pgam` experiments where the liquid water content of Arctic clouds changed significantly in the last half of the year as a response to the climate changes induced by the employed changes in liquid droplet size distribution (see Fig. 4.23).

6

Conclusion

Cloud microphysical properties play a significant role in the Arctic climate. By conducting numerical climate model experiments using the CESM, it is shown that the variation of single cloud parameters, i.e. cloud fraction, liquid droplet size distribution, radiative effective diameter of ice crystals, LWP and IWP, has an effect on Arctic climate. Additionally, the effect of Arctic clouds, modified according to Arctic clouds in a $2\times CO_2$ environment, on Arctic climate was studied. An overview of the main findings follows.

It was shown that changes in Arctic clouds due to global climate change contribute positively to the warming, particularly during winter. In contrast, during summer, these changes negatively affect Arctic warming by cooling the climate and hindering the melting of sea ice.

The general occurrence of clouds, as well as the cloud fraction have a strong impact on the Arctic climate. While Arctic clouds do not warm or cool the Arctic climate on an annual average, according to the CESM, a cooling is observed in the first half of the year while a warming is observed in the second half. Reducing the cloud fraction by 50 % leads to a significant cooling throughout the whole year and an increase in sea ice, especially during the sea ice minimum. If the reduction only takes place in summer, no substantial change in temperature is observed, but the sea ice decreases significantly during the summer season. A reduction of cloud cover in winter has a cooling effect and a positive impact on summer sea ice extent.

The size of liquid cloud droplets was also found to have a strong impact on Arctic climate. Enlarged droplets caused a warming alongside with a decrease in summer sea ice extent, shrunken droplets caused a cooling accompanied by

a significant increase in sea ice extent.
Enlarging the size of the ice crystals caused little response. A warming in summer leads to a decrease in sea ice extent, but the impact is not as severe compared to when the size of the liquid cloud droplets are changed.
Doubling the liquid cloud water content in the Arctic causes a cooling of temperature and an increase in sea ice extent. It could be shown that the cooling effect in summer outweighs the warming effect this change has in winter. This is due to the general higher amount of liquid cloud water in summer compared to winter.
When keeping the overall Arctic cloud water content constant and changing the ratio between Arctic liquid and ice water content, no significant changes were observed when the IWP was reduced. A conversion of liquid water into ice in Arctic clouds, on the other hand, showed a strong negative effect on Arctic temperature and a positive effect on sea ice extent. The severity of the mentioned effects varied with the amount of conversed liquid condensate, getting stronger with increasing amount of conversed liquid condensate.
Several experiments showed a strong negative response in temperature in October when the minimum sea ice extent in September was anomalously small.
Overall, this research has provided valuable insights into the primary impacts of cloud microphysical properties on the Arctic climate. Future studies could further expand on this by exploring the effects of climate change-induced changes in Arctic cloud properties across various regions of the Arctic as well as examining both changes of individual parameters and combinations of several modified parameters.

Bibliography

[1] R. Przybylak, *The Climate of the Arctic*. Springer International Publishing, 2016. [Online]. Available: http://dx.doi.org/10.1007/978-3-319-21696-6

[2] A. D. McGuire, F. Chapin, J. E. Walsh, and C. Wirth, "Integrated regional changes in arctic climate feedbacks: Implications for the global climate system," *Annual Review of Environment and Resources*, vol. 31, no. 1, p. 61–91, November 2006. [Online]. Available: http://dx.doi.org/10.1146/annurev.energy.31.020105.100253

[3] R. Brown, *The Polar Regions: A Physical and Economic Geography of the Arctic and Antarctic*, ser. Methuen's geographical series. Methuen & Company Limited, 1927.

[4] W. Bruce, *Polar Exploration*, ser. Home University Library. Williams & Norgate, 1911.

[5] M. C. Serreze and R. G. Barry, *The Arctic Climate System*. Cambridge University Press, July 2014. [Online]. Available: http://dx.doi.org/10.1017/CBO9781139583817

[6] R. A. Houze Jr., "Cloud dynamics," ser. International geophysics series. Elsevier, 2014.

[7] K. Dethloff, A. Rinke, A. Benkel, M. Køltzow, E. Sokolova, S. Kumar Saha, D. Handorf, W. Dorn, B. Rockel, H. von Storch, J. E. Haugen, L. P. Røed, E. Roeckner, J. H. Christensen, and M. Stendel, "A dynamical link between the arctic and the global climate system," *Geophysical Research Letters*, vol. 33, no. 3, February 2006. [Online]. Available: http://dx.doi.org/10.1029/2005GL025245

[8] T. Koenigk, J. Key, and T. Vihma, *Climate Change in the Arctic*. Cham: Springer International Publishing, 2020, pp. 673–705. [Online]. Available: https://doi.org/10.1007/978-3-030-33566-3_11

[9] U. S. Bhatt, D. A. Walker, J. E. Walsh, E. C. Carmack, K. E. Frey, W. N. Meier, S. E. Moore, F.-J. W. Parmentier, E. Post, V. E. Romanovsky, and W. R. Simpson, "Implications of arctic sea ice decline for the earth system," *Annual Review of Environment and Resources*, vol. 39, no. 1, p. 57–89, October 2014. [Online]. Available: http://dx.doi.org/10.1146/annurev-environ-122012-094357

[10] M. C. Serreze and R. G. Barry, "Processes and impacts of arctic amplification: A research synthesis," *Global and Planetary Change*, vol. 77, no. 1–2, p. 85–96, May 2011. [Online]. Available: http://dx.doi.org/10.1016/j.gloplacha.2011.03.004

[11] J. Stroeve and D. Notz, "Changing state of arctic sea ice across all seasons," *Environmental Research Letters*, vol. 13, no. 10, p. 103001, September 2018. [Online]. Available: http://dx.doi.org/10.1088/1748-9326/aade56

[12] R. V. Bekryaev, I. V. Polyakov, and V. A. Alexeev, "Role of polar amplification in long-term surface air temperature variations and modern arctic warming," *Journal of Climate*, vol. 23, no. 14, p. 3888–3906, July 2010. [Online]. Available: http://dx.doi.org/10.1175/2010JCLI3297.1

[13] C. K. Folland, T. R. Karl, J. R. Christy, R. A. Clarke, and G. V. Gruza et al., "Observed Climate Variability and Change," in *Climate change 2001: the scientific basis, Intergovernmental panel on climate change*, 2001. [Online]. Available: https://hal.science/hal-03333964

[14] J. E. Walsh, J. E. Overland, P. Y. Groisman, and B. Rudolf, "Ongoing climate change in the arctic," *AMBIO*, vol. 40, no. S1, p. 6–16, December 2011. [Online]. Available: http://dx.doi.org/10.1007/s13280-011-0211-z

[15] L. Sandberg Sørensen, S. B. Simonsen, R. Forsberg, K. Khvorostovsky, R. Meister, and M. E. Engdahl, "25 years of elevation changes of the greenland ice sheet from ers, envisat, and cryosat-2 radar altimetry," *Earth and Planetary Science Letters*, vol. 495, p. 234–241, August 2018. [Online]. Available: http://dx.doi.org/10.1016/j.epsl.2018.05.015

[16] E. A. G. Schuur, A. D. McGuire, C. Schädel, G. Grosse, J. W. Harden, D. J. Hayes, G. Hugelius, C. D. Koven, P. Kuhry, D. M. Lawrence, S. M. Natali, D. Olefeldt, V. E. Romanovsky, K. Schaefer, M. R. Turetsky, C. C. Treat, and J. E. Vonk, "Climate change and the permafrost carbon feedback," *Nature*, vol. 520, no. 7546, p. 171–179, April 2015. [Online]. Available: http://dx.doi.org/10.1038/nature14338

[17] E. A. Schuur, B. W. Abbott, R. Commane, J. Ernakovich, E. Euskirchen,

G. Hugelius, G. Grosse, M. Jones, C. Koven, V. Leshyk, D. Lawrence, M. M. Loranty, M. Mauritz, D. Olefeldt, S. Natali, H. Rodenhizer, V. Salmon, C. Schädel, J. Strauss, C. Treat, and M. Turetsky, "Permafrost and climate change: Carbon cycle feedbacks from the warming arctic," *Annual Review of Environment and Resources*, vol. 47, no. 1, p. 343–371, October 2022. [Online]. Available: http://dx.doi.org/10.1146/annurev-environ-012220-011847

[18] R. G. Graversen, S. Drijfhout, W. Hazeleger, R. van de Wal, R. Bintanja, and M. Helsen, "Greenland's contribution to global sea-level rise by the end of the 21st century," *Climate Dynamics*, vol. 37, no. 7–8, p. 1427–1442, October 2010. [Online]. Available: http://dx.doi.org/10.1007/s00382-010-0918-8

[19] R. M. van Westen, M. Kliphuis, and H. A. Dijkstra, "Physics-based early warning signal shows that amoc is on tipping course," *Science Advances*, vol. 10, no. 6, February 2024. [Online]. Available: http://dx.doi.org/10.1126/sciadv.adk1189

[20] T. Vihma, "Effects of arctic sea ice decline on weather and climate: A review," *Surveys in Geophysics*, vol. 35, no. 5, pp. 1175–1214, mar 2014. [Online]. Available: https://doi.org/10.1007%2Fs10712-014-9284-0

[21] J. M. Wallace and P. V. Hobbs, "Atmospheric science." Elsevier, 2006.

[22] J. R. Norris, R. J. Allen, A. T. Evan, M. D. Zelinka, C. W. O'Dell, and S. A. Klein, "Evidence for climate change in the satellite cloud record," *Nature*, vol. 536, no. 7614, p. 72–75, July 2016. [Online]. Available: http://dx.doi.org/10.1038/nature18273

[23] H. Chepfer, V. Noel, D. Winker, and M. Chiriaco, "Where and when will we observe cloud changes due to climate warming?" *Geophysical Research Letters*, vol. 41, no. 23, p. 8387–8395, December 2014. [Online]. Available: http://dx.doi.org/10.1002/2014GL061792

[24] Y. Liu, J. R. Key, Z. Liu, X. Wang, and S. J. Vavrus, "A cloudier arctic expected with diminishing sea ice," *Geophysical Research Letters*, vol. 39, no. 5, March 2012. [Online]. Available: http://dx.doi.org/10.1029/2012GL051251

[25] A. L. Morrison, J. E. Kay, W. R. Frey, H. Chepfer, and R. Guzman, "Cloud response to arctic sea ice loss and implications for future feedback in the cesm1 climate model," *Journal of Geophysical Research: Atmospheres*, vol. 124, no. 2, p. 1003–1020, January 2019. [Online].

Available: http://dx.doi.org/10.1029/2018JD029142

[26] J. E. Kay and A. Gettelman, "Cloud influence on and response to seasonal arctic sea ice loss," *Journal of Geophysical Research: Atmospheres*, vol. 114, no. D18, September 2009. [Online]. Available: http://dx.doi.org/10.1029/2009JD011773

[27] I. N. Esau and A. V. Chernokulsky, "Convective cloud fields in the atlantic sector of the arctic: Satellite and ground-based observations," *Izvestiya, Atmospheric and Oceanic Physics*, vol. 51, no. 9, p. 1007–1020, December 2015. [Online]. Available: http://dx.doi.org/10.1134/S000143381509008X

[28] M. H. Dore, "Climate change and changes in global precipitation patterns: What do we know?" *Environment International*, vol. 31, no. 8, p. 1167–1181, October 2005. [Online]. Available: http://dx.doi.org/10.1016/j.envint.2005.03.004

[29] M. R. McCrystall, J. Stroeve, M. Serreze, B. C. Forbes, and J. A. Screen, "New climate models reveal faster and larger increases in arctic precipitation than previously projected," *Nature Communications*, vol. 12, no. 1, November 2021. [Online]. Available: http://dx.doi.org/10.1038/s41467-021-27031-y

[30] P. Ceppi, F. Brient, M. D. Zelinka, and D. L. Hartmann, "Cloud feedback mechanisms and their representation in global climate models," *WIREs Climate Change*, vol. 8, no. 4, May 2017. [Online]. Available: http://dx.doi.org/10.1002/wcc.465

[31] T. Stocker, *Introduction to Climate Modelling*. Springer Berlin Heidelberg, 2011. [Online]. Available: http://dx.doi.org/10.1007/978-3-642-00773-6

[32] S. H. Schneider and R. E. Dickinson, "Climate modeling," *Reviews of Geophysics*, vol. 12, no. 3, p. 447–493, August 1974. [Online]. Available: http://dx.doi.org/10.1029/RG012i003p00447

[33] S. Manabe, "Climate and the ocean circulation1: I. the atmospheric circulation and the hydrology of the earth's surface," *Monthly Weather Review*, vol. 97, no. 11, p. 739–774, November 1969. [Online]. Available: http://dx.doi.org/10.1175/1520-0493(1969)097<0739:CATOC>2.3.CO;2

[34] P. N. Edwards, "History of climate modeling," *WIREs Climate Change*, vol. 2, no. 1, p. 128–139, December 2010. [Online]. Available: http://dx.doi.org/10.1002/wcc.95

[35] J. E. Kay, T. L'Ecuyer, H. Chepfer, N. Loeb, A. Morrison, and G. Cesana, "Recent advances in arctic cloud and climate research," *Current Climate Change Reports*, vol. 2, no. 4, p. 159–169, October 2016. [Online]. Available: http://dx.doi.org/10.1007/s40641-016-0051-9

[36] Community Earth System Model Developers And Affiliates, "Community earth system model - cesm2.0," 2017. [Online]. Available: http://www.cesm.ucar.edu/models/cesm2.0

[37] World Meteorological Organization, "Definitions of clouds," https://cloudatlas.wmo.int/en/clouds-definitions.html, 2017, accessed 13.11.2023.

[38] V. Spiridonov and M. Ćurić, *Fundamentals of meteorology*. Cham, Switzerland: Springer Nature, Nov. 2020.

[39] W. Demtröder, *Experimentalphysik 1*, 6th ed., ser. Springer-Lehrbuch. Berlin, Germany: Springer, Oct. 2012.

[40] D. Meschede, *Gerthsen Physik*, 25th ed., ser. Springer-Lehrbuch. Berlin, Germany: Springer, Apr. 2015.

[41] (1998) Übersättigung. https://www.spektrum.de/lexikon/physik/uebersaettigung/14854, accessed: 19.10.2023.

[42] P. V. Hobbs, *Basic physical chemistry for the atmospheric sciences*, 2nd ed. Cambridge, England: Cambridge University Press, Sep. 2000.

[43] G. K. Vallis, *Atmospheric and oceanic fluid dynamics*, 2nd ed. Cambridge, England: Cambridge University Press, Jun. 2017.

[44] U. Schumann, Ed., *Atmospheric Physics*. Springer Berlin Heidelberg, 2012. [Online]. Available: https://doi.org/10.1007%2F978-3-642-30183-4

[45] G. Vali, P. J. DeMott, O. Möhler, and T. F. Whale, "Technical note: A proposal for ice nucleation terminology," *Atmospheric Chemistry and Physics*, vol. 15, no. 18, pp. 10 263–10 270, sep 2015. [Online]. Available: https://doi.org/10.5194%2Facp-15-10263-2015

[46] C. Magono and C. W. Lee, "Meteorological classification of natural snow crystals," *Journal of the Faculty of Science, Hokkaido University. Series 7, Geophysics*, vol. 2, no. 4, pp. 321–335, nov 1966. [Online]. Available: http://hdl.handle.net/2115/8672

[47] B. van Diedenhoven, *Remote Sensing of Crystal Shapes in Ice Clouds*.

Springer International Publishing, December 2017, p. 197–250. [Online]. Available: http://dx.doi.org/10.1007/978-3-319-70808-9_5

[48] A. J. Heymsfield, S. Lewis, A. Bansemer, J. Iaquinta, L. M. Miloshevich, M. Kajikawa, C. Twohy, and M. R. Poellot, "A general approach for deriving the properties of cirrus and stratiform ice cloud particles," *Journal of the Atmospheric Sciences*, vol. 59, no. 1, p. 3–29, January 2002. [Online]. Available: http://dx.doi.org/10.1175/1520-0469(2002)059<0003:AGAFDT>2.0.CO;2

[49] M. D. Shupe, T. Uttal, and S. Y. Matrosov, "Arctic cloud microphysics retrievals from surface-based remote sensors at sheba," *Journal of Applied Meteorology*, vol. 44, no. 10, p. 1544–1562, October 2005. [Online]. Available: http://dx.doi.org/10.1175/JAM2297.1

[50] S. J. Ling, J. Sanny, and W. Moebs, *University Physics*, Aug. 2016.

[51] M. B. Baker, "Cloud microphysics and climate," *Science*, vol. 276, no. 5315, pp. 1072–1078, may 1997. [Online]. Available: https://doi.org/10.1126%2Fscience.276.5315.1072

[52] M. L. Salby, *Physics of the Atmosphere and Climate*. Cambridge University Press, Jan. 2012. [Online]. Available: http://dx.doi.org/10.1017/CBO9781139005265

[53] I. M. Vardavas and F. W. Taylor, *Radiation and Climate*, ser. International Series of Monographs on Physics. London, England: Oxford University Press, Sep. 2007.

[54] K. N. Liou, *An Introduction to Atmospheric Radiation*, 2nd ed., ser. International Geophysics. Academic Press, May 2014.

[55] (1999) Mie-Streuung. https://www.spektrum.de/lexikon/optik/mie-streuung/2019, accessed: 10.01.2024.

[56] F. Weng, *Cloud Liquid Water*. New York, NY: Springer New York, 2014, pp. 68–70. [Online]. Available: https://doi.org/10.1007/978-0-387-36699-9_18

[57] K. N. Liou, *An Introduction to Atmospheric Radiation*, 2nd ed., ser. International Geophysics. Academic Press, May 2002.

[58] K.-N. Liou, *Radiation and cloud processes in the atmosphere*, ser. Oxford Monographs on Geology and Geophysics. New York, NY: Oxford Uni-

versity Press, Sep. 1992.

[59] (2001) Albedo. https://www.spektrum.de/lexikon/geographie/albedo/241, accessed: 09.11.2023.

[60] J. Marshall and R. A. Plumb, *Atmosphere, ocean and climate dynamics*. San Diego, CA: Academic Press, Dec. 2007.

[61] A. Slingo, "A gcm parameterization for the shortwave radiative properties of water clouds," *Journal of the Atmospheric Sciences*, vol. 46, no. 10, p. 1419–1427, May 1989. [Online]. Available: http://dx.doi.org/10.1175/1520--469(1989)046<1419:AGPFTS>2.0.CO;2

[62] A. A. M. Society, "Single-scatter albedo," https://glossary.ametsoc.org/wiki/Single-scatter_albedo , 2012, accessed 21.03.2024.

[63] H. Savijärvi and P. Räisänen, "Long-wave optical properties of water clouds and rain," *Tellus A*, vol. 50, no. 1, p. 1–11, January 1998. [Online]. Available: http://dx.doi.org/10.1034/j.1600-0870.1998.00001.x

[64] M. D. Shupe and J. M. Intrieri, "Cloud radiative forcing of the arctic surface: The influence of cloud properties, surface albedo, and solar zenith angle," *Journal of Climate*, vol. 17, no. 3, p. 616–628, February 2004. [Online]. Available: http://dx.doi.org/10.1175/1520-0442(2004)017<0616:CRFOTA>2.0.CO;2

[65] A. Gettelman and S. C. Sherwood, "Processes responsible for cloud feedback," *Current Climate Change Reports*, vol. 2, no. 4, pp. 179–189, oct 2016. [Online]. Available: https://doi.org/10.1007%2Fs40641-016-0052-8

[66] A. Arking, "The radiative effects of clouds and their impact on climate," *Bulletin of the American Meteorological Society*, vol. 72, no. 6, pp. 795–813, jun 1991. [Online]. Available: https://doi.org/10.1175%2F1520-0477%281991%29072%3C0795%3Atreoca%3E2.0.co%3B2

[67] Z. Sun and K. P. Shine, "Studies of the radiative properties of ice and mixed-phase clouds," *Quarterly Journal of the Royal Meteorological Society*, vol. 120, no. 515, pp. 111–137, jan 1994.

[68] C. F. Bohren and D. R. Huffman, *Absorption and Scattering of Light by Small Particles*. Wiley, April 1998. [Online]. Available: http://dx.doi.org/10.1002/9783527618156

[69] M. Tjernström, M. D. Shupe, I. M. Brooks, P. O. G. Persson,

J. Prytherch, D. J. Salisbury, J. Sedlar, P. Achtert, B. J. Brooks, P. E. Johnston, G. Sotiropoulou, and D. Wolfe, "Warm-air advection, air mass transformation and fog causes rapid ice melt," *Geophysical Research Letters*, vol. 42, no. 13, p. 5594–5602, July 2015. [Online]. Available: http://dx.doi.org/10.1002/2015GL064373

[70] W. Demtröder, *Experimentalphysik 3*, 4th ed., ser. Springer-Lehrbuch. Berlin, Germany: Springer, Mar. 2010.

[71] A. Kokhanovsky and C. Tomasi, *Physics and chemistry of the Arctic atmosphere*. Cham, Switzerland: Springer Nature, Jan. 2020.

[72] A. Chernokulsky and I. Esau, "Cloud cover and cloud types in the eurasian arctic in 1936–2012," *International Journal of Climatology*, vol. 39, no. 15, p. 5771–5790, July 2019. [Online]. Available: http://dx.doi.org/10.1002/joc.6187

[73] R. Eastman and S. G. Warren, "Interannual variations of arctic cloud types in relation to sea ice," *Journal of Climate*, vol. 23, no. 15, p. 4216–4232, August 2010. [Online]. Available: http://dx.doi.org/10.1175/2010JCLI3492.1

[74] M. D. Shupe, "Clouds at arctic atmospheric observatories. part ii: Thermodynamic phase characteristics," *Journal of Applied Meteorology and Climatology*, vol. 50, no. 3, p. 645–661, March 2011. [Online]. Available: http://dx.doi.org/10.1175/2010JAMC2468.1

[75] J. M. Intrieri, M. D. Shupe, T. Uttal, and B. J. McCarty, "An annual cycle of arctic cloud characteristics observed by radar and lidar at sheba," *Journal of Geophysical Research: Oceans*, vol. 107, no. C10, August 2002. [Online]. Available: http://dx.doi.org/10.1029/2000JC000423

[76] A. V. Matus and T. S. L'Ecuyer, "The role of cloud phase in earth's radiation budget," *Journal of Geophysical Research: Atmospheres*, vol. 122, no. 5, p. 2559–2578, March 2017. [Online]. Available: http://dx.doi.org/10.1002/2016jd025951

[77] T. Uttal, J. A. Curry, M. G. Mcphee, D. K. Perovich, R. E. Moritz, J. A. Maslanik, P. S. Guest, H. L. Stern, J. A. Moore, R. Turenne, A. Heiberg, M. C. Serreze, D. P. Wylie, O. G. Persson, C. A. Paulson, C. Halle, J. H. Morison, P. A. Wheeler, A. Makshtas, H. Welch, M. D. Shupe, J. M. Intrieri, K. Stamnes, R. W. Lindsey, R. Pinkel, W. S. Pegau, T. P. Stanton, and T. C. Grenfeld, "Surface heat budget of the arctic ocean," *Bulletin of the American Meteorological Society*,

vol. 83, no. 2, p. 255–275, February 2002. [Online]. Available: http://dx.doi.org/10.1175/1520-0477(2002)083<0255:SHBOTA>2.3.CO;2

[78] M. D. Shupe, S. Y. Matrosov, and T. Uttal, "Arctic mixed-phase cloud properties derived from surface-based sensors at SHEBA," *Journal of the Atmospheric Sciences*, vol. 63, no. 2, pp. 697–711, feb 2006. [Online]. Available: https://doi.org/10.1175%2Fjas3659.1

[79] A. P. Siebesma, S. Bony, C. Jakob, and B. Stevens, Eds., *Clouds and climate*. Cambridge, England: Cambridge University Press, Aug. 2020.

[80] R. P. Lawson, B. A. Baker, C. G. Schmitt, and T. L. Jensen, "An overview of microphysical properties of arctic clouds observed in may and july 1998 during fire ace," *Journal of Geophysical Research: Atmospheres*, vol. 106, no. D14, p. 14989–15014, July 2001. [Online]. Available: http://dx.doi.org/10.1029/2000JD900789

[81] J. A. Curry, "Interactions among turbulence, radiation and microphysics in arctic stratus clouds," *Journal of the Atmospheric Sciences*, vol. 43, no. 1, p. 90–106, January 1986. [Online]. Available: http://dx.doi.org/10.1175/1520-0469(1986)043<0090:IATRAM>2.0.CO;2

[82] J. Verlinde, J. Y. Harrington, G. M. McFarquhar, V. T. Yannuzzi, A. Avramov, S. Greenberg, N. Johnson, G. Zhang, M. R. Poellot, J. H. Mather, D. D. Turner, E. W. Eloranta, B. D. Zak, A. J. Prenni, J. S. Daniel, G. L. Kok, D. C. Tobin, R. Holz, K. Sassen, D. Spangenberg, P. Minnis, T. P. Tooman, M. D. Ivey, S. J. Richardson, C. P. Bahrmann, M. Shupe, P. J. DeMott, A. J. Heymsfield, and R. Schofield, "The mixed-phase arctic cloud experiment," *Bulletin of the American Meteorological Society*, vol. 88, no. 2, p. 205–222, February 2007. [Online]. Available: http://dx.doi.org/10.1175/BAMS-88-2-205

[83] Y. Liu, J. R. Key, S. A. Ackerman, G. G. Mace, and Q. Zhang, "Arctic cloud macrophysical characteristics from cloudsat and calipso," *Remote Sensing of Environment*, vol. 124, p. 159–173, September 2012. [Online]. Available: http://dx.doi.org/10.1016/j.rse.2012.05.006

[84] J. M. Intrieri and M. D. Shupe, "Characteristics and radiative effects of diamond dust over the western arctic ocean region," *Journal of Climate*, vol. 17, no. 15, p. 2953–2960, August 2004. [Online]. Available: http://dx.doi.org/10.1175/1520-0442(2004)017<2953:CAREOD>2.0.CO;2

[85] J. A. Curry, F. G. Meyer, L. F. Radke, C. A. Brock, and E. E. Ebert, "Occurrence and characteristics of lower tropospheric

ice crystals in the arctic," *International Journal of Climatology*, vol. 10, no. 7, p. 749–764, November 1990. [Online]. Available: http://dx.doi.org/10.1002/joc.3370100708

[86] J. Intrieri and M. Shupe, "Sensitivity of surface cloud radiative forcing to arctic cloud properties," in *Preprints, 11th Conf. on Atmospheric Radiation, Ogden, UT, Amer. Meteor. Soc., CDROM, JP2*, vol. 2, 2002.

[87] J. M. Intrieri, C. W. Fairall, M. D. Shupe, P. O. G. Persson, E. L. Andreas, P. S. Guest, and R. E. Moritz, "An annual cycle of arctic surface cloud forcing at sheba," *Journal of Geophysical Research: Oceans*, vol. 107, no. C10, September 2002. [Online]. Available: http://dx.doi.org/10.1029/2000JC000439

[88] J. A. Curry, J. L. Schramm, and E. E. Ebert, "Impact of clouds on the surface radiation balance of the arctic ocean," *Meteorology and Atmospheric Physics*, vol. 51, no. 3–4, p. 197–217, 1993. [Online]. Available: http://dx.doi.org/10.1007/BF01030494

[89] A. Devasthale, J. Sedlar, M. Tjernström, and A. Kokhanovsky, *A Climatological Overview of Arctic Clouds*. Springer International Publishing, 2020, p. 331–360. [Online]. Available: http://dx.doi.org/10.1007/978-3-030-33566-3_5

[90] D. N. Thomas and G. S. Dieckmann, Eds., *Sea Ice*. Wiley, jan 2017. [Online]. Available: https://doi.org/10.1002%2F9781444317145

[91] Y. Yu, P. C. Taylor, and M. Cai, "Seasonal variations of arctic low-level clouds and its linkage to sea ice seasonal variations," *Journal of Geophysical Research: Atmospheres*, vol. 124, no. 22, p. 12206–12226, November 2019. [Online]. Available: http://dx.doi.org/10.1029/2019JD031014

[92] R. G. Barry, M. C. Serreze, J. A. Maslanik, and R. H. Preller, "The arctic sea ice-climate system: Observations and modeling," *Reviews of Geophysics*, vol. 31, no. 4, p. 397–422, November 1993. [Online]. Available: http://dx.doi.org/10.1029/93RG01998

[93] J. A. Curry, J. L. Schramm, and E. E. Ebert, "Sea ice-albedo climate feedback mechanism," *Journal of Climate*, vol. 8, no. 2, p. 240–247, February 1995. [Online]. Available: http://dx.doi.org/10.1175/1520-0442(1995)008<0240:SIACFM>2.0.CO;2

[94] National Center for Atmospheric Research, "Home | Community Earth

System Model," https://www.cesm.ucar.edu/, accessed: 14.03.2024.

[95] G. Danabasoglu, J. Lamarque, J. Bacmeister, D. A. Bailey, A. K. DuVivier, J. Edwards, L. K. Emmons, J. Fasullo, R. Garcia, A. Gettelman, C. Hannay, M. M. Holland, W. G. Large, P. H. Lauritzen, D. M. Lawrence, J. T. M. Lenaerts, K. Lindsay, W. H. Lipscomb, M. J. Mills, R. Neale, K. W. Oleson, B. Otto-Bliesner, A. S. Phillips, W. Sacks, S. Tilmes, L. van Kampenhout, M. Vertenstein, A. Bertini, J. Dennis, C. Deser, C. Fischer, B. Fox-Kemper, J. E. Kay, D. Kinnison, P. J. Kushner, V. E. Larson, M. C. Long, S. Mickelson, J. K. Moore, E. Nienhouse, L. Polvani, P. J. Rasch, and W. G. Strand, "The community earth system model version 2 (cesm2)," *Journal of Advances in Modeling Earth Systems*, vol. 12, no. 2, Feb. 2020. [Online]. Available: http://dx.doi.org/10.1029/2019MS001916

[96] National Center for Atmospheric Research, "Slab ocean model," 2018, https://ncar.github.io/CAM/doc/build/html/cam5_scientific_guide/slab_ocean.html, accessed: 14.03.2024.

[97] ——, "Model physics," 2017, https://ncar.github.io/CAM/doc/build/html/cam6_scientific_guide/physics.html, accessed: 14.03.2024.

[98] D. L. Mitchell, "Parameterization of the mie extinction and absorption coefficients for water clouds," *Journal of the Atmospheric Sciences*, vol. 57, no. 9, p. 1311–1326, May 2000. [Online]. Available: http://dx.doi.org/10.1175/1520-0469(2000)057<1311:potmea>2.0.co;2

[99] A. Gettelman and H. Morrison, "Advanced two-moment bulk microphysics for global models. part i: Off-line tests and comparison with other schemes," *Journal of Climate*, vol. 28, no. 3, p. 1268–1287, February 2015. [Online]. Available: http://dx.doi.org/10.1175/JCLI-D-14-00102.1

[100] D. L. Mitchell, "Effective diameter in radiation transfer: General definition, applications, and limitations," *Journal of the Atmospheric Sciences*, vol. 59, no. 15, p. 2330–2346, August 2002. [Online]. Available: http://dx.doi.org/10.1175/1520-0469(2002)059<2330:EDIRTG>2.0.CO;2

[101] M. J. Iacono, J. S. Delamere, E. J. Mlawer, M. W. Shephard, S. A. Clough, and W. D. Collins, "Radiative forcing by long-lived greenhouse gases: Calculations with the aer radiative transfer models," *Journal of Geophysical Research: Atmospheres*, vol. 113, no. D13, 2008. [Online]. Available: https://agupubs.onlinelibrary.wiley.com/doi/abs/10.1029/2008JD009944

[102] X. Lan, P. Tans, K. Thoning, and NOAA Global Monitoring Laboratory,

"Trends in globally-averaged co2 determined from noaa global monitoring laboratory measurements." 2023. [Online]. Available: https://gml.noaa.gov/ccgg/trends/global.html?doi=10.15138/9noh-zh07

[103] NSIDC, "Arctic Sea Ice News and Analysis," https://nsidc.org/arcticseaicenews/, 2024, accessed 15.02.2024.

[104] A. Raval and V. Ramanathan, "Observational determination of the greenhouse effect," *Nature*, vol. 342, no. 6251, p. 758–761, December 1989. [Online]. Available: http://dx.doi.org/10.1038/342758a0

[105] H. Haken and H. C. Wolf, *The physics of atoms and quanta*, 7th ed., ser. Advanced Texts in Physics. Berlin, Germany: Springer, Sep. 2005.

A

Planck's law

Planck's law can only be derived considering the quantum hypothesis, especially that energy absorbed or emitted is always a multiple of the product of the Planck constant h and the frequency of the radiation ν. Considering a thermal equilibrium, the ratio of unexcited (n) and excited (n^*) atoms or molecules is Boltzmann distributed [40]:

$$\frac{n^*}{n} = e^{-h\nu/k_\mathrm{B}T}. \tag{A.1}$$

Particles and radiation can exchange energy through three different processes. For one, particles absorb radiation with the energy $h\nu$. The frequency of this process is proportional to the number of unexcited particles as well as the intensity of radiation in the required frequency range ($\sim B\varrho(\nu, T)n$). The proportionality factor B is called *Einstein coefficient* and describes the probability of such an event per time and unit of radiation density [40, 105].
Secondly, spontaneous emission of radiation with energy $h\nu$ is another possibility of energy exchange. Its frequency is proportional to the number of excited particles ($\sim An^*$). A is the proportionality factor and another *Einstein coefficient*. It describes the probability of spontaneous emission per time [40, 105].
Lastly, excited particles can emit radiation with energy $h\nu$ simultaneously with incoming radiation with the same frequency ν. This process is called stimulated emission and its frequency is proportional to the number of excited particles and the intensity of radiation in the required frequency range ($\sim B\varrho(\nu, T)n^*$). The same proportional constant B as for the absorption process is used as this is the direct reversal process to it [40, 105].

In an equilibrium situation, there are as many absorptions as there are emissions of radiation. Hence:

$$B\varrho(\nu,T)n = An^* + B\varrho(\nu,T)n^*. \tag{A.2}$$

The ratio of the Einstein coefficients A and B can be derived using Eq. (A.1). Combining Eqs. (A.1) and (A.2) gives [105]:

$$\varrho(\nu,T) = \frac{A}{B\left(1 - e^{-h\nu/k_\mathrm{B}T}\right)}. \tag{A.3}$$

For small frequencies ($h\nu \ll k_\mathrm{B}T$), the Rayleigh-Jeans law:

$$\varrho(\nu,T) = \frac{8\pi\nu k_\mathrm{B}T}{c^3} \tag{A.4}$$

holds and $e^{-h\nu/k_\mathrm{B}T}$ can be approximated to:

$$e^{-h\nu/k_\mathrm{B}T} = 1 - \frac{k_\mathrm{B}T}{h\nu} \tag{A.5}$$

using a Taylor expansion to the first order. Combining Eqs. (A.3), (A.4) and (A.5), the ratio of the Einstein coefficients becomes [105]:

$$\frac{A}{B} = \frac{8\pi h\nu^3}{c^3}. \tag{A.6}$$

Using this ratio and the Boltzmann distribution (Eq. (A.1)), Eq. (A.2) becomes Planck's law [40]:

$$\varrho(\nu,T)\mathrm{d}\nu = \frac{8\pi h\nu^3}{c^3}\frac{1}{\exp\left(h\nu/k_\mathrm{B}T\right) - 1}\mathrm{d}\nu, \tag{A.7}$$

B

Additional material regarding the sensitivity studies

B.1 Cloud fraction

Looking at the `no_cloud` experiment, Fig. B.2 shows net LW and SW fluxes at the surface, both with clouds and with a clear sky, as well as the cloud coverage and the cloud coverage as seen by the radiation model. The sea ice extent is included as a white line in all figures. The data displayed in the figure is the averaged data for August during the years 51-70.
When comparing the net fluxes on the lefthand side to the clear sky net fluxes on the righthand side of the figure, it becomes apparent that in the Arctic region, hence North of 70 °N, those fluxes are identical. This is coincides with what was to be expected since no clouds are present in the Arctic due to the applied forcing.
The LW fluxes are directed upwards while the SW fluxes are directed downwards. It can be seen that the SW flux over ice-covered areas (namely sea ice and the Greenlandic ice sheet) is smaller than over the open ocean or land that is not covered by ice. This is due to the higher albedo of ice and snow covered surfaces, thus more SW radiation is getting reflected. Further, FSNS is larger in the areas that are not covered with clouds. This is due to the reflective properties of clouds as they reflect SW radiation before it can reach the surface.

The LW net flux is larger when no clouds are present. In this case, there is no greenhouse effect induced by clouds and the LW radiation can escape into space without being absorbed and re-emitted by clouds. The net LW flux is smallest over areas covered by sea ice and parts of the Greenland ice shield.

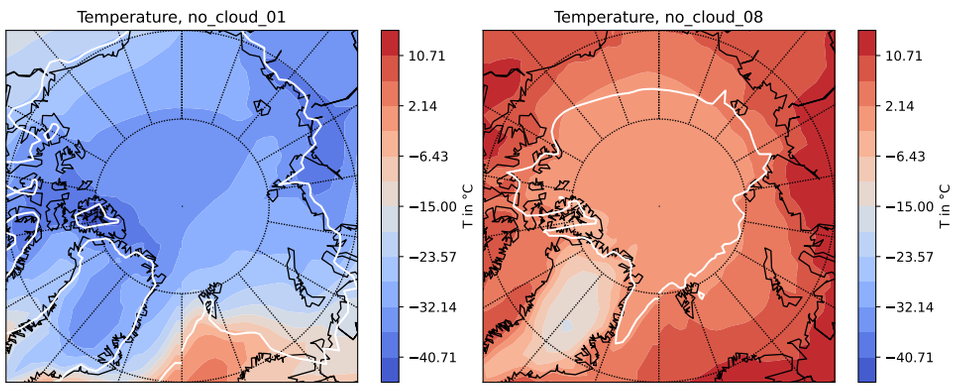

(a) January **(b)** August

Figure B.1: Reference height temperature in January and August, averaged over the years 51-70 for the `no_cloud` experiment. The white line indicates the sea ice extent.

Further, the reference height temperature in August, averaged over the years 51-70 is shown in Fig. B.1b for the `no_cloud` experiment. Here, it can be seen that the temperature is decreases with increasing latitude with Greenland being the exception and the coldest area.
Considering the radiation fluxes in January (see Fig. B.3), it can be seen FLNS is greatest at areas without sea ice (namely north of Norway/south of Svalbard). Here, the ice cannot act as an insulator between the warm ocean and the cold atmosphere. This area is also the warmest (see Fig. B.1a).
The SW flux is constant and 0 for all grid points in the Arctic in January, whether the clear-sky or cloudy-sky flux is considered. This is due to the fact that in January, no sun light reaches the Arctic due to the tilt of Earth's rotational axis.

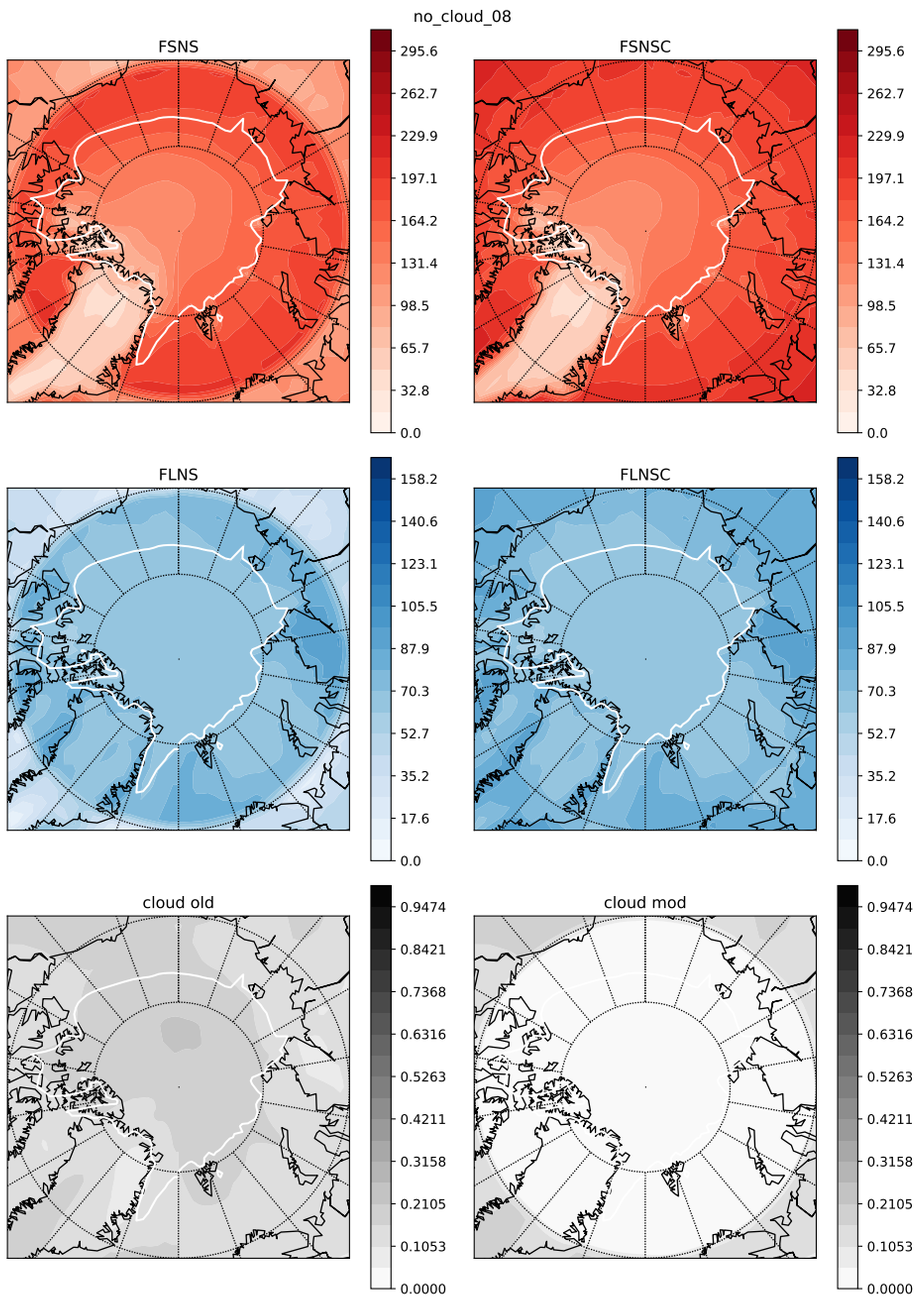

Figure B.2: Net radiation fluxes at surface and cloud coverage in August, averaged over the years 51-70 for the `no_cloud` experiment. From upper left to lower right: FSNS, clear-sky FSNS, FLNS, clear-sky FLNS, cloud coverage prior to modification, modified cloud coverage. The white line in the figures indicates the sea ice extent.

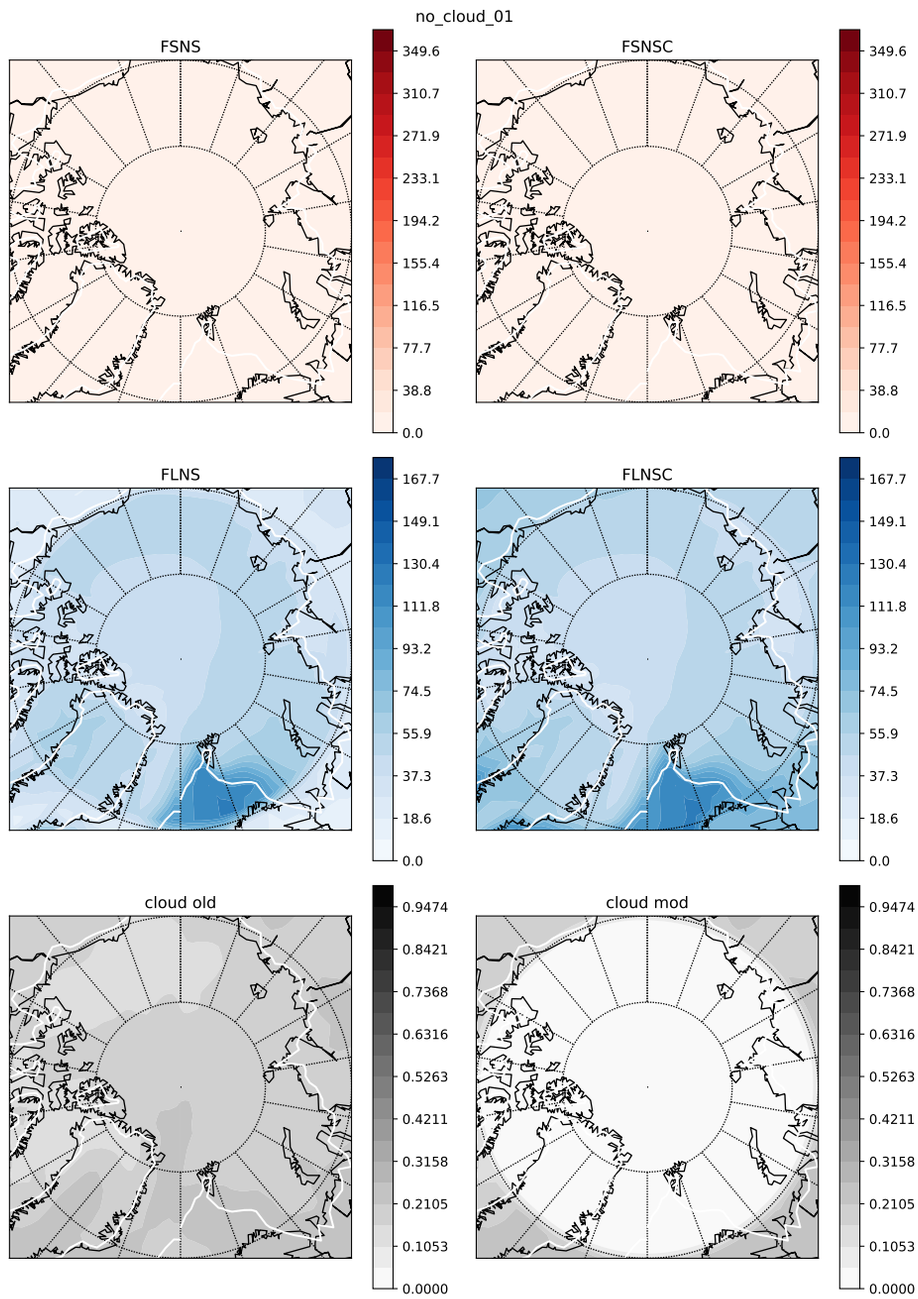

Figure B.3: Net radiation fluxes at surface and cloud coverage in January, averaged over the years 51-70 for the `no_cloud` experiment. From upper left to lower right: FSNS, clear-sky FSNS, FLNS, clear-sky FLNS, cloud coverage prior to modification, modified cloud coverage. The white line in the figures indicates the sea ice extent.

B.2 Liquid and ice water path

B.2.1 Additional experiments

During `+liq`, the mean Arctic reference height temperature during the years 51-70 decreases on average by about 0.4 °C. This is within the 2-σ range of `ctrl`. Converting all solid cloud condensate into liquid during `no_ice` leads to a insignificant increase of this average reference height temperature by 0.2 °C which is within the 1-σ range of `ctrl` (see Tab. 4.3).

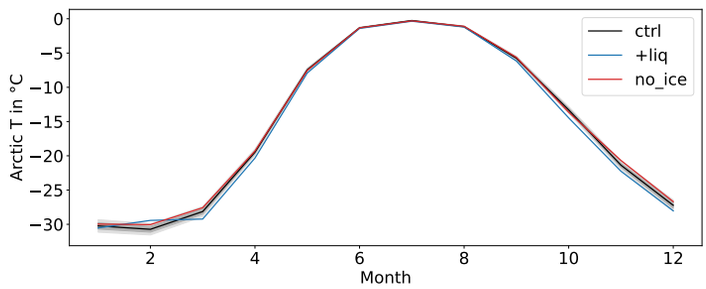

(a) Monthly means

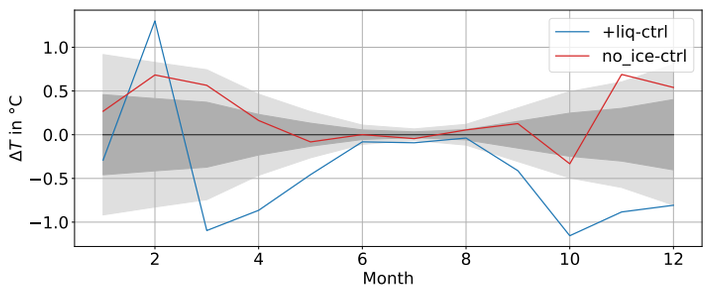

(b) Differences

Figure B.4: Monthly means of the reference height temperature and difference between these monthly means averaged over the Arctic and years 51-70 of the experiments with increased LWP and decreased IWP. The 20-year monthly means of `ctrl` were derived using a MC simulation.

Considering the monthly means of the average Arctic reference height temperature, a general warming trend in all months except for summer can be observed during `no_ice`. The warming is always within the 2-σ range of `ctrl` (see Fig. B.4b).

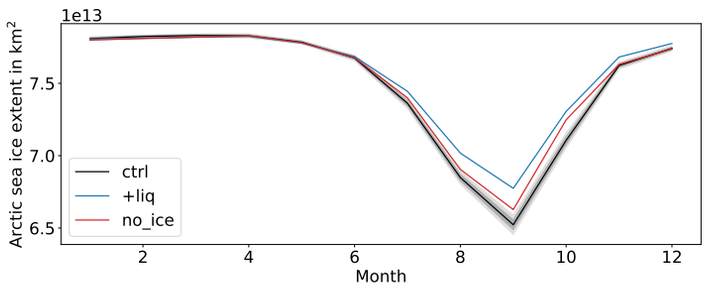

Figure B.5: 20-year averages (years 51-70) of the monthly means of Arctic sea ice extent of the experiments with increased LWP and decreased IWP. The values for `ctrl` were derived using a MC simulation.

An exception here is November, when the temperature is just out of that range by less than 0.1 °C. Additionally, in October, a cooling within the 2-σ range of `ctrl` can be observed.

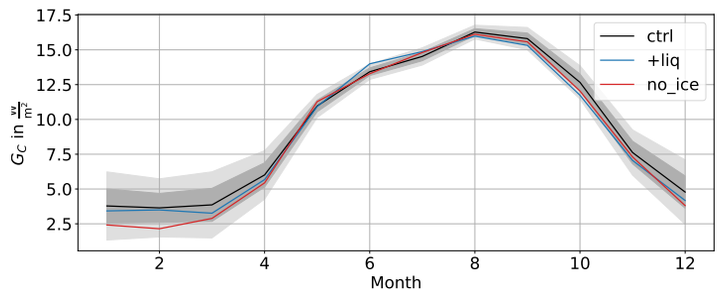

(a) Monthly means

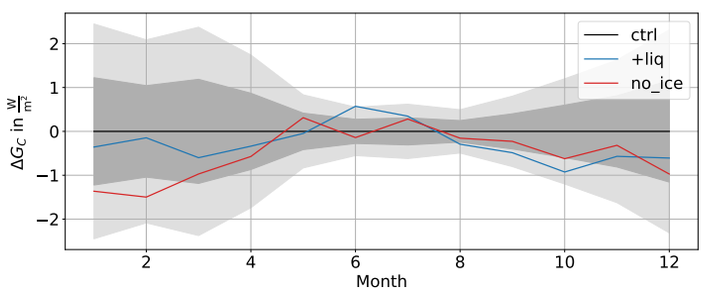

(b) Differences

Figure B.6: 20-year averages of the monthly means of the Arctic cloud greenhouse effect of the experiments with increased LWP and decreased IWP (over the years 51-70) and `ctrl` (derived by a MC simulation) and their differences.

In early summer, it is slightly cooler during `no_ice` compared to `ctrl`, even though temperatures are locked by sea ice melt. A minor increase in cloud

albedo (see Fig. B.7) that can be explained with liquid cloud droplets being more reflective than ice crystals (see Ch. 2.3) possibly leads to the slightly greater sea ice minimum (see Fig. B.5).

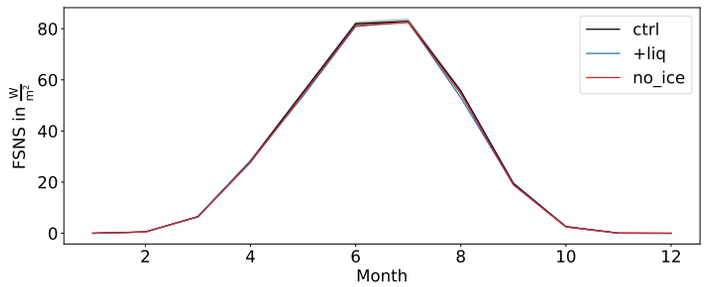

(a) Monthly means of the FSNS

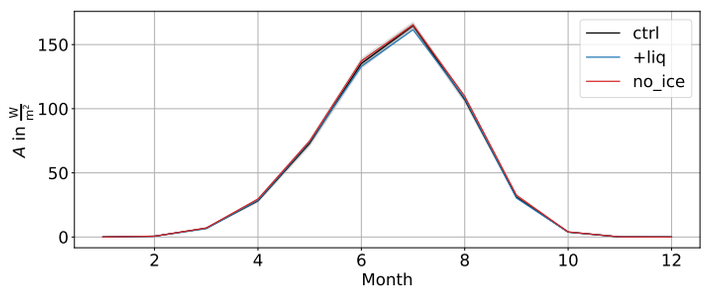

(b) Monthly means of the Arctic cloud albedo effect

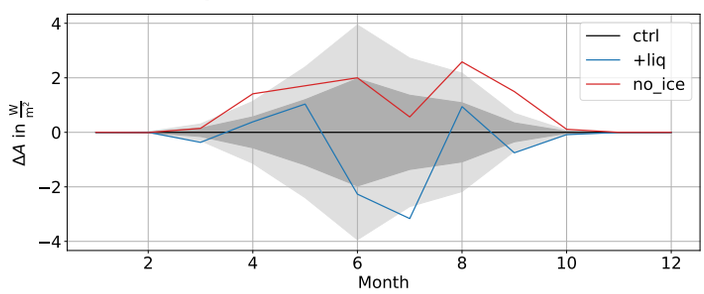

(c) Differences between the monthly means of the Arctic cloud albedo effect

Figure B.7: 20-year averages of the monthly means of the FSNS, the Arctic cloud albedo effect A of the `ctrl` (derived by a MC simulation) and experiments with increased LWP and decreased IWP (over the years 51-70) and the difference between the Arctic cloud albedo effect monthly means. The net SW flux is directed downwards.

The slight drop in temperature during October could be explained by the greater sea ice extent inhibiting the energy exchange between the ocean and the atmosphere. This effect is suspected to be largest in October due to a

larger deviation in sea ice extent between `no_ice` and `ctrl` as the temperature difference between ocean and atmosphere is not as big in September compared to October and the sea ice extent of the two experiments is about the same in November.
Furthermore, the greenhouse effect of the clouds does not change significantly during `no_ice` (see Fig. B.6).
During `+liq`, temperatures are lower during all months, except for February (see Fig. B.4). The largest deviations from `ctrl` can be found in February, March and October when the differences between the average Arctic temperatures are greater than 1 °C. Due to the consistently lower temperatures, it is reasonable to observe a greater sea ice extent throughout the summer and autumn seasons. Moreover, the greater sea ice extent helps to sustain the colder temperatures throughout the winter season by acting as an insulator between ocean and atmosphere.
The warming in February cannot be explained by just considering cloud effects. Even though there is a small increase in cloud condensate in February (see Fig. B.9), the greenhouse effect is not significantly increased (see Fig. B.6).

B.2.2 Water contents

Figs. B.8 - B.14 show the Arctic LWC, IWC and combined water content for the experiments with modified water paths. *old* refers to the water content suggested by the model, *mod* refers to the modified parameters.

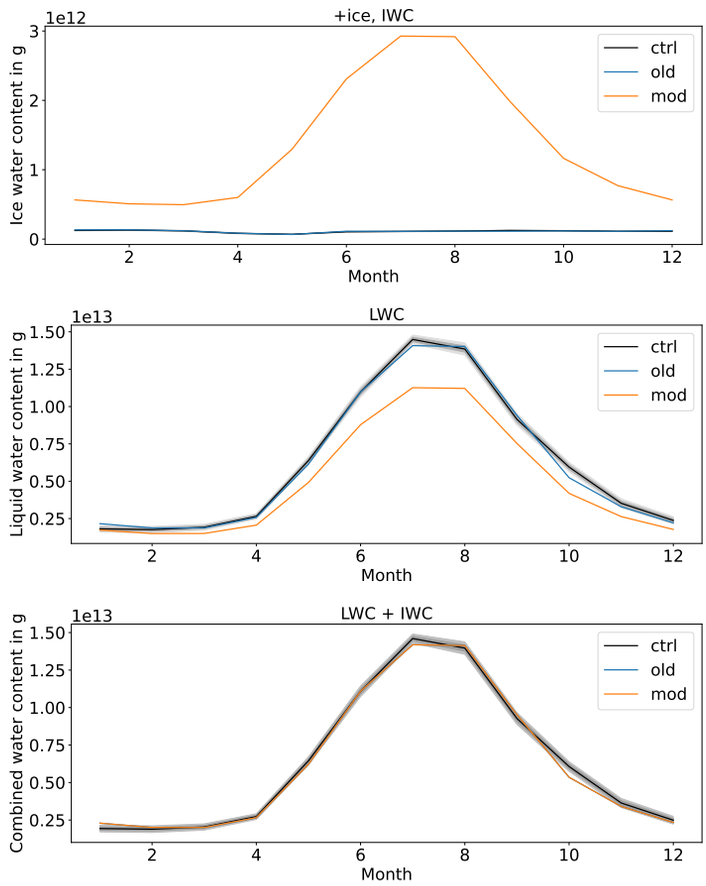

Figure B.8: 20-year averages of the monthly means of the Arctic LWC, IWC and combined water content of the `+ice` experiment (over the years 51-70) prior and after the modifications and `ctrl` (derived by a MC simulation) experiments.

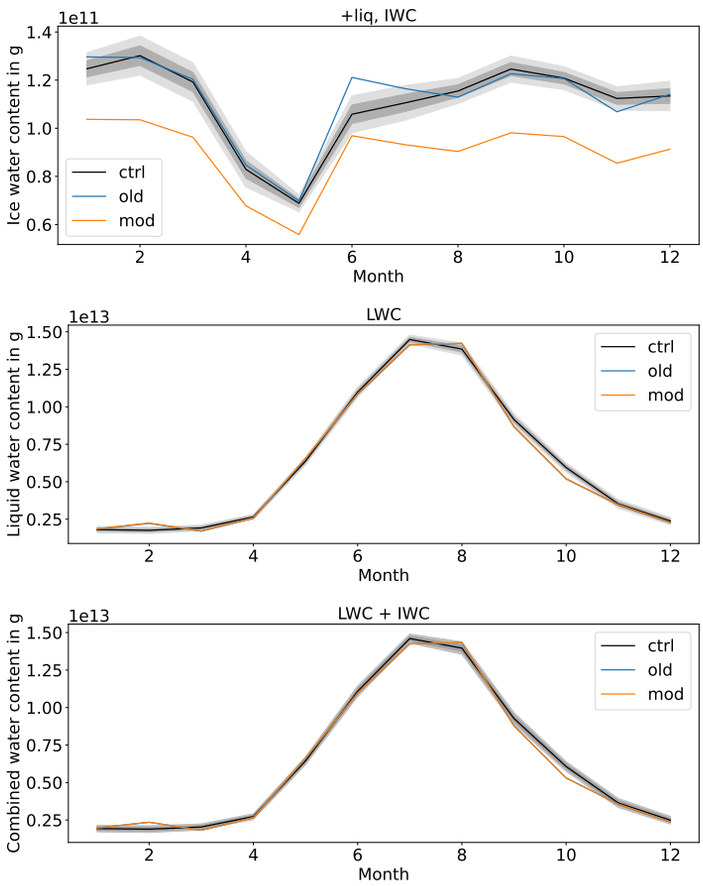

Figure B.9: 20-year averages of the monthly means of the Arctic LWC, IWC and combined water content of the `+liq` experiment (over the years 51-70) prior (old) and after (mod) the modifications and `ctrl` (derived by a MC simulation) experiments.

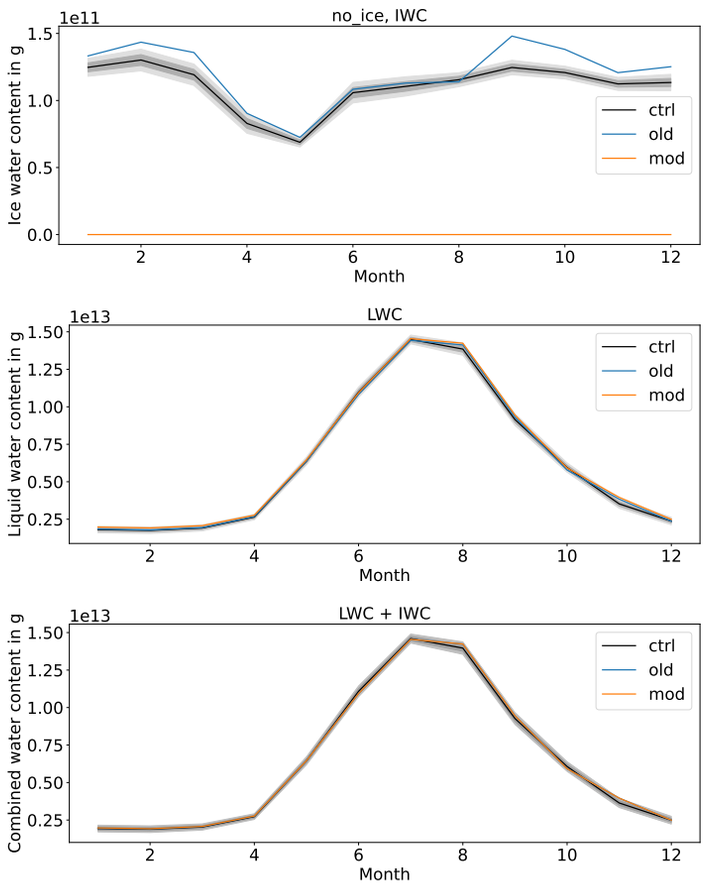

Figure B.10: 20-year averages of the monthly means of the Arctic LWC, IWC and combined water content of the `no_ice` experiment prior (old) and after (mod) the modifications (over the years 51-70) and `ctrl` (derived by a MC simulation) experiments.

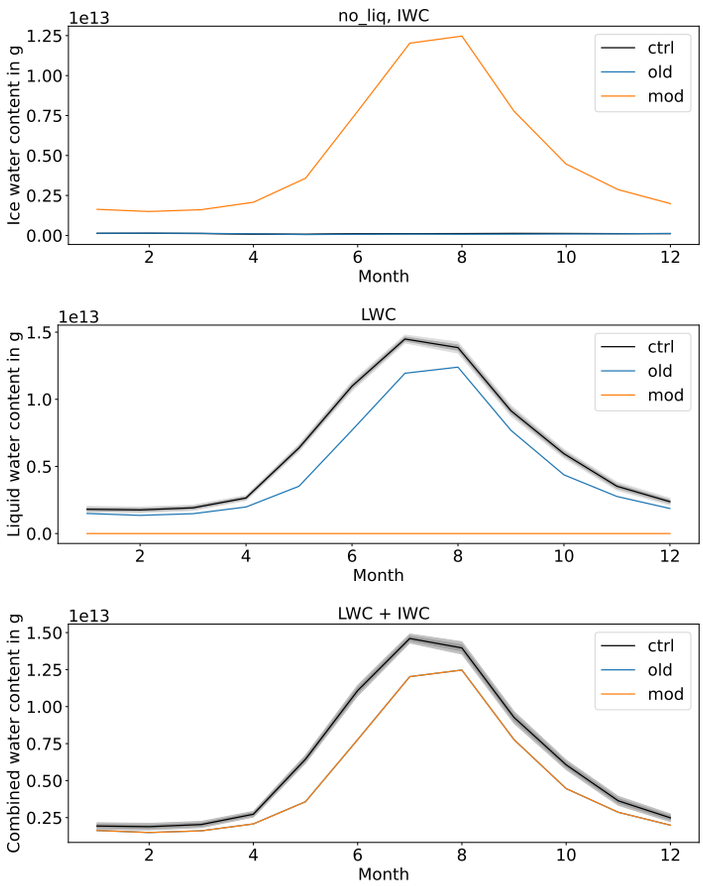

Figure B.11: 20-year averages of the monthly means of the Arctic LWC, IWC and combined water content of the `no_liq` experiment (over the years 51-70) before (old) and after (mod) the modifications and `ctrl` (derived by a MC simulation) experiments.

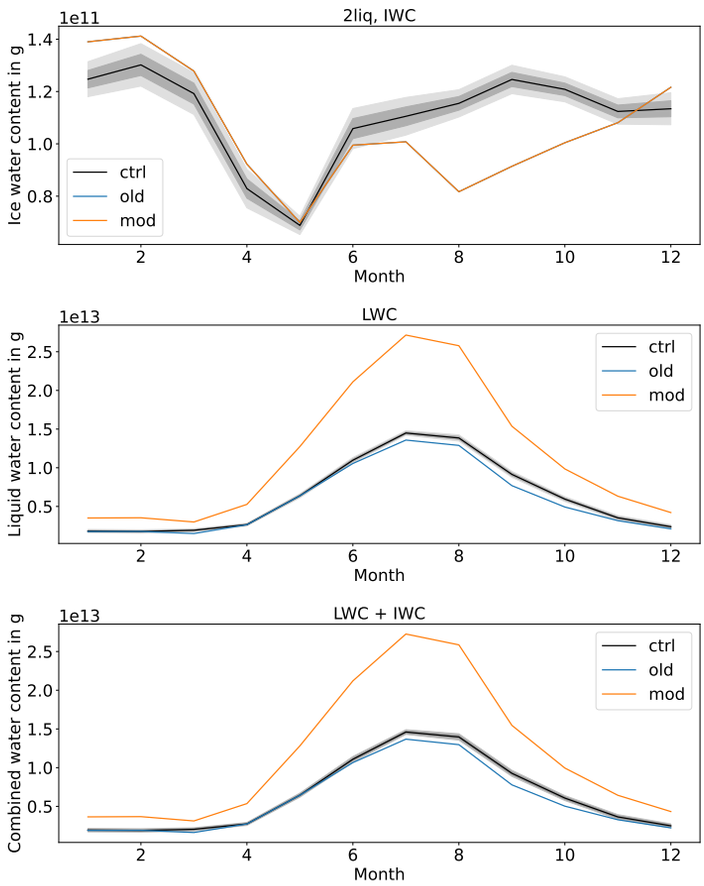

Figure B.12: 20-year averages of the monthly means of the Arctic LWC, IWC and combined water content of the `2liq` experiment (over the years 51-70) before (old) and after (mod) the modifications and `ctrl` (derived by a MC simulation) experiments.

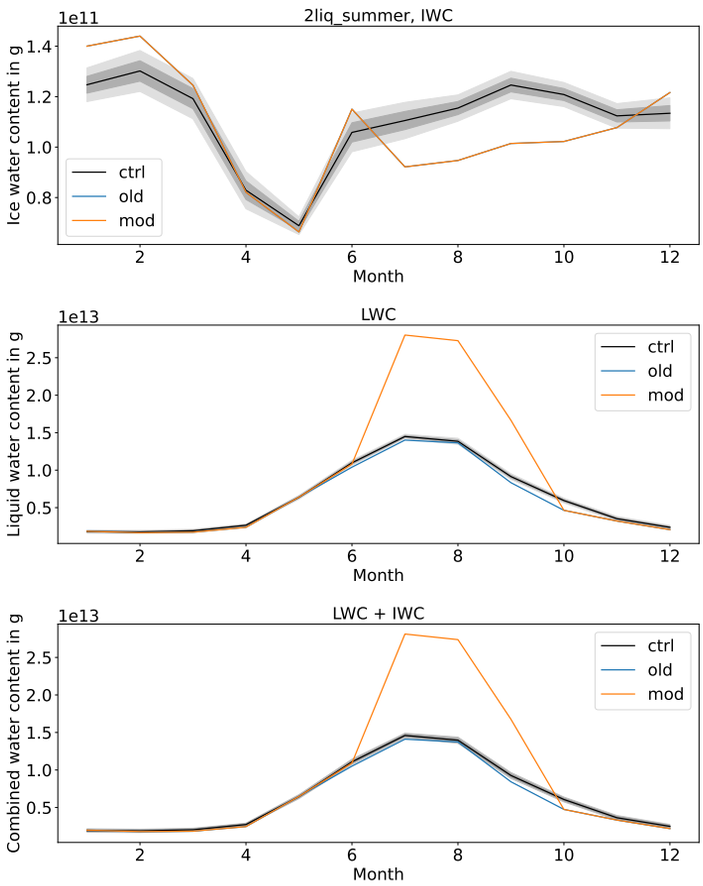

Figure B.13: 20-year averages of the monthly means of the Arctic LWC, IWC and combined water content of the `2liq_summer` experiment (over the years 51-70) before (old) and after (mod) the modifications and `ctrl` (derived by a MC simulation) experiments.

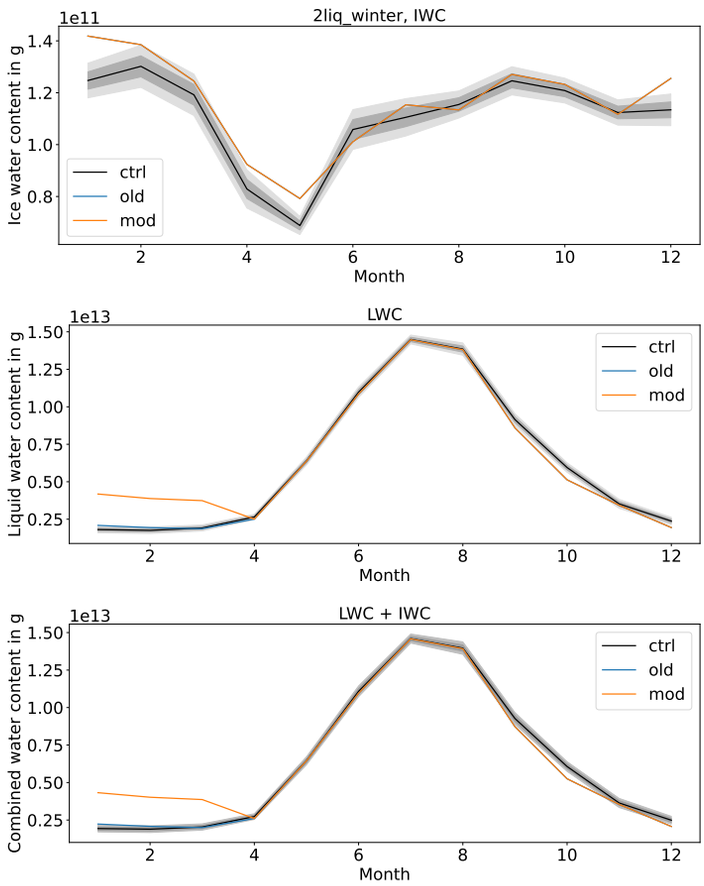

Figure B.14: 20-year averages of the monthly means of the Arctic LWC, IWC and combined water content of the `2liq_winter` experiment (over the years 51-70) before (old) and after (mod) the modifications and `ctrl` (derived by a MC simulation) experiments.

B.3 Doubling of CO_2

Fig. B.15 shows the mean values of microphysical cloud properties relevant for interaction with radiation averaged over the Arctic and all pressure levels over the years 51-80 of `ctrl` and `cld_force`, before and after the modifications. Differences in `cld_force` (mod) and 2C02 can result from underlying cloud changes as well as the fact that the mean displayed in Fig. B.15 is a very broad one, ignoring large spatial variability, vertically and horizontally.

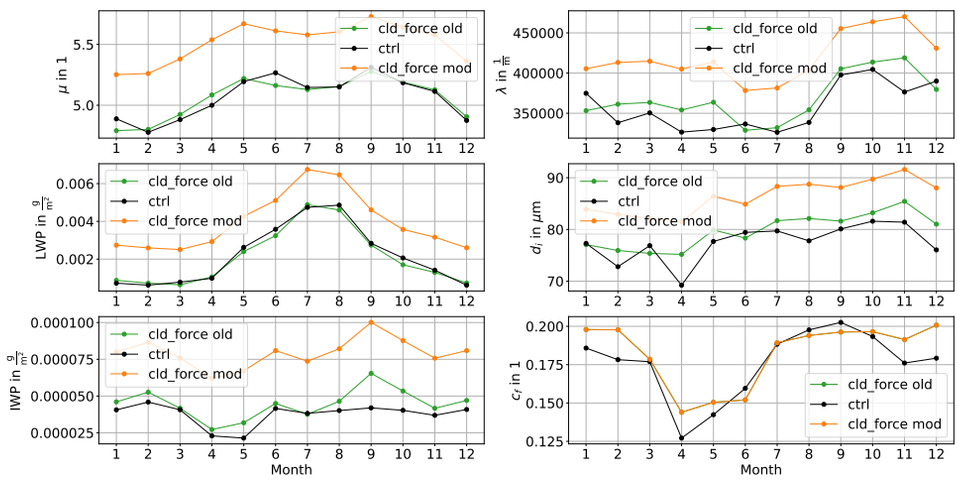

Figure B.15: Mean values of microphysical cloud properties relevant for interaction with radiation averaged over the Arctic, all pressure levels and the years 51-80 of `ctrl` and `cld_force` before (old) and after (mod) the modifications.

Fig. B.16 shows the Arctic LWC, IWC and combined water content for the `params` experiment. *old* refers to the water content suggested by the model, *mod* refers to the modified parameters.

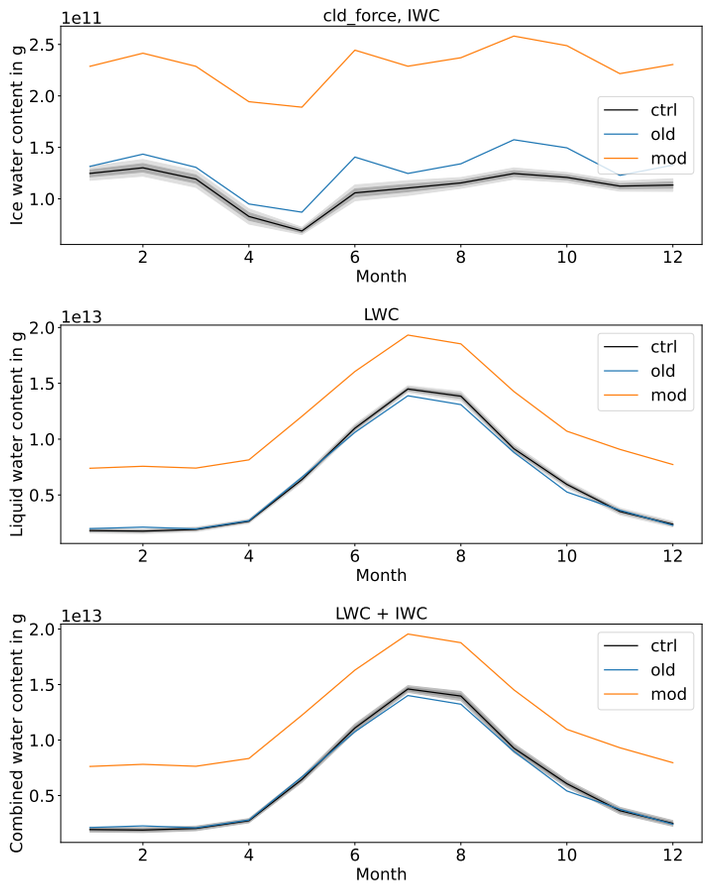

Figure B.16: 20-year averages of the monthly means of the Arctic LWC, IWC and combined water content of the `params` experiment (over the years 51-70) before (old) and after (mod) the modifications and `ctrl` (derived by a MC simulation) experiments.